Materials and Design 204 (2021) 109651

Contents lists available at ScienceDirect

Materials and Design

journal homepage: www.elsevier.com/locate/matdes

# Heat treatment of aluminium alloys produced by laser powder bed fusion: A review

J. Fiocchi *, A. Tuissi, C.A. Biffi

*CNR ICMATE, National Research Council, Institute of Condensed Matter Chemistry and Technologies for Energy, Unit of Lecco, Via Previati 1/e, 23900 Lecco, Italy*

## HIGHLIGHTS

- Heat treatment of LPBFed aluminium parts must be redefined due to LPBF's peculiar solidification conditions.
- Matrix supersaturation and presence of metastable phases often make direct ageing more effective than solution treatment.
- Modified alloys require specific treatment procedures due to the peculiar microstructures induced by rapid solidification.

## GRAPHICAL ABSTRACT

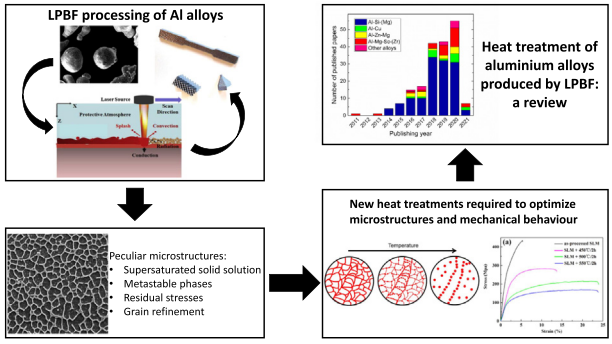


## ARTICLE INFO

*Article history:*
Received 19 October 2020
Received in revised form 1 February 2021
Accepted 6 March 2021
Available online 10 March 2021

*Keywords:*
Laser powder bed fusion
Selective laser melting
Aluminium alloys
Heat treatment
Microstructure
Mechanical behaviour

## ABSTRACT

Laser powder bed fusion (LPBF) is the most widely used additive manufacturing technique and has received increasing attention owing to the high design freedom it offers. The production of aluminium alloys by LPBF has attracted considerable interest in several fields due to the low density of the produced alloys. The peculiar solidification conditions experienced by molten metal during the SLM process and its layer-by-layer nature causes a variety of microstructural peculiarities including the formation of metastable phases and supersaturated solid solutions, extreme microstructural refinement, and generation of residual stresses. Therefore, post-build heat treatments, which are commonly applied to conventionally produced aluminium alloys, may need to be modified in order to be adapted to the peculiar metallurgy of aluminium alloys manufactured using LPBF and address the specific issues resulting from the process itself. A number of studies have investigated this topic in recent years, proposing different approaches and dealing with various alloying systems. This paper reviews scientific research results in the field of heat treatment of selective laser melted aluminium alloys; it aims at providing a comprehensive understanding of the relationship between the induced microstructure and the resulting mechanical behaviour, as a function of the various treatment strategies.



**Contents**



* Corresponding author.
*E-mail address:* jacopo.fiocchi@icmate.cnr.it (J. Fiocchi).

https://doi.org/10.1016/j.matdes.2021.109651

## 1. Introduction

Since the 1990s, the additive manufacturing (AM) of metallic alloys has attracted considerable attention in both research and industrial communities. Therefore, enormous efforts have been devoted to improve various aspect of the production techniques belonging to this family including the technological aspect [1], metallurgical aspect [2] and design [3]. Particularly, laser powder bed fusion (LPBF), also commonly named selective laser melting (SLM), has emerged as one of the most widespread AM technique, and has evolved from being a rapid prototyping technique to becoming a well-established industrial reality [4]. LPBF has been applied in the production of several engineering alloys such as steel [5], titanium [6], nickel [7], and aluminium alloys. Aluminium alloys usually suffer from production related issues such as high reflectivity and thermal conductivity, strong oxidation tendency, and wide solidification range [8]. These limitations have been addressed and widely investigated. First, several studies have focussed on alloys of the aluminium-silicon system, which are directly derived from alloys designed for casting. Thereafter, alloys with higher mechanical performance have been developed, such as those belonging to the 2xxx and 7xxx series of wrought alloys. These alloys, which present numerous processing issues (e.g., solidification cracking), have been modified to obtain improved products: similarly to what is sometimes done in laser welding through the use of filler material, eutectic inducing elements (e.g. Si) or inoculants (e.g. SiC, TiC, $TiB_2$), have been introduced in poorly processable alloys in order to change the solidification dynamics or induce heterogeneous nucleation [9]. Finally, some new formulations, specifically dedicated to LPBF processing, which are frequently based on the addition of Sc, have been proposed and are attracting considerable attention. In addition to the optimisation of processing parameters, the detailed analysis of the arising microstructure and mechanical or functional properties, strong attention has been devoted in the past few years to the identification of suitable thermal treatments, able to improve the performance of laser powder bed fused (LPBFed) aluminium components. Particularly, the importance of on-purpose developed heat treatments has been recognized early [10] and arises from the peculiar metallurgical features, which are induced by the LPBF process. The LPBF process, which is based on the localised melting of small powder volumes by a high-energy source, is rightfully considered as a rapid solidification technique, akin to melt spinning or copper mould casting. Therefore, LPBF presents a number of peculiarities:

- Extremely high cooling rates in the range of $10^3$–$10^7$ K/s
- Building of the part due to the solidification of new melt pools overlapped with each other, due to the layer-by-layer construction
- Successive heating and cooling cycles on the solidified material caused by laser scans on adjacent tracks or overlying layers.

These technological features have a significant influence on the metallurgy of the LPBFed parts, which among others, display the following characteristics, which will be later deeply addressed:

- Formation of strongly supersaturated solid solutions (SSSSs)
- Generation of residual stresses
- Epitaxial growth on the underlying layers, which results in directional solidification and mechanical anisotropy
- In situ heat treatment of previously solidified material, which in turn causes local phase transformations and precipitation.

This indicates that the metallurgical characteristics of LPBFed alloys differ inherently from those of conventionally produced alloys. Therefore, heat treatments, which are commonly applied to conventionally produced aluminium alloys, may need to be recalibrated in terms of the holding temperatures and durations, or even completely reformulated to obtain satisfactory microstructural modifications, and consequently, mechanical properties. In recent years, a considerable number of scientific papers have addressed this issue by exploring several heat treatment routes and developing new methods for improving the alloys' behaviour. In 2011 and 2013, for the first time, two pioneering papers by Palm and Schmidtke reported the heat treatment of an LPBFed aluminium alloy focussing on the now renowned Scalmalloy® [11,12]. Nevertheless, in the following years, most

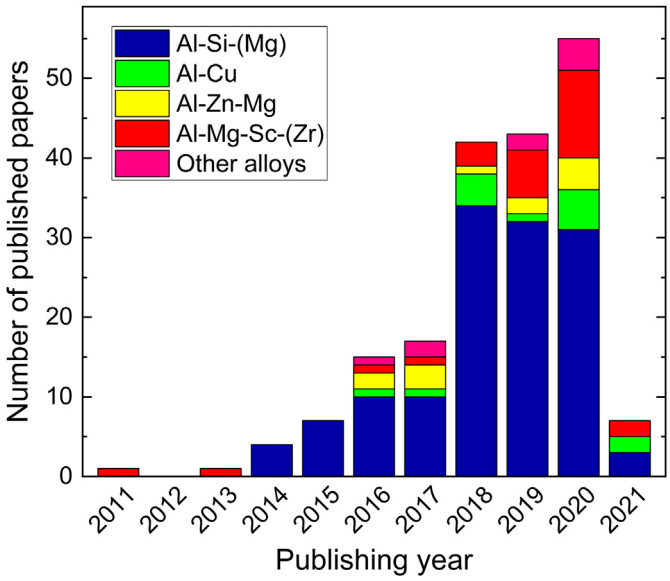


**Fig. 1.** Published papers dealing with heat treatment of LPBFed aluminium alloys, classified by alloying system, updated to July 2020 (Source: Scopus database).

researchers have dealt with Al-Si alloys, due to their relative ease of production, availability, and growing industrial interest. As shown in Fig. 1, since 2014, a growing number of studies have addressed the heat treatment of LPBFed aluminium alloys. Most of these studies have focussed on alloys based on the Al–Si system, but an increasing variety of different compositions are now being considered. Even though previsions are difficult to make, it is reasonable to expect that interest in the present topic will not fade in the next years, and that greater efforts will be devoted to systems other than the Al-Si system due to their greater performance potential and increasing maturity in terms of the processing. Particularly, Al-Cu and Al-Zn-Mg alloys are likely to attract considerable interest with the hope of replicating the advantageous properties of the corresponding 2xxx and 7xxx wrought alloy series, respectively.

Since 2015, some papers have reviewed the scientific literature regarding the LPBF of aluminium alloys, both from a generic perspective [13–22] and with focus on specific issues such as aluminium matrix composites [23], process optimisation [24], alloy design [2], mechanical properties [25], and corrosion [26]. However, although heat treatments have been discussed in the abovementioned papers, no systematic effort has been directed towards comprehensively summarising and critically analysing the various heat treatment strategies and their effect on the alloy properties. On the contrary, such an effort has been undertaken regarding Ti alloys, resulting in a recent review by Teixeira et al. [27]. Considering this lack of a specific review, the present paper aims to review the scientific literature produced in the last few years (since 2011), which addresses the response of the studied LPBFed aluminium alloys to heat treatment. To provide a complete perspective on this, the noteworthy metallurgical characteristics of such alloys are briefly discussed. Then, the starting as-built microstructures are described, with particular focus on those features that may affect the subsequent behaviour during heat treatment. Finally, studies on the heat treatment of different alloying systems are discussed one at a time. These studies are grouped according to the type of applied heat treatment and the type of properties considered as output.

## 2. Precipitation in relevant aluminium alloys

This section briefly describes the physical metallurgy of the main alloy systems, whose responses to heat treatments will be examined later. Particularly, precipitation sequences are described and, whenever possible, the influence of specific initial conditions (e.g., supersaturation, presence of lattice defects, etc.) on the yield and kinetics of the precipitation process was discussed.

Precipitation hardening is induced by solid-state transformations, which is caused by a decrease in the solid solubility of one or more of the alloying elements with a decrease in temperature [28]. This enables the dissolution of the alloying elements during holding at elevated temperatures. After rapid quenching, the formation of an out-of-equilibrium SSSS is induced, which decomposes by diffusion upon holding at room (natural ageing) or elevated temperatures (artificial ageing), thus leading to the controlled formation of finely dispersed precipitates. The decomposition of the SSSS involves several intermediate steps, which minimise the required activation energy. First, small coherent clusters of solute atoms are usually formed, which in turn strengthen the alloy by elastically straining the surrounding matrix. Then, intermediate precipitates evolve, which are larger than the initial clusters and exhibit a definite, although varying, composition and crystal structure. Finally, a stable precipitate is formed, which is usually relatively bulkier and incoherent with respect to the matrix and is thus less effective in strengthening the alloy. Precipitation hardening is caused by three main mechanisms: lattice distortion, chemical hardening (i.e., resistance to shearing by dislocations), and dispersion hardening (i.e., Orowan strengthening) [29,30].

### 2.1. Al-Si-(Mg) system

Alloys based on the Al-Si system, which often contain Mg to achieve precipitation hardening, belong to families optimised for both casting (e.g., A357 – AlSi7Mg) and plastic deformation (i.e., the AA6000 series). The precipitation sequences of the two families are remarkably similar and are based on the face-centred cubic $Mg_2Si$ phase:

SSSS → Mg/Si atom clusters → GP zones → β" (coherent needles) → β' (semi-coherent rods/laths) → β (incoherent platelets)

The B' precipitate ($Al_3Mg_9Si_7$) has also been described as a possible phase. Several literature results have pointed out that the formation of solute clusters and GP zones is affected by the abundance of retained vacancies [31–34], which in turn may be influenced by the quenching rate and possible pre-aging treatment. In addition to the formation of $Mg_2Si$, thermal treatments may also induce the precipitation of dissolved Si [35,36], and/or a change in the morphology of the eutectic Si, as reported in [37,38]. This latter process has been reported to likely be caused by Si interdiffusion rather than by surface diffusion.

### 2.2. Al-Cu system

Several studies have been carried out on the precipitation sequence of Cu-containing alloys (e.g., those belonging to the AA2000 series), and the following main series, based on body-centred tetragonal $Al_2Cu$ phase, has been established:

SSSS → GP zones → θ" (coherent) → θ' (semi-coherent plates) → θ (incoherent)

A further sequence, based on the orthorhombic S ($Al_2CuMg$) phase, may be realised if Mg is present in the alloy according some definite proportions with respect to Cu [39]:

SSSS → GP zones → S" (fully coherent) → S' / S (incoherent).

The precipitation of the GP zones in both sequences is based on short-range diffusion and requires the presence of quenched-in vacancies, therefore being favoured if rapid quenching / solidification of the alloy takes place [40]. On the contrary, the intermediate precipitate θ', presenting a fluorite-type structure, is known to heterogeneously precipitate at dislocations [41,42], and a similar behaviour has been described for the S phase [43]. The formation of such phases, and therefore hardening, are thus boosted in conventionally produced alloys by plastic deformation. Finally, the equilibrium phase θ nucleates at the interface of the grown θ' precipitates or by the direct formation from the supersaturated α-Al matrix, preferentially at grain boundaries

[44]. The formation of other strengthening phases, such as Q ($Al_5Mg_8Cu_2Si_6$) or Ω (with composition close to $Al_2Cu$ but in the presence of Ag), is possible depending on the alloy's composition.

A particular case is represented by Al-Cu-Li alloys, which had been initially developed for obtaining precipitation hardening and later in the view of obtaining high-modulus and low-density alloys [45]. Upon ageing they are effectively strengthened by precipitates belonging to both the previously described θ and S sequences, and the ones based on δ' ($Al_3Li$, appearing as FCC coherent spheres) and $T_1$ ($Al_2CuLi$, characterized by plate shape and hexagonal crystal structure) precipitates, which are specific to Al-Cu-Li alloys. $T_1$ phase is known to precipitate heterogeneously on dislocations and grain boundaries.

### 2.3. Al-Zn-Mg system

The most important alloys based on the Al-Zn-Mg system are those belonging to the 7xxx series of wrought alloys; they are widely known for their excellent mechanical properties and good response to age hardening. The precipitation sequence of this system is based on the hexagonal $MgZn_2$ phase:

SSSS → GP zones → η' (semi-coherent disks) → η (incoherent)

Alternatively to the formation of GP zones, vacancy-solute clusters have been reported to play a role in early ageing stages [46]. The formation of an incoherent cubic T phase, with composition close to $Mg_3Zn_3Al_2$, may take place if ageing is performed at high temperature [47]. In addition, the presence of high dislocation density have been shown to suppress the formation of GP zones and clusters (presumably by annihilating vacancies), while simultaneously promoting the precipitation of η by providing nucleation sites [48].

### 2.4. Al-Mg-Sc-Zr

In recent years, the modification of Al-Mg alloys belonging to the 5xxx series by the addition of Sc and Zr has been extensively studied. The addition of Sc induces several benefits. For example, upon solidification, primary $Al_3Sc$ particles with an $L1_2$ crystal structure are formed, which act as heterogeneous nucleation sites owing to their low lattice misfit with respect to Al. This in turn reduces solidification cracking and induces general grain refinement. Moreover, secondary $Al_3Sc$ precipitates may also be formed upon ageing, thus improving the alloys' mechanical resistance. Such precipitates are coherent to the aluminium matrix, with a very low lattice misfit ($\delta = 1{,}33\ \%$). This coherency is maintained even after annealing at relatively high temperatures for prolonged time (e.g. 300 °c – 450 °C for 168 h): the theoretical value of the critical radius for coherent to semi-coherent transition of $Al_3Sc$ precipitates is 20 nm, but coherency is actually maintained by larger particles thanks mainly to the presence of Mg in the aluminium matrix [49]. Since Sc has a low solid solubility in aluminium matrix under equilibrium conditions (0,38 wt.% at 660 °C [50]), enormous efforts have been devoted to improve the solid solubility through rapid solidification [51,52], thus improving the precipitation strengthening. Therefore, this family of alloys are highly promising candidates for the LPBF process, considering that the high cooling rates typical of LPBF is expected to extend the solid solubility of Sc and may represent a further advantage if ageing treatments are to be applied [53,54]. Moreover, higher amounts of dissolved Sc have been shown to bolster the kinetics of the precipitation process, suggesting that an at least moderately faster precipitation could be expected in LPBFed alloys [51]. The addition of Zr to the alloy leads to the formation of $Al_3(Sc,Zr)$ precipitates, which exhibit high thermal stability [55] and a core-shell structure [56].

## 3. Microstructure of the as-built parts

In this section, the microstructural peculiarities, which are common among LPBFed aluminium alloys, are briefly discussed. Particularly, those aspects that may influence the heat treatment strategy or its outcome are emphasised.

The microstructure of LPBFed aluminium alloys under as-built conditions has been extensively described in literature. Owing to the nature of the process itself, the as-built parts appear intrinsically non-isotropic. As depicted in Fig. 2, along the building direction, usually labelled as z, the bulk parts consist of continuous stacking of solidified melt pools with a half-cylindrical shape. Conversely, such structures are observed in the xy plane (i.e., perpendicular to the building direction) as rounded or elongated stripes, thus clarifying the laser scanning strategy.

The anisotropic nature of the process is often reflected by the grain shape and size, too. As visible in Fig. 3 a, LPBFed Al-Si alloys are characterized by elongated grains (approximately 50 μm in length and 5-10 μm in width) pointing towards the centre of melt pools and displaying some degree of epitaxy, mainly at the centreline of the melt pools [58]. Moreover, smaller equiaxed grains are present along melt pool boundaries and are associated with locally faster cooling rates [59]. On the other hand, an example of a completely different grain structure is shown in Fig. 3 b: alloys containing some kind of in-situ or ex-situ inoculants ($TiB_2$, $Al_3Sc$, $LaB_6$, alumina or SiC nanoparticles etcetera) are indeed characterized by a fine distribution of equiaxed grains [60], showing little or no preferred orientation nor epitaxy with respect to underlying grains [61]. In fact, inoculant particles can stimulate the heterogeneous nucleation of new grains from the liquid melt, thus limiting grain growth and making the equiaxed microstructure more favourable.

At a lower scale, the morphology and size scale characterizing the microstructure of LPBFed aluminium alloys after solidification depend on the temperature gradient, G, and solidification rate, R, as shown in Fig. 4 [63,64]. The cooling rate is denoted as G*R and determines the size of the solidification structure, whereas the G/R ratio indicates the morphology of the solidifying front. The cooling rates experienced by the solidifying melt pool during the LPBF process have been reported to be of the order of $10^6$ K/s, which can be attributed to the reduced dimensions of the pool and the underlying bulk metal acting as a large heat sink [65]. In addition, the value of the G/R parameter is approximately 20 $Ks/mm^2$ for an AlSi10Mg alloy. Consequently, the high cooling rate and moderate temperature gradient are such that the solidification process of an aluminium alloy during LPBF lies at the boundary between the columnar dendritic and equiaxed dendritic dominions [66], as shown in the schematic in Fig. 4: in particular, a high cooling rate induces the formation of a very fine structure. Moreover, the solidification conditions may vary slightly from the lower boundary to the top of the melt pool. This is because the progressive lowering of the temperature gradient may induce a transition from the columnar to the equiaxed morphology. Liu et al. [67] numerically predicted and then experimentally demonstrated this transition in an AlSi10Mg alloy by means of EBSD analysis and similar effects were shown to be induced by varying process parameters in an Al-Mg-Sc-Zr alloy too [68].

Due to these solidification conditions, LPBFed aluminium alloys possesses very fine microstructure, often described as cellular, which may be markedly anisotropic. As shown in Fig. 5, Al-Si alloys are characterized by cells composed of an α-aluminium matrix and an almost-continuous fibrous eutectic silicon network. However, based on the solidification conditions, a coarser area is formed along the melt pool boundaries and a finer area is formed in the centre. Moreover, a heat-affected zone, which is induced by the heating cycles occurring during successive laser scans, is often visible [62]. Although less defined, similar structures are also formed in other as-built alloys: eutectic phases containing Cu, Mg, and Zn with a cell-like structure have been amply observed to be dispersed across the aluminium matrix [69–72]. The dimension and morphology of such eutectic cells depend on the process parameters, as recently observed in AlSi10Mg by Liu et al. [73]. ince the microstructure and, consequently, the mechanical behaviour of the alloys depends on process parameters, it is reasonable to expect that the same alloy, produced under varying conditions, may behave differently when subjected to heat treatments. In this respect,

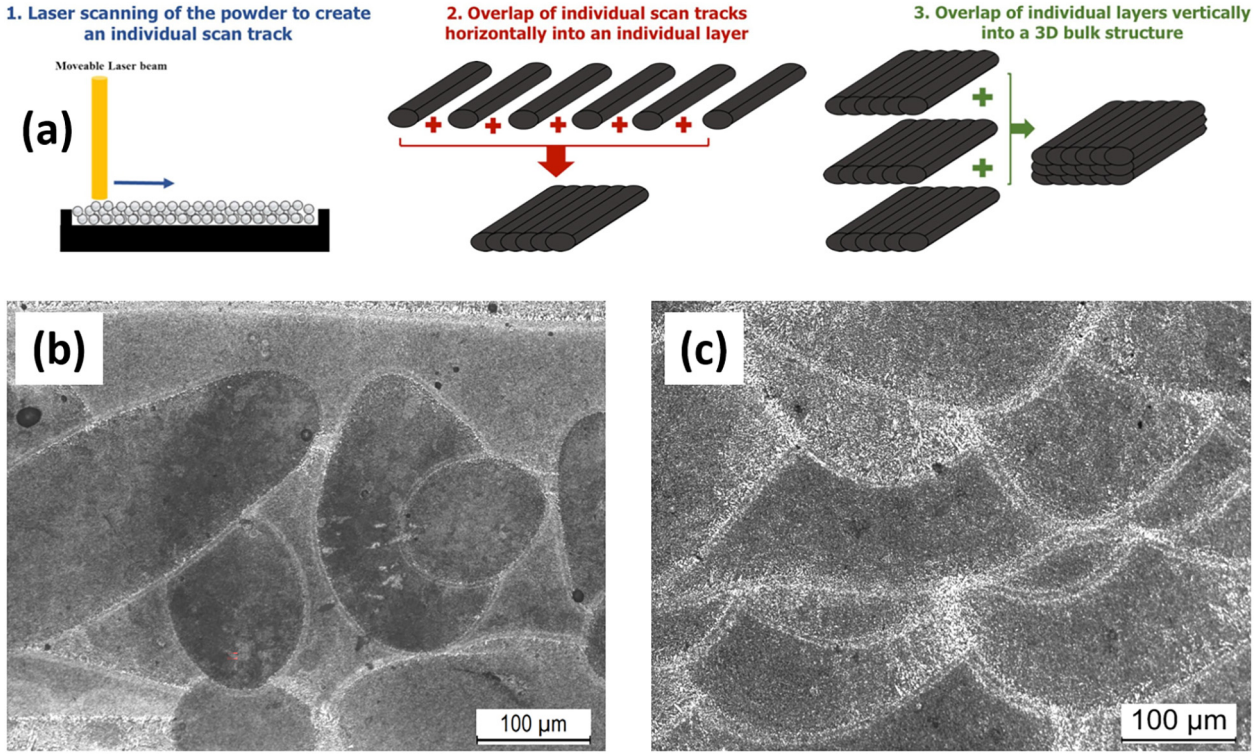


**Fig. 2.** (a) schematic depicting the overlapping of scan tracks and layers during the LPBF process; representative microstructure of an LPBFed AlSi10Mg alloy in the xy (b) and xz (c) planes. Reproduced from [20] (a) and [57] (b, c).

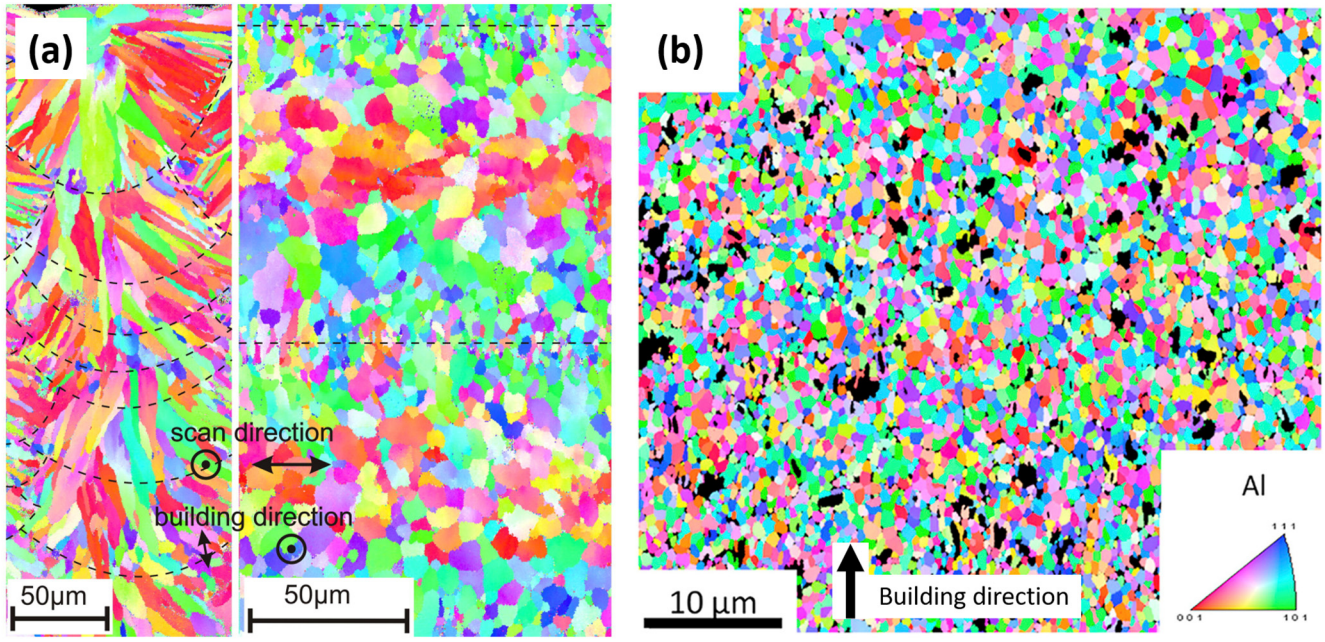


**Fig. 3.** EBSD orientation maps of LPBFed alloys: (a) AlSi10Mg alloy, showing both vertical and horizontal sections; (b) $TiB_2$-modified Al-Cu alloy, showing a vertical section. The different morphologies of grain distributions (columnar vs. equiaxed), deriving from different solidification conditions, can be appreciated. Reproduced from [62] (a) and [61] (b).

it would be interesting if the machine-learning assisted optimization process developed in [73] could be expanded and implemented in order to a priori identify a correct heat treatment procedure for LPBFed alloys. At a smaller scale (Fig. 5 b), the eutectic structure characteristic of Al–Si alloys consists of a fibrous network surrounding the α-aluminium cells and is often enriched in other solute elements which segregate during solidification, such as Mg, Fe, Cu or Sc [74]. This feature appears of paramount importance, since such segregated elements may not be readily available for diffusion and may thus prevent the full exploitation of the alloy's precipitation hardening potential during direct ageing

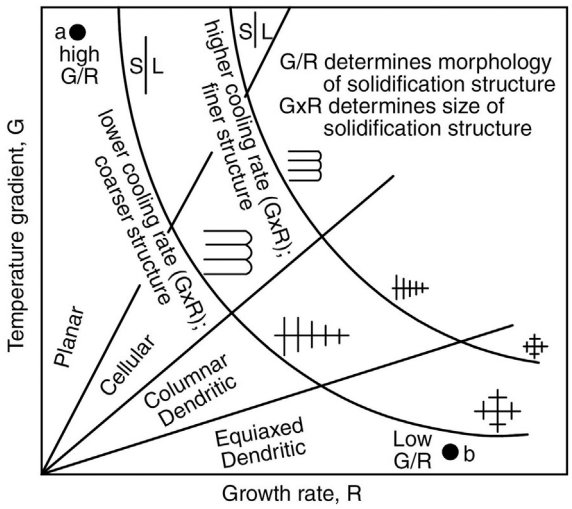


**Fig. 4.** influence of temperature gradient G and growth rate R on the morphology and size of solidification microstructure. Reproduced from [63].

treatments. In fact, the activation of some precipitation sequences (e.g. $Mg_2Si$ in Al-Si-Mg alloys) may be severely hindered. The inner α-aluminium cells in turn have been reported to contain nanometric solute clusters (Fig. 5 c), which play a fundamental role in enhancing the strength and strain hardening ability of the as-built alloy [75,76]. The presence of such a unique microstructure should be considered when designing the appropriate heat treatments. For example, in [77] the authors specifically designed heat treatments that can break or keep the Si network intact.

Another unique property of LPBFed aluminium alloys is the formation of SSSSs due to the high cooling rates experienced by the melt pools upon solidification. Marola et al. [78] studied an as-built AlSi10Mg alloy and computed the amount of Si dissolved in the FCC (face centred cubic) matrix by investigating the change in the lattice parameter of Al. They found that the dissolved Si concentration was approximately 4 %. In contrast, Rao et al. [79] attributed the Si supersaturation of up to 6 wt.% in AlSi7Mg to the presence of crystallographic-dependent strains, rather than directly to the fast cooling. For post-building heat treatments, the presence of such high amounts of dissolved solute in the matrix may allow to avoid solubilisation treatments and promotes direct precipitation upon ageing.

Residual stresses are a well-known problem that affects LPBFed parts [80]. They are caused by the hardening induced by fast cooling, as well as by the volumetric changes of the material during solidification; moreover, the layer-by-layer nature of the process further aggravates the problem [10,81]. These residual stresses influence heat treatment procedures in two ways: (i) they often need to be relieved to improve the fatigue resistance of the built parts [82]; and (ii) they

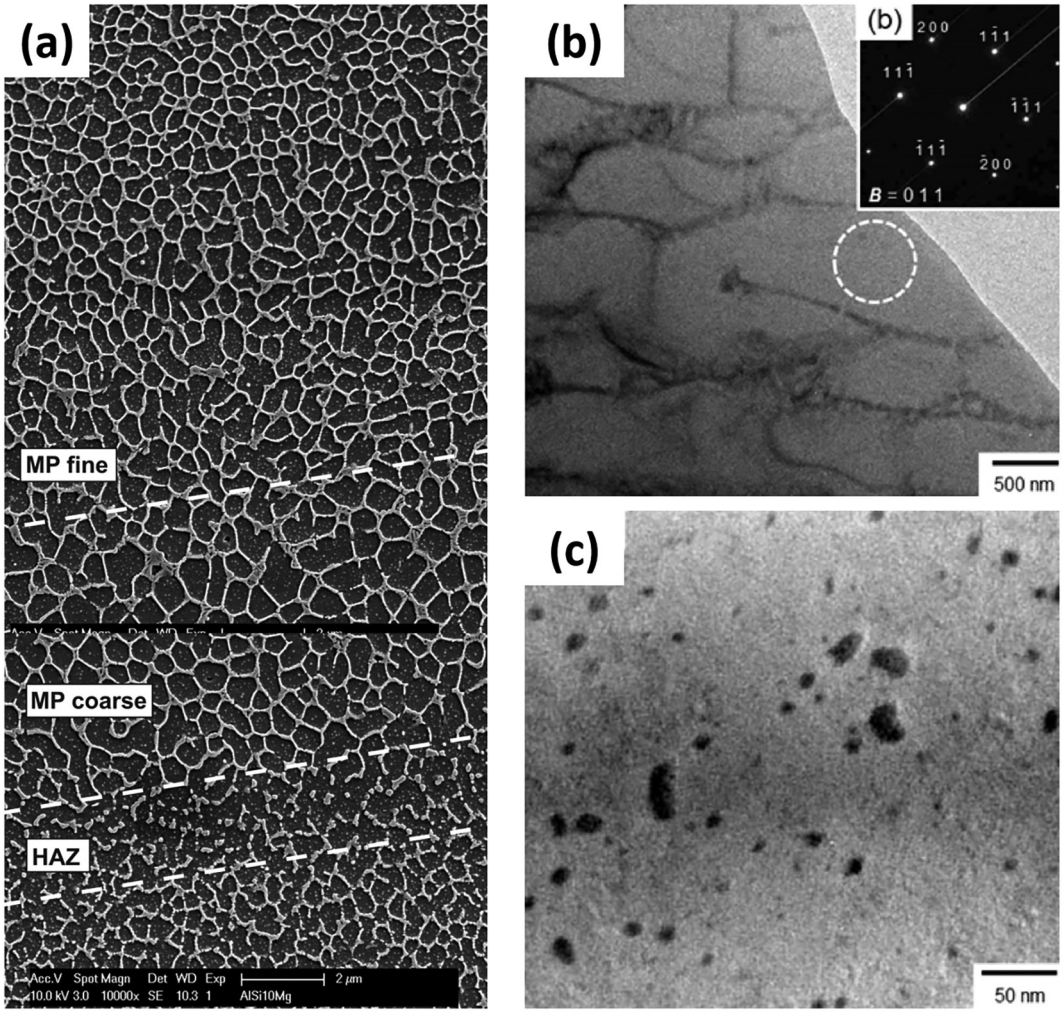


**Fig. 5.** SEM micrographs of an as-built AlSi10Mg sample, taken along xy plane and depicting fine area, coarse area and heat affected zone in a melt pool (a); TEM micrographs depicting Al-Si cellular structure (b) and Si nanoprecipitates inside Al cells (c) in an as-built AlSi10Mg alloy. Reproduced from [62] (a) and [76] (b, c).

may influence precipitation processes by altering the kinetics of atomic diffusion across the aluminium matrix [83,84].

It is also important to note that the solidified portion of an LPBFed part inevitably experiences further thermal cycles during the building of the remaining volume due to three distinct causes. First, the metallurgical cause lies in the recalescence phenomenon, that is the release of latent heat during the formation of a solid solution upon solidification, which is likely to cause local heating, and thus, precipitation [78,85]. Additionally, the repeated heating–cooling cycles induced by successive laser scans and the use of a preheated platform may induce precipitation or other thermally-induced phenomena across the solidified volume. In fact, the solidified material goes on experiencing successive heating and cooling cycles caused by the movement of the laser along tracks next to the solidified ones. As shown in Fig. 6 a, after melt tracks are first melted and solidified (first peak above melting temperature), the laser movement induces relatively low temperature oscillations during the scanning of the same powder layer; thereafter, when the following layer is scanned on top of the previous one, remelting occurs in the first layer ensuring proper metallurgical bonding (second peak above melting temperature). Therefore, while temperature peaks above melting temperature are important for the soundness of the LPBFed part, lower temperature peaks still play an important role in causing successive "in-situ" thermal treatments, which may partially trigger precipitation or other thermally induced phenomena. Moreover, the use of base-plate preheating causes a proper in-situ heat treatment of the built volume [86]: this feature may cause serious inhomogeneities across the built part due to the different exposures of the volumes at different heights to high temperatures, possibly inducing different levels of local age-hardening or even softening due to over-ageing (Fig. 6 b). In this light, the post-building precipitation treatments may be rendered less effective or even unnecessary by these features [79,87].

Finally, it is important to consider lattice defects, i.e. dislocations and vacancies, which may arise during the building process. As briefly discussed in Section 2, the presence and relative abundance of such features are of particular interest, since they may affect the kinetics of the precipitation processes. The presence of dislocation tangles in the as-built material is related to the relaxation of stresses induced by solidification and shrinkage. The presence of dislocation tangles has been reported by some studies on Si-based [89–91], Sc-containing [92], Cu- and Mg-containing [72] and Cu- and Li-containing [93] alloys. However, their abundance has been questioned in [94] and it has not been noted in other studies that have performed transmission electron microscopy based microstructural analysis of undeformed samples [76,95]. It should be noted that in [92], the authors reported the absence of dislocations in finer grains, and concluded that the process parameters including platform heating, if present, may influence the presence or absence of such defects; this may explain the different conclusions drawn by different authors. Vacancies are known to be readily trapped in rapidly solidified alloys [96,97] thus forming concentrations that may largely exceed those of the equilibrium alloys. Therefore, even though no detailed study on vacancy concentrations in LPBFed alloys could be found, it can be concluded that a similar condition holds for LPBFed alloys, provided that the repeated heating–cooling cycles do not considerably alter this original condition. For example, Rao et al. [94], assumed the presence of numerous quenched-in vacancies in an LPBFed AlSi7Mg alloy, and discussed their influence on the formation of precipitates belonging to the β series.

## 4. Heat treatment of LPBFed Al-Si-(Mg) alloys

As far as most of the initial research work on LPBF of aluminium alloys has dealt with Si containing ones, the search for proper heat treatments has also been mainly focussed on such alloys. Particularly, the majority of these studies have dealt with three alloys: the hypereutectic AlSi12 and the hypoeutectic, age-hardenable AlSi7Mg and AlSi10Mg alloys. Since the importance of the post-production heat treatment of LPBFed aluminium parts has been first recognised, considerable research efforts have been devoted to developing new annealing procedures that can improve the mechanical (strength, ductility, fatigue resistance) and functional properties (corrosion resistance, thermal, and electrical conductivity) of the alloys. Initially, two research trends emerged: first, traditional thermal treatments (e.g., T6) were adapted in terms of temperature and duration to improve the properties of LPBFed aluminium alloys; later, annealing treatments at different temperatures were trialled to understand the induced phase transformations. Consequently, direct ageing (T5) and tailored annealing treatments were developed, which consider the microstructural peculiarities of the LPBFed Al-Si alloys. Particularly, several studies have been carried out to describe the phase transformations taking place upon heating in Al-Si-Mg alloy by using differential scanning calorimetry (DSC). Understanding such transformations constitutes a fundamental step towards mastering the alloys' metallurgy and their response to heat treatments. The recorded thermograms, an example of which is shown in Fig. 7, are characterised by the presence of two exothermic peaks: peak A, lying at approximately 260 °C, and peak B at 320 °C [87,98,99]. The reason for the presence of these peaks has been widely discussed and justified in

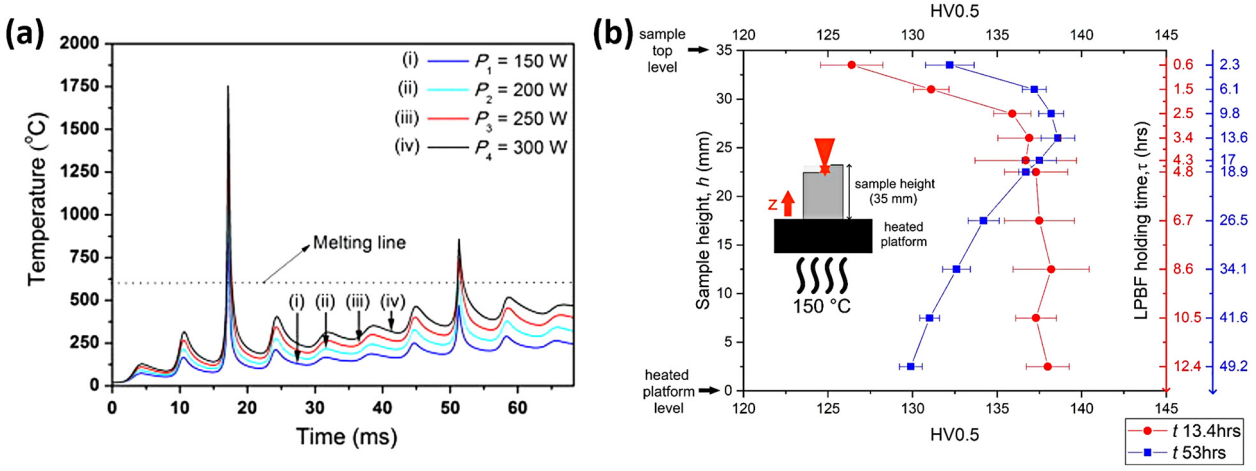


**Fig. 6.** Side-effects of laser scanning and base-plate preheating during LPBF processing of aluminium alloys: (a) Local variation of temperature during successive laser scans with the employment of different laser powers; (b) hardness trends induced by base-plate preheating along the height of massive ASi10Mg components produced by LPBF. Reproduced from [88] (a) and [86] (b).

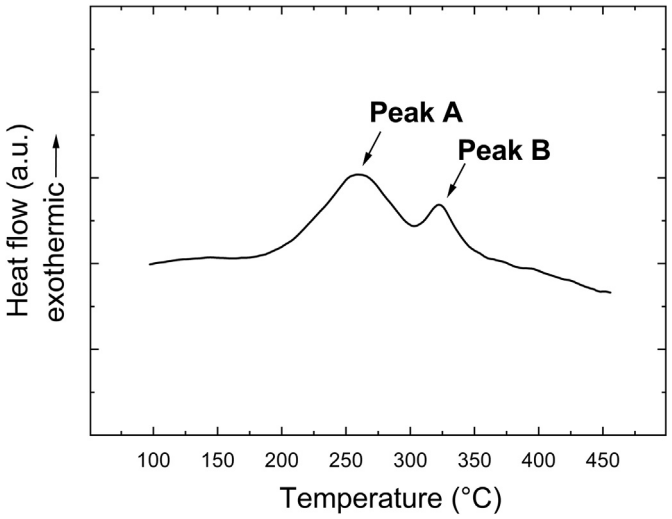


**Fig. 7.** typical DSC thermogram of an LPBFed AlSi10Mg alloy, in as-built condition. Elaborated from the authors' own data.

different ways, based on the interpretations of different authors. Fiocchi et al. [77,100] attributed peak A to the precipitation of the $Mg_2Si$ phase in its coherent β" form and peak B to the superposition of two effects (i.e., the precipitation of β' and the rupture and spheroidization of the Si network). This interpretation was later confirmed in other studies [101–103] based on the temperature position and computed activation energies. Particularly, peak A displays an activation energy in the 110 - 120 KJ/mol range, which is consistent with the values reported in [104] for $Mg_2Si$ precipitation, whereas a higher activation energy of 163 – 211 KJ/mol was observed to characterise peak B. These latter values are extremely close to those commonly reported for the diffusion of Si through an aluminium matrix [37,38,105,106]. Similarly, Yang et al. [107] attributed peak A to β" precipitation and peak B to β', suggesting that this second process causes the collapse of cellular Si walls. In contrast, based on their respective enthalpies, Marola et al. [78], attributed peak A to the precipitation of Si from the supersaturated aluminium matrix and peak B to the concurrent formation of $Mg_2Si$ and Fe-containing precipitates. Similar conclusions were drawn in [108] and were further supported by the fact that a single exothermic peak, between 196 °C and 299 °C, was observed in a binary Al-50Si alloy [109]. Girelli et al. [99] concluded that peak B cannot be definitively attributed to β' formation or Si diffusion as the peak displays features of both phenomena. Based on the reviewed experimental results, as well as on further discussion which will take place in the next sections, the authors of the present work believe that peak A should be attributed to Si precipitation from the supersaturated matrix and peak B to the superposition of two the effects, namely, $Mg_2Si$ formation and Si diffusion along the eutectic network. Regardless of the precise attribution of each peak, it is worth noting that the various papers agree on the presence of an exothermic phenomenon related to Si diffusion, which is made possible by the non-equilibrium state of the as-built material, which in turn is due to the solidification conditions characteristic of LPBF. Moreover, it has been reported that such precipitation processes are influenced in terms of intensity, temperature and activation energy by the processing parameters used during the LPBF process [87,110] and, accordingly, by the type of LPBF equipment employed [111]. Therefore, particular care should be taken to optimise the ad-hoc heat treatment procedures for LPBFed Al–Si alloys because parts made of the same alloy but produced with different LPBF systems or with different process parameters are likely to react differently.

The following sections will explore the results available in open literature on the heat treatment of Al-Si and Al-Si-Mg alloys produced by LPBF. Ideally, two different approaches would be needed to effectively describe and compare the collected papers: one is based on the type of applied heat treatment (T6, T5, and annealing at intermediate temperatures) and the second focusses on the property, which was studied as the output of the treatment itself (e.g., mechanical resistance, fatigue life, corrosion, etc. ). However, to avoid redundancy and excessive length, only the first approach will be discussed in the next sections. Particular attention will be devoted to the output properties, and due comparisons will be made to provide a general overview.

### 4.1. Solution and ageing treatment

The first step of this treatment is based on a high-temperature solution annealing. It aims at dissolving pre-existing precipitates and intermetallic phases and is followed by quenching, to produce an out-of-equilibrium SSSS. Subsequently, the SSSS is annealed at a relatively low temperature, usually in the range of 150–250 °C, thus leading to the formation of finely dispersed precipitates, which in turn strengthen the aluminium matrix. In particular, the commonly used T6 label refers to the maximum strength condition that is achieved during ageing. Since this type of treatment is commonly applied to Al-Si-Mg casting alloys, it has been extensively studied during the early development of LPBFed Al-Si-Mg alloys. As shown in Fig. 8, the appearance and characteristic dimension of the microstructure are heavily changed by solution and ageing treatment and, as a consequence mechanical and functional properties of the treated alloys are revolutionized too. Hence, the next

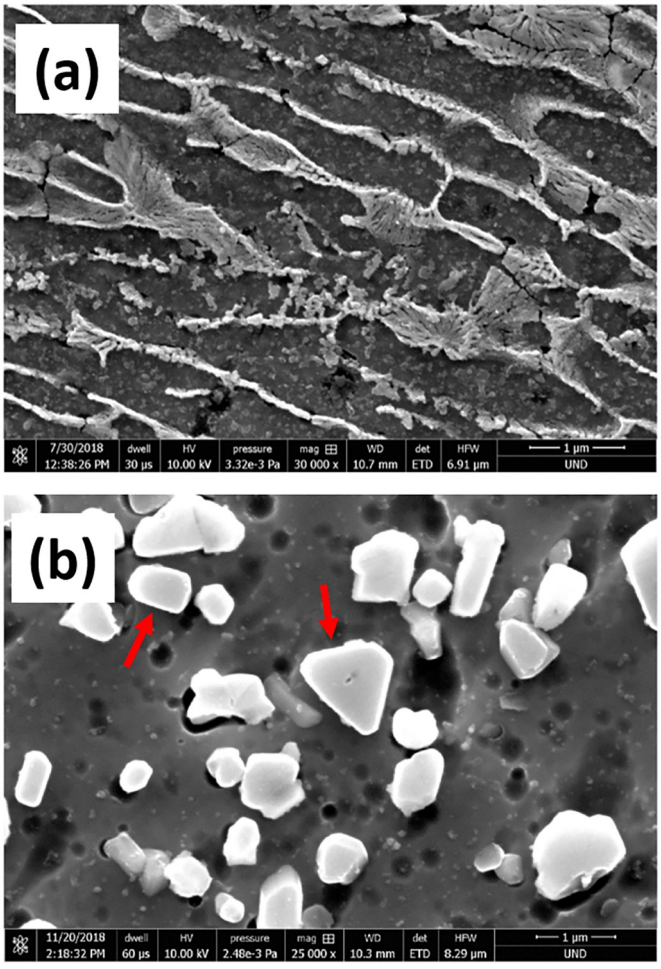


**Fig. 8.** SEM micrographs of as-built (a) and solution treated and quenched (b) LPBFed AlSi10Mg alloy. The disappearance of the eutectic network and the coarsening of Si particles after solution treatment can be appreciated. Reproduced from [112].

paragraphs will deal with these profound modifications and the correlations among them.

*4.1.1. Optimisation of the heat treatment procedure*

Several studies have been carried out to optimise the heat treatment of alloys and understand its influence on the mechanical and microstructural characteristics. The optimal combination of temperature and treatment time has been mainly searched for through a typical procedure based on ageing solution-treated samples at different temperatures for different times, to individuate the peak hardness in ageing curves.

Girelli et al. [113] performed solution treatments at 510 °C and 540 °C for 6 h, and found no significant difference in the resulting microstructure and hardness. However, they reported a marked decrease in density at 540 °C (-4.5 %) with respect to the as-built condition and attributed it to diffusion of dissolved hydrogen and the growth of gas porosities. Consequently, a superposition of T6 treatment and hot isostatic pressing was proposed in [114] by performing the T6 temperature cycle while holding at high pressure. In [115] different durations of solution treatment at 520 °C were trialled on an AlSi10Mg alloy: it was reported that the 1 h treatment was not sufficient to dissolve scan tracks, whereas the boundaries between successive layers became less definite after treatments lasting for 2 h or more. In addition, an increase in time facilitates Si diffusion, thus leading to particle growth, whose dimension got stable after 3, 4 h-long treatments. Furthermore, the quenching rate was also observed to have a significant effect on the mechanical properties [112,116]. To achieve satisfactory precipitation during successive ageing, LPBFed AlSi10Mg and AlSi7Mg alloys require higher quenching rates at the end of solution treatment. This can be attributed to the fine microstructure and shorter diffusion paths, which hindered achieving metastable supersaturation. Subsequently, age hardening was supposed to take place for short durations during ageing at 160 °C. This supposition was confirmed in an earlier work by Mertens et al. [117], which showed that ageing at 170 °C or 190 °C induced peak hardness in the initial 4 h, whereas much longer times, higher than 10 h, were needed at 150 °C. Regardless, it should be noted that this last condition (150 °C) enabled the highest hardening, even though the required times were deemed excessively long for effective application. Similarly, other works [103,108] have reported peak hardness after 4 h of ageing at 160 °C and almost no decrease in the hardness (overageing) after 24 h. Moreover, another interesting point was demonstrated in [103]: a 1 week natural ageing at room temperature before artificial ageing was detrimental for maximum hardness, since it reduced the number of sites available for β" nucleation.

Indeed, the reported treatment durations needed to achieve peak hardness are similar to those reported for conventionally produced AlSi7Mg [118] and AlSi10Mg [119] alloys at similar temperatures, which is consistent with the fact that the activation energies for $Mg_2Si$ precipitation were similar in LPBFed and conventional Al-Si-Mg alloys. In addition, a similar result was described through a direct LPBF – casting comparison in [99].

*4.1.2. Modification of the microstructure*

Solution heat treatment transforms the as-built microstructure of LPBFed Al-Si-Mg alloys through two concomitant and interdependent mechanisms, as clearly visible in Fig. 9, that shows the evolution of Si morphology and the concurrent reduction of the matrix supersaturation. The original eutectic fine fibrous network is completely cancelled and substituted by more or less uniformly distributed blocky particles, whose numerosity and dimension depend on the treatment temperature and duration [120,121]. First, Si atoms, which are dissolved in the as-built supersaturated matrix, are rejected and precipitate along the pre-existing cellular boundaries, which consequently become blurred [122,123]. Thereafter, fragmentation and spheroidization of the Si branches takes place, presumably by Al–Si interdiffusion, which is energetically favoured over surface self-diffusion [37,124]. An alternative mechanism was proposed in [125], wherein the fragmentation at the necking locations of the Si network is considered to be induced by cracks emerging during heat treatment as a consequence of the different thermal expansion coefficients displayed by Al and Si. The cracks would then be filled by an Al melt driven by capillary forces. Although fascinating, this explanation appears nebulous. For example, it is not clear why molten aluminium should be present at temperatures equal to or lower than 500 °C. Regardless of the specific mechanism, coarse independent Si particles are formed, which grow upon further annealing through the Ostwald ripening mechanism. Consequently, this induces a steep decrease in the matrix supersaturation (see Fig. 9 f). The decrease in the amount of Si present as solute in the α-Al matrix can be as high as 5.4 wt.% in an AlSi12 alloy, and mostly takes place in the initial 0.5 h of the solution treatment at temperatures equal to or higher than 500 °C [126]. Predictably, the change in Si morphology has been linked to a marked decrease in the electrical resistivity in solution-treated AlSi10Mg parts [127].

During solution heat treatment, less evident but equally important changes regarding the distribution of other elements and the formation and dissolution of precipitates also occur. The presence of nm-sized Si precipitates inside the α-Al matrix, which are typical of as-built samples, has been confirmed even after high-temperature solution treatment [128]. In addition, the formation of the needle-like monoclinic β-$Al_5FeSi$ phase has been widely reported upon solution treatment. In the as-built condition, Fe segregates at the cell and grain boundaries, eventually forming the π - $Al_8Si_6Mg_3Fe$ phase; during subsequent high-temperature holding it diffuses to form $Al_5FeSi$, which is considered to be embrittling and thus detrimental to the alloy's mechanical behaviour [128].

On the contrary, solution treatment has no significant effect on the grain size, although a slight growth of the small equiaxed grains at the melt pool boundaries has been reported [129], with the vast majority of the columnar grains remaining unchanged. Accordingly, the texture type and intensity are also not influenced by heat treatment. However, there is no full consensus regarding the effect of solution treatment on residual stresses. Maamoun et al. [130] reported the presence of tensile stresses in the 26.8–78.9 MPa range along the Z direction in both solution-treated and solution-treated + aged conditions. In contrast, a reduction in the residual stresses from –111 MPa (as-built condition) to –42 MPa (T6) was reported in [131]. A definitive understanding of the trend cannot be proposed in this study, since the first work presents an unusually low residual stress in the as-built condition, while the second work reports very high data. Further studies should be conducted to clarify this point.

When the considered alloys are subjected to artificial ageing after solution treatment and quenching, no major changes are induced in the microstructure at a large scale (i.e., in Si morphology and grain size). However, as expected, the precipitation of the reinforcing $Mg_2Si$ phase occurs. A similar precipitation sequence has been reported for the corresponding cast Al-Si-Mg alloy, but there are controversies on the exact order of precipitation, and whether the B' precipitate ($Al_3Mg_9Si_7$) should also be considered. A noteworthy work by Rao et al. [94] clearly showed that different precipitation pathways are possible, depending on the starting condition of the alloy. In addition, the authors found that, after short solution treatment (1 h at 535 °C), the peak-aged condition was characterised by numerous B' precipitates, whereas the presence of β" was almost negligible. However, an 8 h-long solution treatment reversed the previous situation, and largely increased the number of β" in the peak-aged condition. This can be attributed to the presence of higher number of vacancies, whose formation was aided by residual strains, and were retained in the samples subjected to shorter solution treatment, thus, speeding up the precipitation processes favouring the formation of B'. In contrast, Zhou et al. [128] detected the presence of GP zones and fine β" precipitates lying along the (100) directions in the peak hardness condition (solution treatment at 520 °C for 2 h, ageing at 160 °C for 10 h), as shown in the TEM images

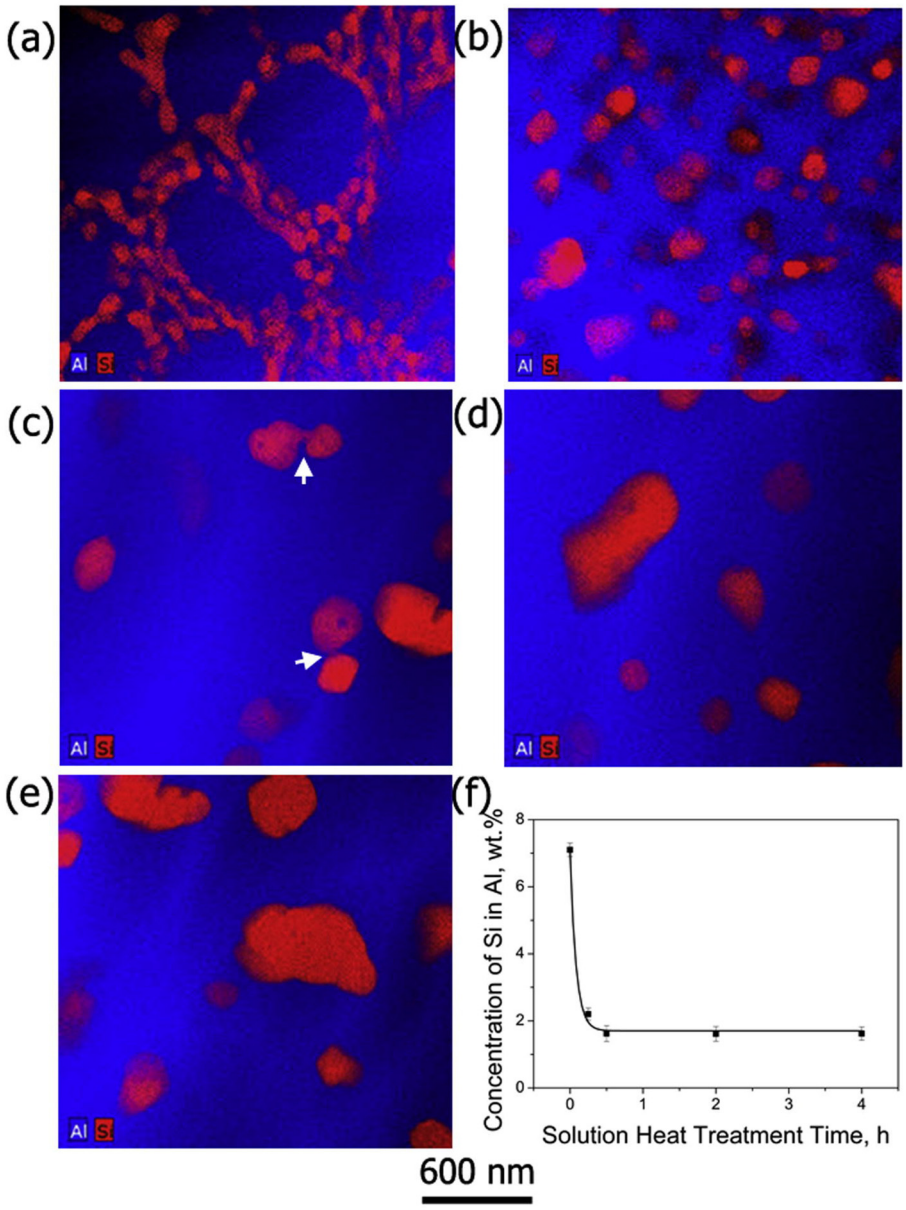


**Fig. 9.** STEM-EDX maps depicting the distribution of Al and Si in a LPBFed AlSi12 alloy in as-built condition (a) and after solution treatment at 500 °C for 15 min (b); 30 min (c); 2 h (d); and 4 h (e); progressive reduction of the concentration of dissolved Si in Al for increasing solution heat treatment times (f). Reproduced from [126].

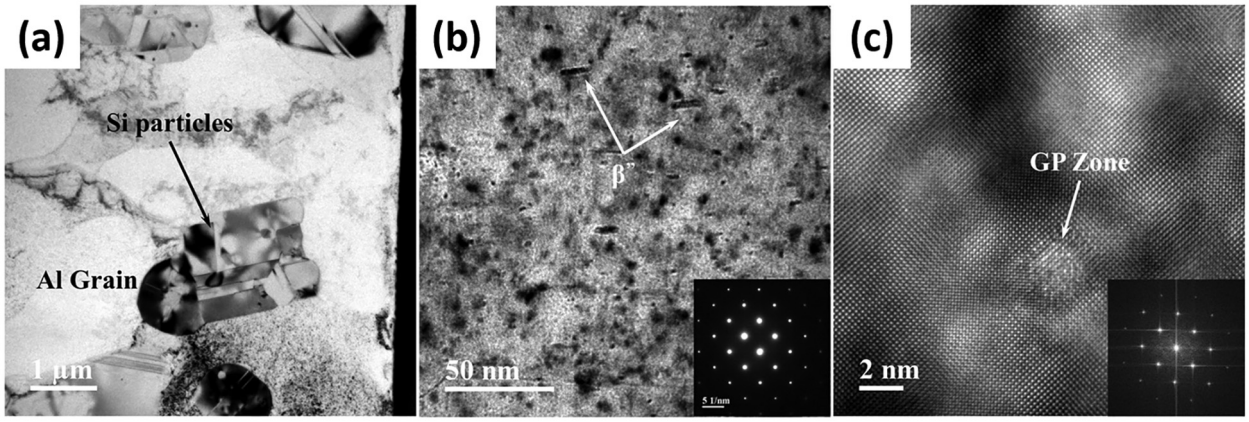


**Fig. 10.** TEM micrographs of an LPBFed AlSi10Mg alloy in T6 condition: low magnification general view (a); micrograph of GP zones and β″ precipitates on Al [001] crystal plane (b); HRTEM of a GP zone (c). Reproduced from [128].

in Fig. 10. β", although coarsened, was also shown to be present in over-aged conditions (24 h at 160 °C), whereas no sign of β' or β was observed. These discrepancies indicate a call for caution when discussing the possible precipitation sequences. Different heat treatment procedures as well as different manufacturing conditions may radically alter the final outcome, thereby increasing the difficulties inherent to the already complex recognition of precipitates in aluminium alloys.

*4.1.3. Evolution of the mechanical properties*

The evolution of the mechanical properties during solution treatment strictly depends on the microstructural changes. All the reviewed papers reported a decrease in strength after solution treatment, which becomes more intense with an increase in the temperature or duration of the treatment (Fig. 11). Conversely, ductility is constantly improved [132,133]. In addition, a reasonably stable plateau is reached for both strength and elongation to failure at temperatures exceeding 500 °C ($R_m = 214$ MPa, $e_f = 23.5$ % in AlSi10Mg, [122]) or durations higher than 30 min at 500 °C ( $R_m = 190$ MPa, $e_f = 25$ % in AlSi12, [126]). These modifications of mechanical behaviour follow quite immediately from the progressive reduction of α-Al matrix supersaturation, rupture of the Si network and continuous growth of relatively coarse Si particles. In this respect, it shall nevertheless be noted that a peculiar case has been reported regarding a TiN-AlSi10Mg nanocomposite [134]: in fact a continuous increase in mechanical resistance was induced by raising solution treatment temperature from 460 °C to 540 °C because of the formation of Fe- and Ti-bearing intermetallics. After solution treatment, precipitation hardening upon ageing is expected to increase the hardness and, accordingly, the tensile resistance. In [128] the hardening contribution of $Mg_2Si$ was computed according to the Orowan strengthening mechanism. Based on the TEM observations of the samples aged for different times, a strength increase of 159 MPa at 10 h and 136 MPa at 24 h ageing was computed. These values were consistent with the experimental data and also correctly described the overageing phenomenon.

It has been widely demonstrated that the original resistance of the as-built condition cannot be fully restored [135,136], as may be appreciated by comparing the values reviewed in Table 1. Some early studies reported an overall improvement in the mechanical properties (both strength and ductility) of T6 treated parts compared to the as-built ones, but this unexpected result can be readily attributed to the very poor integrity of the samples built during initial trials [137]. The usual reduction in the mechanical resistance may be very well justified by considering that after solution treatment an important component of strengthening fails. As reported in [138], in the as-built condition, multiple Orowan loops are formed upon plastic deformation by dislocation gliding through cell boundaries, thus highly strengthening the alloy. Moreover, this mechanism induces the continuous production of a large number of dislocations, which increases the alloy's strain-hardening ability. To partially compensate the above-described strength loss, solution and ageing treatments can be used to considerably increase the material's ductility, which may easily overcome the typical values of corresponding cast alloys, although some limited data contradicting such a claim exist, as shown in Table 1. Moreover, another advantageous side effect of solution and ageing treatment is the homogenisation induced by the treatment itself: the complete modification of Si morphology and the solubilisation and re-precipitation of alloying

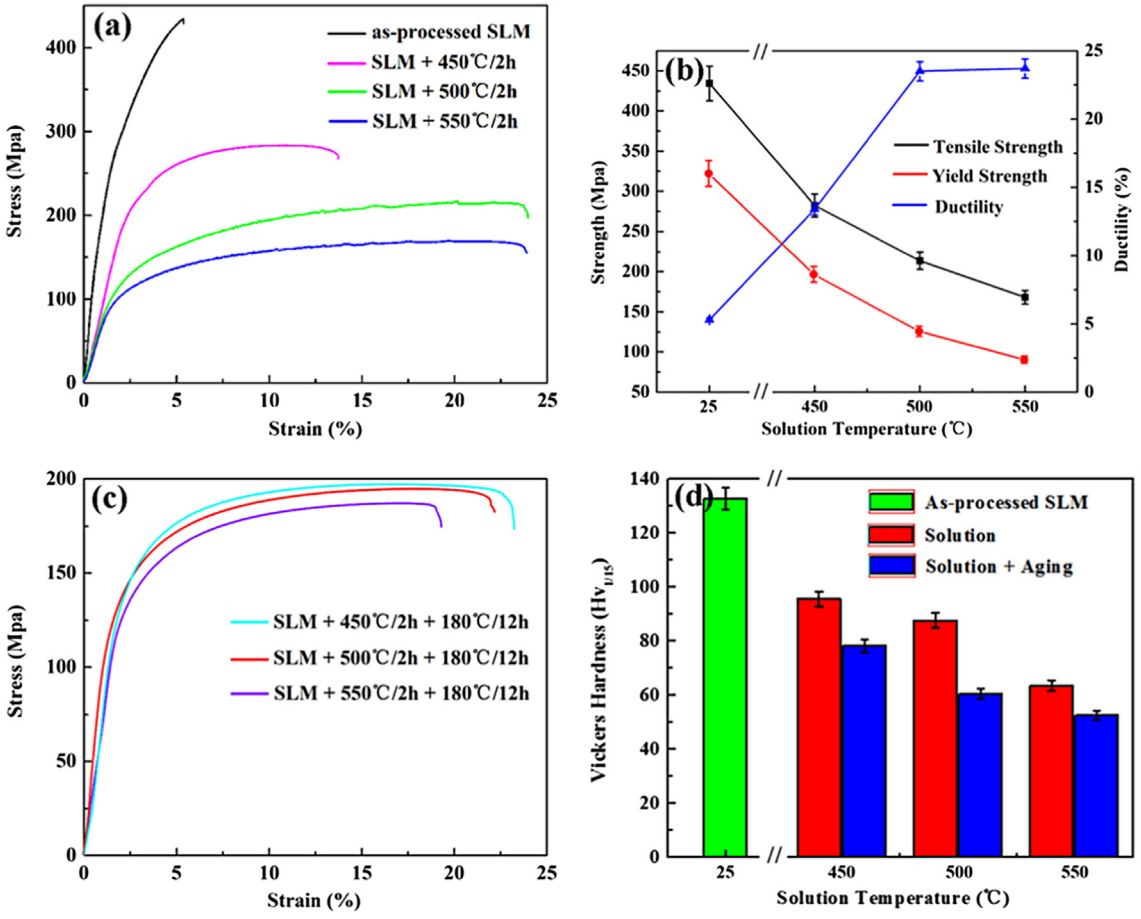


**Fig. 11.** tensile curves of solution treated AlSi10Mg samples (a) and corresponding mechanical properties (b); tensile curves of solution treated and peak aged AlSi10Mg samples (c); Vickers hardness of samples subjected to different heat treatments (d). Reproduced from [122]

**Table 1**
Mechanical properties, evaluated through tensile tests, of LPBFed Al-Si alloys in as-built and T6 conditions.

| Alloy | Reference | Thermal treatment | Sy (MPa) | UTS (MPa) | Ef (%) |
|---|---|---|---|---|---|
| AlSi10Mg | [99] | As-built | 264 | 452 | 8,6 |
| | | 540 °C – 1h, 180 °C – 2h | 277 | 332 | 5,8 |
| AlSi10Mg | [102] | As-built | 226 | 429 | 4 |
| | | 550 °C – 2h, 180 °C – 2h | 270 | 321 | 9 |
| AlSi7Mg | [103] | As-built | 257 | 398 | 7,6 |
| | | 540 °C – 1h, 160 °C – 4h | 256 | 306 | 4,7 |
| AlSi10Mg | [108] | As-built | 275 | 406 | 3,8 |
| | | 540 °C – 1h, 160 °C – 8h | 236 | 288 | 9,3 |
| AlSi10Mg | [131] | As-built | 270 | 446 | 8,1 |
| | | 535 °C – 1 h, 190 °C – 10 h | 164 | 214 | 11 |
| AlSi10Mg | [146] | As-built | 360 | 307 | 1,7 |
| | | 540 – 1 h, 160 °C – 6 h | 290 | 267 | 2,5 |

elements has been reported to cancel property gradients (e.g., hardness variations due to differential precipitation), which are often found in as-built samples, when varying the distance from the building plate [139–141]. The final fracture mode has also been reported to depend on the applied heat treatment. In [142], the authors demonstrated that the fracture of as-built samples occurred along the interfaces between the melt pool boundary and core, whereas, after T6 treatment, cracks nucleated at the Si particles by decohesion and then propagated freely inside the Al matrix. The application of T6 treatment was found to be especially useful for aluminium lattice structures [143].In fact, in [144], they observed that the compressive behaviour radically changed after solution treatment and ageing, as the initial spiky and irregular appearance was substituted by a smooth plateau, which increased the absorbed energy from approximately 0.14 MJ/m$^3$ (as-built) to approximately 0.35 MJ/m$^3$ for the solution-treated samples and to 0.2 MJ/m$^3$ after further ageing at 250 °C. This improved behaviour may be explained by considering the microstructural evolution reported in [145], wherein the solution treatment was found to remove residual stresses and cancel microstructural differences between the upwards and downwards parts of each strut. These modifications are likely to enhance the smoother mechanical behaviour of the entire structure.

A relevant number of studies have also dealt with the influence of heat treatment on fatigue resistance, which indeed constitutes a critical characteristic of LPBFed parts, since the unavoidable presence of pores and defects may adversely affect the components' behaviour. Therefore, before discussing the influence of T6 treatment on the fatigue life, it is important to consider the possibility of an influence of heat treatment on porosity, and hence relative density of LPBFed Al-Si parts. It should be noted that no full consensus regarding this issue is present in the available literature. Some very detailed studies, performed employing X-ray computed tomography, concluded that thermal treatments, even at high temperatures (e.g., solution treatment at 520 °C for 2 h), had no effect on the location, dimension, numerosity, or shape of pre-existing defects [147,148]. Similarly, Larrosa et al. [149] found only minor density variations upon heat treatment and argued that no definitive conclusion could be drawn. In contrast, Girelli et al. [113] reported that a 5% reduction in relative density of LPBFed AlSi10Mg parts was caused by the solution treatment. This variation was ascribed to the formation of new pores. The authors argued that H atoms, which might be trapped inside the metal matrix during solidification, diffused upon heating, thus recombining into a molecular form and giving rise to new gas porosities. This problem may eventually be worsened by the absorption of humidity by the powders during storage and handling and, accordingly, Yang et al. demonstrated that this phenomenon could be limited by pre-drying powders before the manufacturing process [150]. Finally, two works by Majeed et al. [151,152] reported that solution treatment and artificial ageing lowered the relative densities of thick LPBFed parts (from 2.5 mm to 5 mm), whereas it improved the densities of thinner parts (from 0.5 mm to 2 mm). Indeed, the reported differences do not appear large and the proposed explanation, based on microstructural modification and precipitation during heat treatment, seems unclear at best. Most of the reviewed papers on the effect of T6 treatment on the fatigue life of LPBFed parts reported an improvement in the fatigue resistance induced by T6 treatment [153], as demonstrated by the results reported in Fig. 12. Maskery et al. reported that the fatigue strength increased from 85 MPa to 134 MPa owing to solution treatment and ageing [154,155], which is also similar, although translated to lower values, to what was reported in [156]. In addition, higher fatigue strength values (175 MPa and 200 MPa, depending on the amount of defects) were reported in [157]. It should be noted that this value is much higher (almost double) than that displayed by the corresponding cast alloy subjected to T6 treatment [158]. Bagherifard et al. [159] observed an improvement in the fatigue resistance in T6 treated samples despite the reported increase in porosity, and attributed this to a number of factors such as ductility increase, reduction of residual stresses, and microstructural homogenisation, which effectively balanced and outmatched the reduced strength and higher porosity. Lesperance et al. [160] found out that their own data, regarding T6-treated AlSi10Mg specimens, were in better agreement with literature data referring to as-built samples than with the ones regarding heat-treated parts: this point certainly indicates that a better understanding of the influence of microstructure on fatigue phenomena is due. In [161] a detailed analysis of crack growth mechanisms in both as-built and T6 AlSi10Mg samples was conducted, and two main features were highlighted. First, in the T6 samples, the crack propagated through the tough α-Al matrix, occasionally fracturing the spheroidal Si particles (and thus consuming energy); second, compressive residual stresses were generated after heat treatment, thus, favouring fatigue resistance. To the best of our knowledge, only one study reported a definite reduction in the fatigue resistance after a T6 treatment [162], which was ascribed to a reduction in the mechanical resistance.

#### 4.1.4. Modification of the corrosion behaviour

It is reasonable to expect that, as a consequence of the deep microstructural modifications induced by solution treatment and ageing, the corrosion behaviour of LPBFed Al-Si alloys would be modified too. Anyway, such topic has not currently attracted much attention and a limited number of works have dealt with it. In fact, greater efforts have been spent in studying the effect on corrosion behaviour of intermediate temperature annealing treatments, which will be specifically discussed at the end of Section 4.3.

Given that Al and Si present different corrosion potentials, in as-built condition the α-aluminium and continuous Si network act as a large anode and small cathode, respectively [163]. This allows the quick formation of compact films which inhibit further corrosion; moreover, the quasi-continous Si network imedes direct contact between the aluminium matrix and the electrolyte. After solution treatment, two effects are induced: Si forms large and randomly scattered cathodic particles and, concurrently, the aluminium matrix rejects dissolved Si atoms, thus increasing its activity as anode [164]. As a consequence, corrosion is accelerated and may induce large and interconnected pits in the vicinity of coarse Si particles [165]. This behaviour has been experimentally verified in both $HNO_3$ [166] and NaCl solutions. Quite logically, it has also been shown that a progressive increase of solution treatment temperature, causing greater Si rejection from the matrix and giving rise to larger Si particles, corresponds to a continuous increase in mass loss rate or corrosion current density and to a decrease of the corrosion potential, as shown in Fig. 13.

### 4.2. Direct ageing treatment

Studies on direct ageing treatment are relatively rare compared to those on T6 or intermediate annealing. T5 treatment, which properly

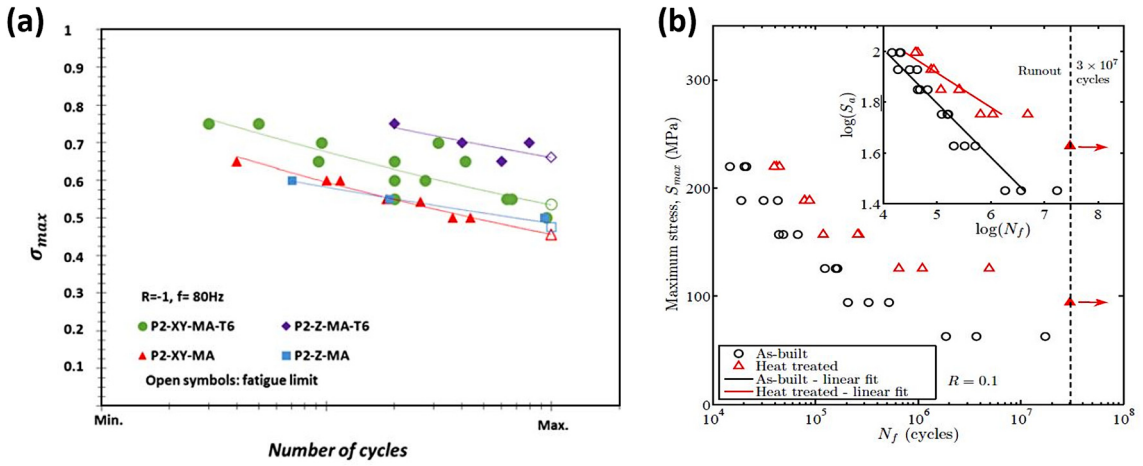


**Fig. 12.** S-N curves of as-built and T6-treated samples, showing the improvement inf fatigue resistance induced by solution treatment and ageing in both horizontally and vertically built samples. Reproduced from [153] (a) and [154] (b).

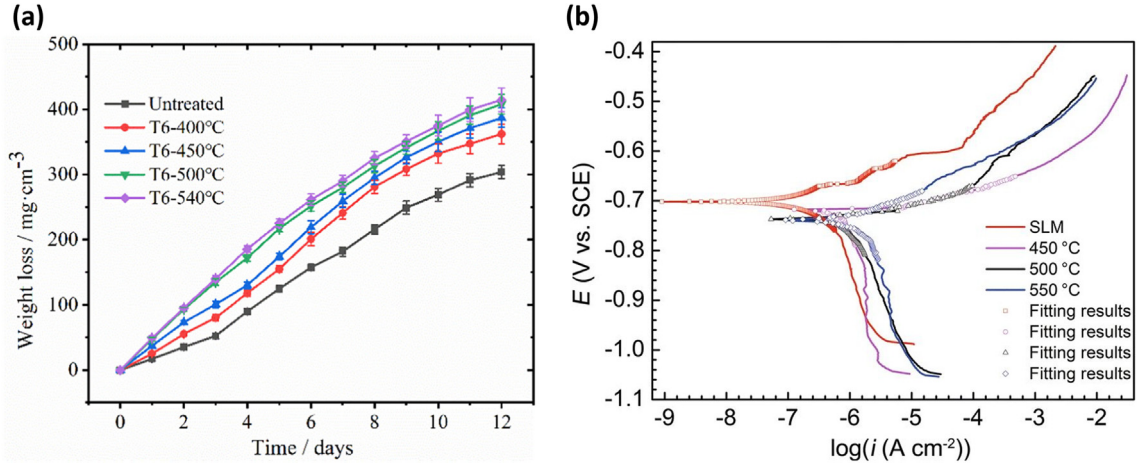


**Fig. 13.** Influence of solution treatment temperature on the corrosion rate of LPBFed AlSi10Mg alloy: (a) mass loss vs. immersion time in 1 M $HNO_3$ solution of T6 treated samples; (b) potentiodynamic polarization curves in 3,5 % NaCl solution of solution treated samples. Reproduced from [166] (a) and [167] (b).

refers to the maximum hardness condition, is based on direct annealing at relatively low temperatures to strengthen the alloy through precipitation hardening. Therefore, this treatment does not entail a previous solution treatment step. The interest for T5 treatment of LPBFed Al-Si alloys is mainly driven by two considerations arising from the experience gained from T6 treatment. First, an abrupt strength loss has been reported to occur due to the spheroidization and coarsening of the eutectic Si phase; second, it has been widely reported that the as-built α-Al matrix displays a high degree of supersaturation by alloying elements and such supersaturation is markedly lowered by solution treatment. Therefore, the absence of the initial high-temperature solution treatment can be expected to yield considerable advantages by retaining the original Si morphology and simultaneously allowing successive precipitation by exploiting the matrix supersaturation induced by the rapid cooling of the LPBF process. Following the same pattern used in the discussion of T6 treatment, the next sections will describe the available results concerning the optimisation of T5 treatment and its effects on the microstructure and mechanical behaviour of LPBFed Al-Si alloys.

*4.2.1. Optimisation of the heat treatment procedure*

Detailed studies have been performed to determine the appropriate heat treatment procedures to achieve maximum hardness using the T5 treatment. Since the T5 treatment is a single step treatment, the set of variable parameters is rather limited and consists of treatment temperature and duration. In [168] direct ageing tests were performed at temperatures in the 120–180 °C range, and the results are shown in Fig. 14. As expected, the hardening process was faster at higher temperatures: peak hardness was reached after 0.5 h at 180 °C, 5 h at 160 °C, 6.5 h at 140 °C; and ageing at 120 °C gave rise to a prolonged and shallow plateau with no definite peak up to 22 h. Except for the last case, overageing and consequent hardness decrease were reported at all temperatures. A similar time to peak hardness was reported in [100] (1.5 h at 170 °C) and in [103] (4 h at 160 °C). Several papers have emphasised that the response of the alloy to direct ageing may strongly depend on the manufacturing conditions. Particularly, Aversa et al. [169] demonstrated that it may be impossible to exploit the alloy's full hardening potential if platform heating is employed during production. An increase in the platform temperature decreases the maximum achievable hardness and the required annealing time. Similarly, in [87] it was demonstrated that samples built at 160 °C underwent only slight softening during ageing at 160 °C, presumably due to stress relaxation and/or overageing. Finally, the effectiveness of T5 treatment was demonstrated to be reduced by delay (i.e., natural ageing) between parts production and heat treatment, in a similar manner to that of T6 treatment [103],

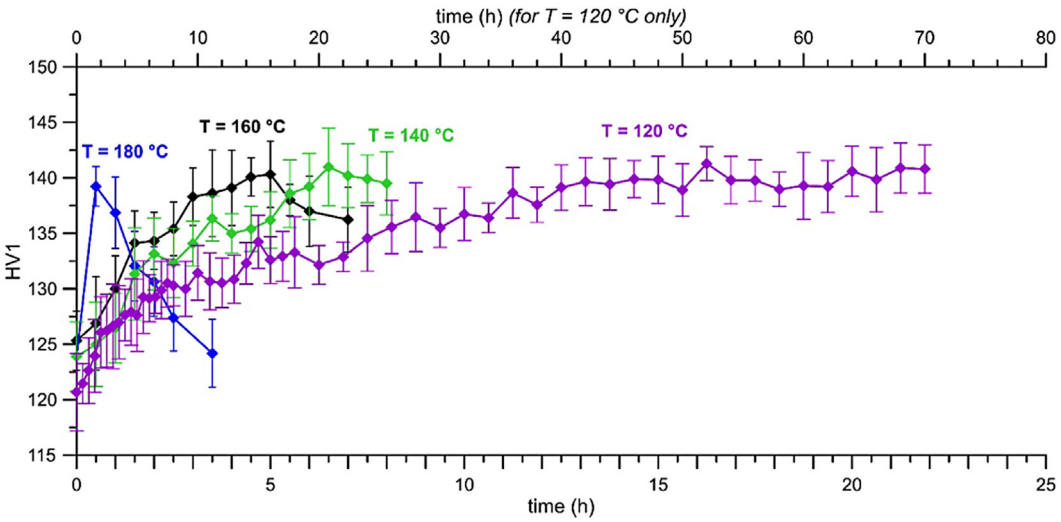


**Fig. 14.** Ageing curves of LPBFed AlSi10Mg alloy upon holding at 120 °C, 140 °C, 160 °C and 180 °C. Reproduced from [168].

which is likely due to the reduction of Si concentration in the matrix [170]. Essentially, all those conditions, which are prone to reduce the supersaturation of the aluminium matrix before the ageing treatment, have to be avoided in order to maximize the effectiveness of direct ageing treatments.

*4.2.2. Evolution of the microstructure*

The most prominent microstructural feature of directly aged Al–Si parts, which may be noticed at first glance, is the persistence of the eutectic Si network. Various papers [98] have reported that the modification of the original as-built microstructure is insignificant on a large

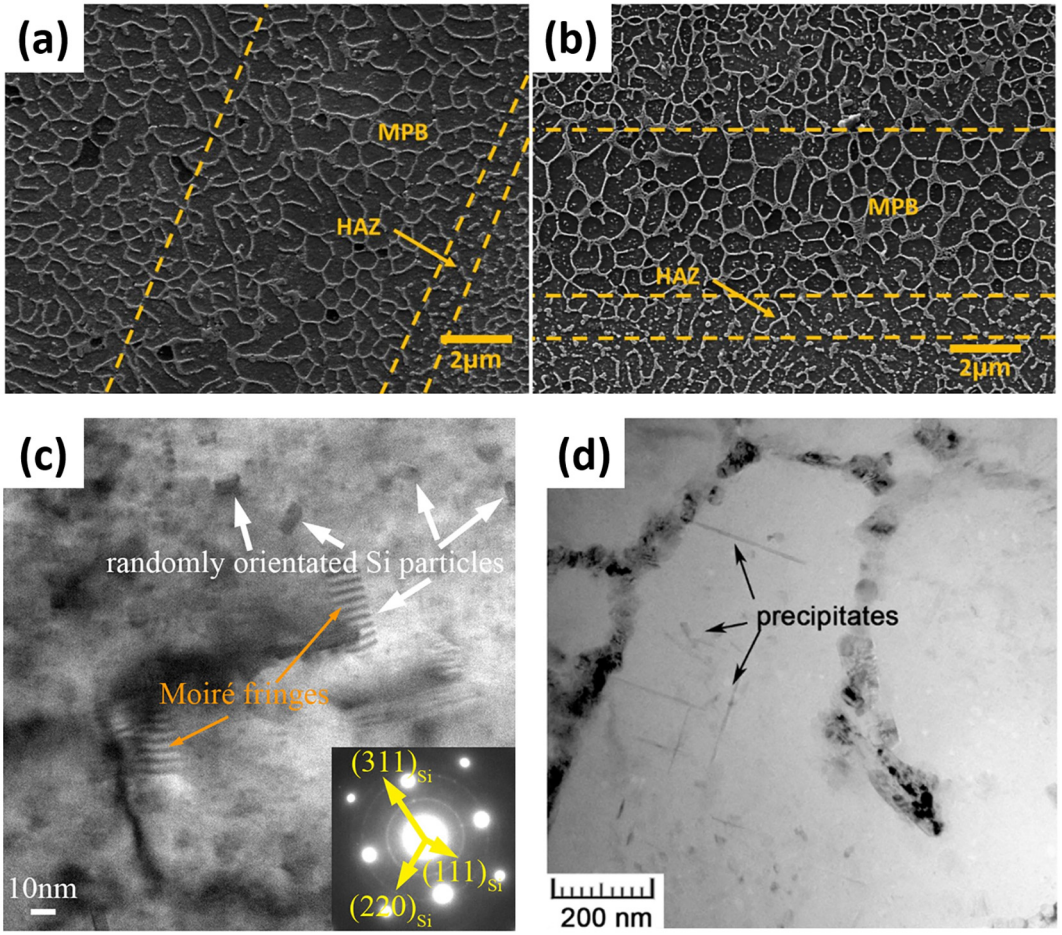


**Fig. 15.** SEM micrographs of an LPBFed AlSi10Mg alloy in as-built (a) and T5 (b) conditions; TEM image of randomly oriented Si precipitates in an LPBFed AlSi7Mg alloy in T5 condition (c); TEM micrograph of rod-like Si precipitates in an LPBFed AlSi10Mg alloy in T5 condition (d). Reproduced from [171] (a,b), [94] (c) and [168] (d).

scale, as clearly visible by comparing Fig. 15 a and b. The differences among the melt pool interior, boundary, and heat-affected zone are retained as well. This can be attributed to the fact that ageing is carried out in a temperature range, which is largely below the temperature related to Si diffusion effects, as suggested by calorimetric studies (see section 4). This was also confirmed in [100], where the authors reported that the enthalpy of the supposedly Si-related peak remained constant for all times during ageing at 170 °C. Similarly, no changes in grain size and texture were observed after ageing at 160 °C for 8 h [129]. The lack of abrupt changes at large scale was shown to be such that the corrosion behaviour of the as-built and T5 samples is extremely similar [171]. At a finer scale, the induced hardening must logically be related to the precipitation of some type of strengthening phase. Although several studies have attributed the improvement of the mechanical resistance to the formation of precipitates belonging to the β ($Mg_2Si$) series [100,103], no direct observation of such particles in directly aged samples has been reported in open literature. In fact, two works described the formation of Mg-free Si precipitates, assuming the form of either (partially) randomly oriented particles (10 nm – 20 nm in size) [94] or acicular needles lying along definite crystallographic orientations (5 nm thick and up to 200 nm long) [168], as depicted in Fig. 15 c, d. Both papers justify the formation of Si precipitates rather than $Mg_2Si$ in the same way. The extremely high Si supersaturation in the as-built state is believed to provide a considerable driving force that allows faster diffusion of Si rather than of Mg. Moreover, Mg has been reported to segregate at cell boundaries in as-built samples, thus further reducing the reservoir of atoms available for precipitation. Accordingly, TEM analyses of in-situ heated AlSi10Mg samples showed the presence of coherent Si precipitates/clusters [172]: their surface was characterized by the presence of segregated Mg atoms but the particles remained far from the stoichiometric β composition. In addition, direct ageing has no significant effect on the grain size and orientation [129]. Finally, residual stresses are considerably reduced but not cancelled by direct ageing. In [100] annealing at 170 °C for 1.5 h induced 48% and 24% reductions of principal stresses along the in-plane and vertical directions, respectively.

#### 4.2.3. Modification of the mechanical properties

Direct ageing has been reported to slightly improve the mechanical behaviour of LPBFed Al–Si alloys, even though the deviation between the as-built and T5 properties is not comparable to that induced by ageing in solution-treated parts. Nevertheless, T5 samples have been unanimously recognised to display the highest mechanical resistance among the various tested heat treatments. This feature may be appreciated by comparing the values reported in Table 2. The increase in the yield strength and ultimate tensile strength of T5 treated alloys has been attributed to precipitation, either of Si nanoparticles or the $Mg_2Si$ phase, which has been reported to balance the expected strength loss caused by the concurrent reduction of matrix supersaturation [87]. Strain hardening is believed to play similar roles in the as-built and T5 parts, since the complete recovery of dislocations is rather unlikely at typical ageing temperatures [129], as confirmed by the fact that residual stresses could not be completely recovered either. Although no specific studies exist, the comparison between the shapes of the as-built and T5 stress-strain curves indicates that the strain hardening rate is also similar under both conditions. Concurrently, ductility remains more or less similar to that displayed by as-built samples in the peak-hardness condition and is slightly reduced after prolonged ageing (overageing) [100]. In addition, due to the partial reduction of residual stresses, the damping ability of the LPBFed AlSi10Mg alloy decreased by 14% after direct ageing at 170 °C [173]. It is remarkable that direct ageing, although unable to completely homogenise the microstructure of LPBFed Al-Si parts, was found to be sufficient in inducing a reasonable homogeneity in parts built at various distances from the building platform, at least in terms of hardness [139]. Finally, with respect to crack propagation, a direct ageing treatment was found to induce a 35– 40% reduction in toughness [174], and the fracture was described as more random and less localised at the melt pool borders in the as-built state [175].

**Table 2**
Mechanical properties at ambient temperature, evaluated through tensile tests, of LPBFed Al-Si alloys in as-built and T5 conditions.

| Alloy | Reference | Thermal treatment | Sy (MPa) | UTS (MPa) | ef (%) |
|---|---|---|---|---|---|
| AlSi10Mg | [175] | As-built | 263 | 473 | 7,8 |
| | | 200 °C – 2 h | 298 | 479 | 5,6 |
| AlSi10Mg | [135] | As-built | 267 | 391 | 5,6 |
| | | 175 °C – 1h | 310 | 440 | 4,4 |
| AlSi10Mg | [168] | As-built | 255 | 377 | 2,2 |
| | | 160 °C – 5 h | 268 | 342 | 0,9 |
| AlSi7Mg | [129] | As-built | 225 | 375 | c.a 7,5 |
| | | 160 °C – 8 h | 280 | 400 | c.a 5,5 |
| AlSi10Mg | [174] | As-built | 257 | 398 | 7,6 |
| | | 160 °C – 4 h | 309 | 411 | 4,8 |
| AlSi10Mg | [176] | As-built | 289 | 414 | 5,6 |
| | | 170 °C – 1,5 h | 309 | 442 | 5,3 |

### 4.3. Intermediate annealing treatments

Annealing at intermediate temperatures, that is in the range between ageing temperatures and solution treatment temperature, has been widely applied to LPBFed Al–Si alloys. In fact, several suppliers of LPBF systems suggest a post-building annealing treatment at temperatures close to 300 °C, which is aimed at stress-relieving the parts before their removal from the building platform [177–179]. Since such treatments have been developed with various aims and cover a wide range of temperatures and durations, it would be improper to discuss the optimisation of treatment parameters; rather, the dependence of the microstructural and mechanical features on temperature and time will be described and discussed in the next sections.

#### 4.3.1. Modification of the microstructure

As previously done during the review of studies dealing with solution treatment and ageing and direct ageing, the possible modifications of the eutectic Si network will be discussed first, since these changes appear to be the most recognisable among microstructural alterations. So far, it has been established that two radically different outcomes could be obtained based on the annealing temperatures. At the lower end of the temperature range, the original interconnected Si network is left almost untouched, as during a direct ageing treatment, with only limited Si precipitation occurring in the particles along the cell boundaries. However, at higher temperatures, the growth of such particles leads to the progressive disappearance of the continuous network [180]. A schematic illustration of this evolution is shown in Fig. 16.

The boundary between these two temperature domains has been identified in different works through the metallographic analysis of samples treated for the same duration at different temperatures. This boundary was reported to lie below 260 °C in [181], between 240

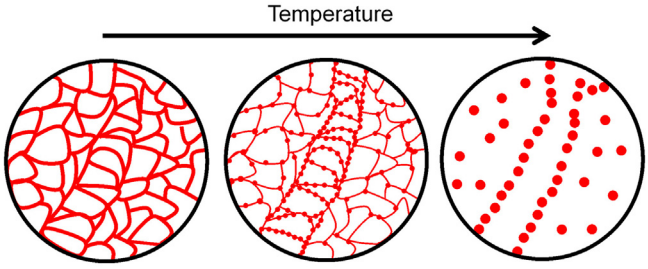


**Fig. 16.** Schematic depicting the evolution of Si morphology in an LPBFed Al-Si alloy during annealing at increasing temperatures. Red areas represent Si. Reproduced from [180].

– 282 °C in [107,182], between 263 –294 °C in [77,183], and between 240 and 290 °C in [100]. It is important to note that these data roughly agree with each other. This bipartition of the treatment temperature field was justified in [77] on the basis of calorimetric analyses, allowing to establish direct relationship between the treatment temperature and the intrinsic thermo-physical properties of the alloy. After recognising the exothermal phenomena, as reported in the introductory part of Section 4, a regression of the peak offset temperatures was performed to a hypothetical "scan speed 0". It was concluded that in the considered AlSi10Mg alloy, Si spheroidization was likely to take place at temperatures close to 294 °C. A similar procedure was applied in [107]. In later works, it has been demonstrated that these temperatures can vary depending on the processing parameters used (i.e., on the induced thermal history), thus justifying the slight variations noticeable in the available literature [100,111].

The changes in the microstructure with treatment time have also been studied by metallography and mechanical tests, as depicted in Fig. 17 [100]. As shown in the image, annealing at 244 °C led to a hardness plateau after 3 h, whereas a stable condition could be reached at 290 °C for approximately 1 h. Accordingly, Si morphology was shown to remain stable for longer durations, showing no rupture of the eutectic network at 244 °C and no evident coarsening of the spheroidal particles at 290 °C. A direct consequence of the disruption of the Si network is the lowering of the material's electrical [127] and thermal [184] resistivity. Simultaneously with Si network break-up, similarly to what happens during solution heat treatment, the supersaturation of Si in the Al matrix decreases and an increase in the Si phase fraction from 7.4% (as-built) to 9.6% (annealed at 300 °C for 2 h) is induced.

In terms of the effect on the grain size and orientation, slightly different results can be found in open literature. Several studies have reported that thermal treatments both above and below the Si network rupture threshold has no significant effect on the grain growth or recrystallisation [76,129,185,186], while some other studies have reported both the growth [182] and reduction [187] of the grain size at temperatures close to 300 °C. Although no definitive conclusion may be drawn, it should be emphasised that the reported variations in the grain size are quite small, and therefore the differences in the result can be attributed to the inherent variability in the local grain size rather than to the actual influence of heat treatments: it is quite reasonable to assume that no recrystallization or grain growth occurs in the considered temperature range. The annealing's ability to remove residual stresses has also been extensively studied, both experimentally [131,188,189] and numerically [190]. Treatment at 300 °C for 3 h was shown to lower residual stresses by more than 200 MPa, even though they could not be completely eliminated, and a certain nonuniformity in stress distribution across the volume persisted even after annealing [81,191]. In [130] the authors suggested that, even though annealing at 300 °C allowed an almost complete recovery of stresses, treating LPBFed AlSi10Mg parts at 200 °C was not sufficient. Colombo et al. [100,176] concluded that residual stresses were practically negligible after annealing at both 244 °C and 290 °C, but the first treatment had the advantage of keeping the Si network intact, thus retaining higher mechanical resistance.

Annealing at temperatures equal to or higher than 300 °C is absolutely necessary for the far-hypereutectic AlSi50 alloy, which is frequently used for producing mirrors, in order to remove residual stresses and homogenise parts. Moreover, heat treatment can induce precipitation of supersaturated Si, thus avoiding in-service precipitation and giving rise to a smooth evolution of the thermal expansion coefficient (CTE) with temperature, which is essential for the actual application of such alloys [109,192]. Heat treatments at intermediate temperatures (200 °C – 400 °C) have been used to homogenise LPBF-produced joints between different Al-Si alloys [193] or welded beads between different LPBFed parts [194].

Finally, it shall be briefly reported that a completely different method of modifying the as-built microstructure, based on electropulsing, has been reported in [195]: it was demonstrated that, by controlling current intensity and pulse duration, different degrees of Si spheroidisation and, consequently, strength and ductility could be induced. Importantly, such treatments were obviously less time-consuming than conventional ones.

#### 4.3.2. Modification of the mechanical properties

It may be easily understood that the previously described microstructural modifications have a profound impact on the mechanical behaviour of the treated alloys and that rather different behaviours correspond to the range of diverse microstructures which can be obtained by annealing LPBFed Al-Si alloys. Li et al. carried out an extensive study on the deformation mechanisms acting in LPBFed AlSi10Mg and investigated the influence of heat treatments on such mechanisms [196]. The differences in the microstructure and mechanical behaviour among fully cellular (as-built), partially cellular (annealed at 300 °C for 4 min), and non-cellular (annealed at 300 °C for 40 min) alloy were studied to highlight differences and propose a description of dislocation behaviour. As reported in [76], annealing induces an abrupt lowering of the strain hardening rate with respect to the as-built condition (see Fig. 18): the work-hardening exponent, n, was lowered from 0.202

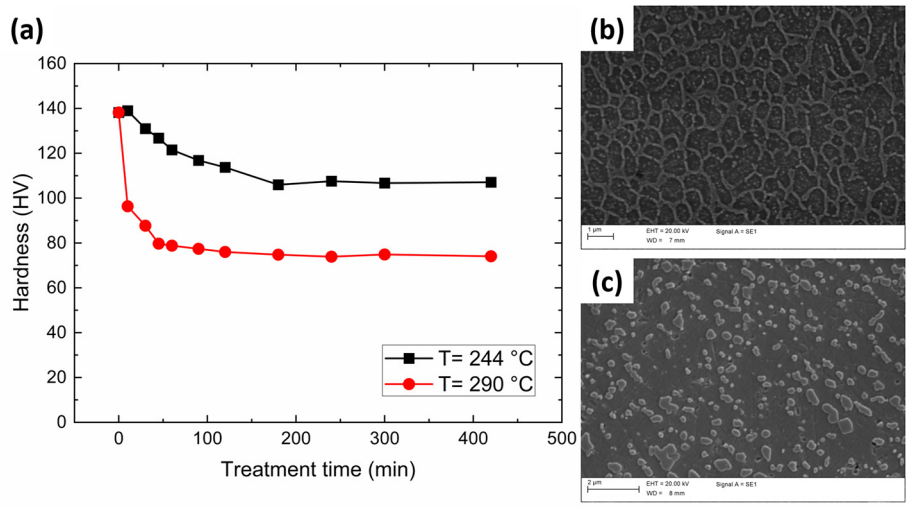


**Fig. 17.** Hardness evolution of an LPBFed AlSi10Mg alloy upon annealing at 244 °C and 290 °C (a); SEM micrographs depicting the microstructure after (b) annealing at 244 °C for 180 min (intact Si network) and (c) at 290 °C for 45 min (spheroidised Si). Elaborated from the authors' own data.

(as-built sample) to 0.143 (partially cellular) and 0.138 (non-cellular). This reduction was attributed to the lower ability of the interrupted Si network to generate dense areas of geometrically necessary dislocations (GND), which hinder the motion of mobile dislocations (generated at the Si nanoparticles lying across the matrix) in the as-built samples. In contrast, in [76], the high strain hardening of the as-built material was attributed to the SSSS and the nanometric Si particles present inside cells; while the reduction in the strain hardening after heat treatment at both 300 °C and 530 °C (solution treatment) was ascribed to the fading of such supersaturation due to Si precipitation.

The dependence of strength and ductility on the annealing temperature is shown in Fig. 19, whose trends are in good agreement with the available literature [197–199]. The roughly continuous decrease in the yield and ultimate strength with increasing treatment temperature can be attributed to the progressive coarsening of Si nanoparticles and reduction in the solid solution supersaturation. At temperatures close to 300 °C, a marked change in both strength and ductility can be readily attributed to the disappearance of the continuous Si network [120,200,201]. This increase in ductility also corresponds to a transition from brittle to ductile fracture behaviour, as evidenced by the formation of numerous equiaxed dimples in samples annealed at 300 °C, whereas as-built parts usually exhibit evident cleavage planes [202,203]. Annealing both above and below the Si network rupture threshold has also been shown to be unable to fully cancel the anisotropic nature of mechanical behaviour [186]. An interesting feature was highlighted by the tensile tests reported in [204], although the authors did not comment on it. It is evident that serrated plastic flow, connected to the dynamic strain ageing phenomenon [205,206], takes place only in samples annealed in a confined temperature interval: samples treated at 450 °C present marked serrations, but neither 300 °C nor 550 °C annealing caused such behaviour. The understanding of this trend and its correlation to the evolution of microstructure would definitely constitute a limited but intriguing research topic.

Annealing appears to be of paramount importance for the effective employment of the LPBFed– Al Si lattice structure and is therefore commonly applied [207] . In [208], the authors demonstrated that annealing at 300 °C could prevent abrupt early failure (≈ 9 %) typical of as-built trabeculae, thus allowing a smooth compression to take place up to full densification (≈ 65 %). This may be connected to the ability of annealing treatments at 300 °C to remove residual stresses and partially homogenize the microstructural inhomogeneities that characterize different portions of lattice structures [145]; this effect has been proven to be even more pronounced if annealing temperature is raise up to 530 °C, which could be properly considered as a solution treatment [209].

As far as dynamic mechanical behaviour is concerned, the effect of various annealing treatments has been tested on both damping capacity and high strain rate compressive performance. Damping tests proved that the loss factor of the LPBFed AlSi10Mg laminas was greatly and similarly reduced by annealing both below and above the critical temperature for Si network rupture, suggesting that the damping ability is determined by residual stresses rather than by the microstructure itself. On the contrary, the compressive behaviour at elevated strain rates (1000 mm/s to 2000 mm/s) was shown to be greatly influenced by the spheroidization of the eutectic Si phase, since samples annealed at 400 °C showed reduced flow stress and increased strain with respect to the ones in as-built and 200 °C – annealed conditions [210]. In [211] annealing at 300 °C was also shown to largely improve the impact resistance, measured by Charpy impact tests, over both the as-built and the T6-treated samples: this was attributed to the ability of the annealed alloy of generating new dislocations and therefore having a different strain sensitivity. Finally, it may be briefly recalled that the tribological performances of LPBFed Al-Si parts are understandably degraded by annealing owing to the induced hardness reduction [212,213].

Considerable effort has been devoted to improving the fatigue resistance of LPBFed Al–Si alloys by annealing at intermediate temperatures [214]. This interest has been mainly driven by the hypothesis that removing residual stresses while maintaining reasonable hardness, higher than that obtained after T6 treatment, could effectively improve the material's behaviour under cyclic loading conditions [215,216]. Moreover, most researchers agree in considering that no variation in internal porosity is expected at the temperatures typical of the currently discussed annealing treatments [147,217], even though Strumza et al. [218] attributed plastic deformation upon thermal expansion tests to the formation of thermally induced porosity at temperatures higher than 240 °. Nevertheless, the improvement of the fatigue resistance by annealing at 300 °C was indeed verified in [219], where it was confirmed that the effect of tensile strength reduction is outmatched by the removal of residual stresses, thus, improving the fatigue strength with respect to the as-built condition. Similarly, Suryawanshi et al. demonstrated that a 300 °C – 6 h treatment increased the fatigue strength of an AlSi10Mg alloy from 60 MPa to 110 MPa [82]. In contrast, a reduction in fatigue resistance was caused by a stress relief treatment (300 °C for 2 h) in [162]. The effect of annealing treatments lying below or above the Si network spheroidization boundary was studied by Tridello et al. on horizontally built samples in the very high cycle fatigue regime [220,221], yielding the results shown in Fig. 20. It was reported that annealing at 320 °C induced a decrease in fatigue resistance (from 68 MPa to 61 MPa), whereas a 244 °C treatment, which was able to keep the Si network

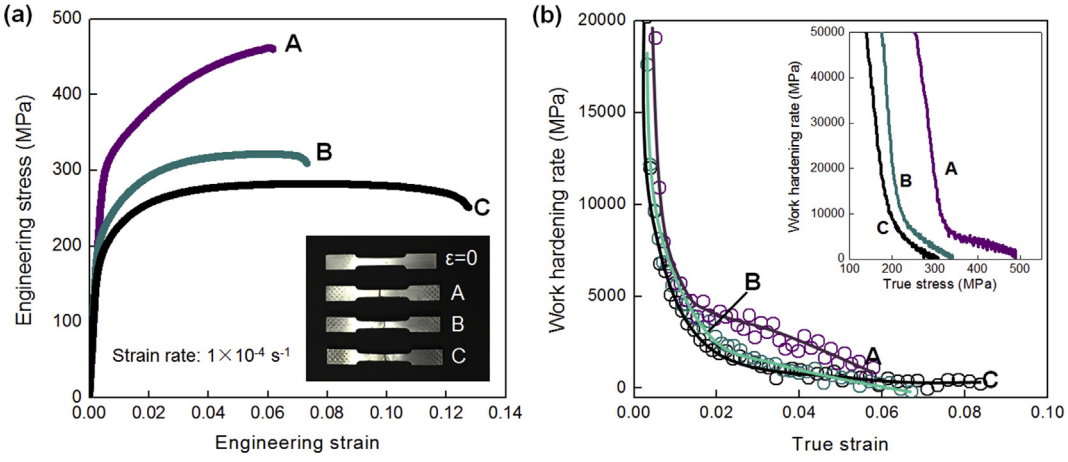


**Fig. 18.** Tensile stress-strain curves of a LPBFed AlSi10Mg alloy (a); corresponding work hardening rate - true strain curves of samples in different conditions (b); inset reports the corresponding work hardening rate - true stress curves. A, B and C indicate samples with full-, partial- and non-cellular structure, respectively. Reproduced from [196].

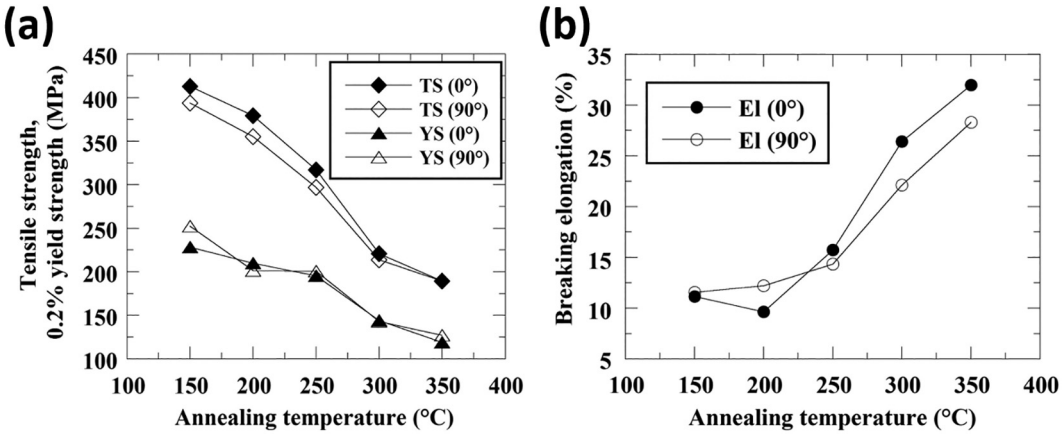


**Fig. 19.** Evolution of mechanical properties of a LPBFed AlSi7Mg alloy upon annealing at different temperatures: ultimate tensile strength (TS) and yield strength (YS) (a) and elongation to failure (El) (b). Reproduced from [120].

intact and remove residual stresses, improved the fatigue resistance (76 MPa). This modification was also reflected in the distribution of the defect types originating fracture: only larger incomplete fusion defects could initiate cracks in samples treated at 244 °C, whereas smaller pores and surface defects were common in the as-built 320 °C-treated samples. These results highlight that a definitive understanding of the influence of annealing temperature on fatigue resistance is yet to be obtained. Still, the currently available data, though partially contradictory, seem to indicate that treatments at temperatures lower than or equal to 300 °C may be more beneficial. Annealing at temperatures below the Si spheroidization threshold may be even more advantageous as they allow removing residual stresses while keeping relatively high hardness.

*4.3.3. Modification of the corrosion behaviour*

Several studies have explored the influence of annealing at various temperatures on the corrosion behaviour. Indeed, the different Si morphologies obtained by treating in the considered temperature range are likely to heavily influence the possible degradation mechanisms of LPBFed Al-Si alloys (Fig. 21). Since it is generally accepted that as-built parts suffer localised attack along melt pool boundaries [26], it is also widely recognised that this same behaviour holds for samples annealed at temperatures below the onset of the Si network rupture process. Particularly, at lower temperatures (i.e., at temperatures lower than or close to 200 °C), the presence of unreleased residual stresses favours the formation of superficial microcracks, but pitting corrosion is prevented owing to the integer Si network [171,222]. Conversely,

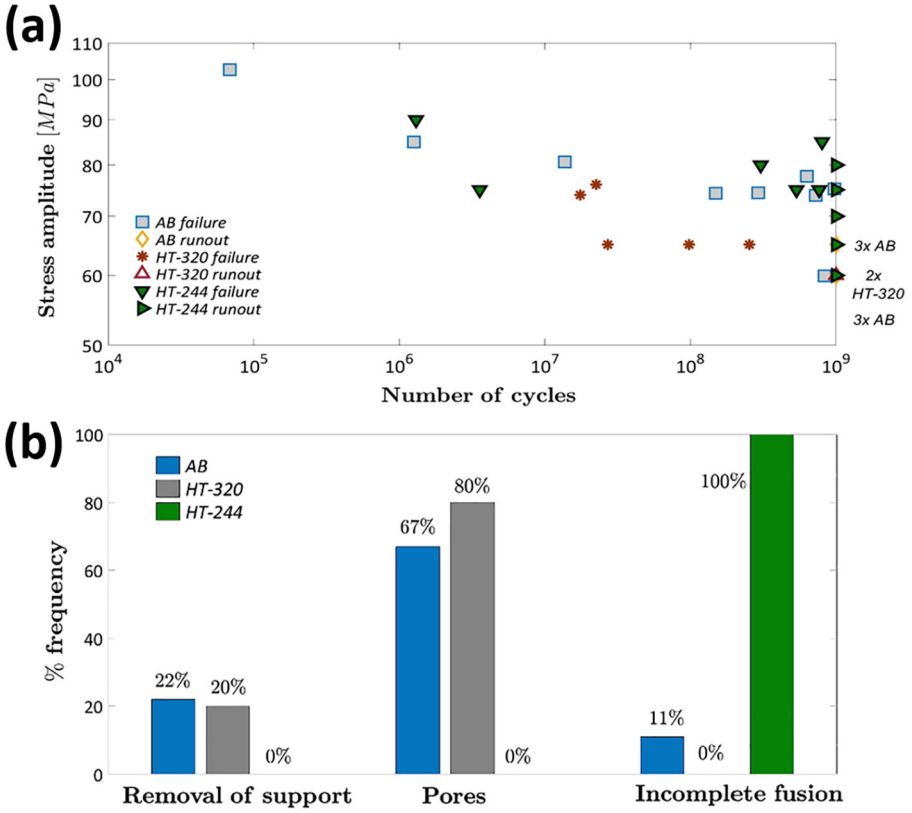


**Fig. 20.** S-N curves of a LPBFed AlSi10Mg (a) and distribution of critical defect types (b) in as-built, annealed-244 °C and annealed-320 °C conditions. Reproduced from [221].

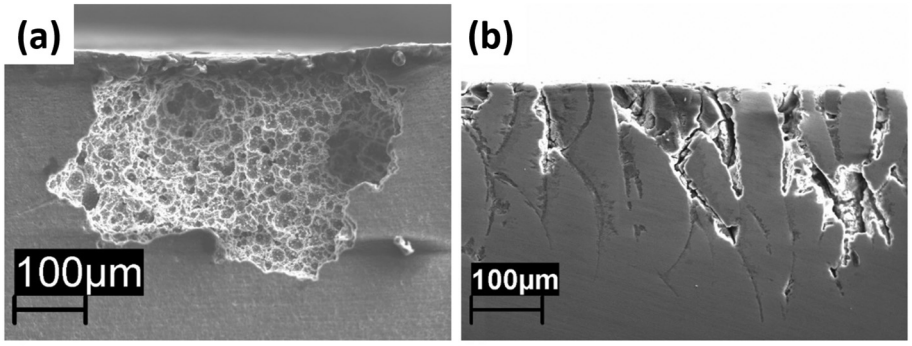


**Fig. 21.** Metallographic sections showing the corrosion morphology in LPBFed AlSi1Mg alloy: pitting in a sample annealed at 450 °C (a) and selective penetrating attack in an as-built sample (b). Reproduced from [223].

annealing temperatures higher than 300 °C are likely to change the corrosion morphology, giving rise to a uniformly distributed penetrating attack caused by the effective galvanic coupling between the Al matrix and the now spheroidized Si particles [101,223–225]. A further increase in temperature does not affect the corrosion mechanism, possibly worsening the galvanic coupling effect due to further Si precipitation and growth [167]. However, due to the different testing conditions and evaluation methods, the quantitative interpretation of results appears not to be fully unanimous among the available works, and different corrosion rates can be found in the literature. The reader is referred to a more focussed review paper ([26]) for further details.

## 5. Heat treatment of other LPBFed aluminium alloys

The number of scientific works dealing with heat treatment of LPBFed aluminium alloys other than those based on Al-Si systems is understandably smaller. In fact, much greater difficulties have been experienced in manufacturing such alloys [2,20] due to the large solidification range and solidification shrinkage: as a consequence, extensive cracking has been reported in high-strength alloys, including Al-Zn-Mg [70] and Al-Cu alloys [226,227]. In order to overcome these processing issues numerous works have explored the modification of such alloys by the addition of either further alloying elements (e.g. Si) or in situ and ex situ inoculants (e.g. $TiB_2$ or SiC nanoparticles). In light of the optimization of heat treatments, particular care shall be devoted to the study of such modified alloys, since their as-built microstructure, as well as their precipitation sequences, may be deeply altered [23]. The introduction of $TiB_2$ inoculants was shown to have no influence on the kinetics of precipitation in Cu-based 2618 [69,228] and Al-3,5Cu-1,5Mg-1Si alloys [229], even though large alterations of the as-built microstructures (grain size and morphology, dislocation density…) were reported. On the contrary, the modification of a Al-Zn-Mg 7075 alloy by the addition of Si resulted in the appearance of the $Mg_2Si$ precipitation sequence beside the usual $Mg_2Zn$ one [70]. Moreover, if Si amount exceeds 3 – 4 wt.% an almost continuous eutectic network, akin to the one typical of LPBFed Al-Si alloys, is formed [230]: consequently, all the transformations regarding such phase, discussed in Section 4, have to be carefully considered when designing dedicated thermal treatments. Finally, a further effect, which has to be carefully considered, is the selective evaporation of low-boiling elements (e.g. Zn), which may totally impede the exploitation of certain precipitation sequences, as reported in [231].

Nevertheless, given the availability of sound samples, an increasing number of studies have focussed their attention on the heat treatment of a variety of alloys to fully exploit their strength potential. The next sections will discuss the output of such research, dealing with one alloying system at a time.

### 5.1. Al-Cu alloys

To the best of our knowledge, only a limited number of papers have discussed the heat treatment of LPBFed Al–Cu alloys. Among these alloys, the considered alloys are the plastic deformation-oriented alloys 2618 [69,228], 2219 [232], and modified 2024 [233], two casting-derived alloys [84,234,235], the on-purpose Al-3Ce-7Cu alloy [71] and the Al-3,5Cu-1,5Mg-1Si alloy [72,229,236]. A brief summary of the mechanical properties of some of the considered alloys, and of their dependance on various heat treatments, is given in Table 3.

Casati et al. [69] demonstrated that T6 heat treatment (solution annealing at 530 °C and ageing at 200 °C) was effective in improving the compression resistance of an LPBFed ENAW 2618 alloy (33% improvement of yield strength with respect to as-built samples). Particularly, they compared the effectiveness of T5 and T6 treatments, concluding that the latter allowed both a higher hardening upon ageing (as confirmed by calorimetric analyses too) and the formation of the stable intermetallic phase $Al_9FeNi$. Moreover, ageing tests and calorimetric tests suggested that similar precipitation kinetics of the S phase exist in the as-built and solution-treated samples. The same alloy, but modified by the addition of Ti and B in order to obtain $TiB_2$ inoculants, was

**Table 3**
Mechanical properties at ambient temperature, evaluated through tensile tests, of LPBFed Al-Cu alloys in as-built and heat treated conditions

| Alloy | Reference | Thermal treatment | Sy (MPa) | UTS (MPa) | ef (%) |
|---|---|---|---|---|---|
| $TiB_2$-modified 2618 | [228] | As-built | 448 | 448 | 7,2 |
| | | 180 °C – 3h | 479 | 460 | 6,1 |
| | | 530 °C – 1 h | 375 | 454 | 8,8 |
| | | 180 °C – 3 h | | | |
| 2219 | [232] | As-built | c.a 120 | c.a 250 | c.a 27,5 |
| | | 530 °C – 10 h | c.a 150 | c.a 380 | c.a 21 |
| | | 190 °C – 18 h | | | |
| Ti-modified 2024 | [233] | As-built | 321 | 365 | 12 |
| | | 495 °C – 1 h | 286 | 432 | 10 |
| | | 190 °C – 12 h | | | |
| Al-3,5Cu-1,5Mg-1Si | [72] | As-built | 223 | 366 | 5,3 |
| | | 493 °C – 1 h | 368 | 455 | 6,2 |
| | | 190 °C – 10 h | | | |
| 2195 (Li-containing) | [237] | As-built | 208 | 341 | 17,2 |
| | | 520 °C – 6 h | 521 | 587 | 6,2 |
| | | 170 °C – 6 h | | | |
| AlSi9Cu3 | [84] | As-built | 266 | 463 | 4,5 |
| | | 470 °C – 6 h | 206 | 319 | 7,8 |
| | | 160 °C – 24 h | | | |
| AlSi11CuMn | [234] | As-built | 350 | 470 | 1,8 |
| | | 250 – 3 h | 250 | 460 | 3,2 |
| | | 515 °C – 1 h | 288 | 354 | 5,4 |
| | | 180 °C – 8 h | | | |

studied in [228]: kinetics aspects were confirmed and the alloy in the overaged state showed improved mechanical resistance at high temperature with respect to the its wrought counterpart. In [232] a 2219 alloy (AlCu6Mn) was subjected to a standard T6 treatment (solution annealing for 10 h at 530 °C, artificial ageing at 190 °C for 18 h), giving rise to a final hardness of 147 HV with respect to 94 HV of the as-built samples. It should be noted that the conventional wrought alloy displays a lower hardness at 130 HV. Tensile tests showed a similar increase in resistance and a decrease in ductility, whereas mechanical anisotropy was not reduced by the T6 treatment. Similarly, the T6 treatment of a 2024 alloy modified by the addition of Ti nanoparticles resulted in increased strength and similar ductility over the as-built samples [233]: homogeneous $Al_7Cu_2Fe$ dispersoids and S precipitates were formed upon solution treatment and ageing, respectively. An LPBFed AlCu5MnCdVa alloy was subjected to solution treatment (530 °C for 6 h) and ageing (150 °C and 170 °C) in [238]: it was found that solid solution strengthening plays a very little role with respect to precipitation strengthening by θ" and θ' and, as a consequence, as-built samples showed the lowest mechanical resistance. Moreover, the evolution of morphology of the precipitates and their contribution to mechanical strengthening were followed upon ageing. The Al-3,5Cu-1,5Mg-1Si alloy studied in [72] consisted of α-Al and Q phases ($Al_5Mg_8Cu_2Si_6$) in the as-built condition, and upon T6 treatment (solution treatment at 493 °C for 1 h, ageing at 190 °C for 10 h), was strengthened by the precipitation of fine rod-like S and θ precipitates, together with some bulkier $Mg_2Si$ particles. This increased the yield strength from 223 MPa (as-built) to 368 MPa (T6); and simultaneously increased the elongation to failure from 5,3. to 6,2 %. Moreover, in [236] the formation of such $Mg_2Si$ phases was found to be instrumental in improving the corrosion resistance of the alloy in NaCl solution: in fact, $Mg_2Si$ acted as anode, passivating the Al matrix and providing some self-healing capacity too. In [229] the same alloy was strengthened by adding micrometric $TiB_2$ powder. The authors claimed that no influence on the precipitation process was induced by the reinforcing particles. However, as clearly visible by comparing Figs. 22 a and c, the dislocation density of the composite was shown to be considerably reduced in the $TiB_2$-containing alloy: considering that the precipitation of θ and S phases is heavily influenced by dislocations, that act as high-diffusional paths, it would have been reasonable to expect a variation in the intensity or kinetics of precipitation. These seemingly contrasting results can be explained by considering that the performed solution treatment step, whose resulting microstructure was not analysed, likely smoothed the differences between the two alloys by annihilating excess dislocations.

The precipitation sequence of the AlSi9Cu3 alloy, which is a well-known foundry alloy, was studied by calorimetry in [84]. The authors concluded that the formation of phases belonging to the θ sequence could occur at a similar pace as in the conventionally produced alloy, whereas a good resistance to overageing was envisioned. A T6 treatment (solution treatment at 470 °C for 6 h, ageing at 160 °C for 24 h) was shown to cause a sharp decrease in tensile strength and an increase in ductility. In [239] the authors studied the response of the same AlSi9Cu3 alloy to a stress relief treatment (300 °C) and solution treatment and ageing. In both cases, a clear improvement of mechanical behaviour over the as-built condition was achieved, even though the initial strength appears to be rather low. Pozdniakov et al. [234] explored another Si-containing alloy, namely AlSi11CuMn, and trialled different heat treatments, including annealing in the 215 – 275 °C range and a T6 treatment. Although a finely dispersed precipitation of S' ($Al_2CuMg$) was induced, all the treatments led to a marked decrease in hardness due to Si diffusion. Indeed, the response of Al-Si-Cu alloys to heat treatments appears to be markedly similar to the one of Al-Si-Mg alloys, as their as-built microstructures are dominated by the same eutectic structure and by a Si-supersaturated matrix. As a result, similar conclusions regarding the effectiveness of the various heat treatment strategies can be likely drawn. Finally, the Al-3Ce-7Cu alloy [71], where Ce addition gives rise to a eutectic phase useful in mitigating hot cracking, was shown to be characterised by a negative response to age-hardening. Neither T6 treatment (solution treatment at 540 °C for 3 h, ageing at 190 °C) nor direct annealing at temperatures in the 250 – 400 °C range produced an increase in hardness. Nevertheless, it is interesting to note that the hardness resulting from direct annealing increases if the treatment temperature is increased. This was explained by suggesting that the precipitation of nanosized $Al_3Zr$ particles might balance the hardness reduction due to stress relieving.

To the best of the authors' knowledge, a limited number of works have studied the heat treatment of LPBFed Al-Cu-Li alloys. Two papers by Raffeis et al. [93,240] explored the precipitation of different phases ($Al_2CuLi$-$T_1$, $Al_{7.5}Cu_4Li$-$T_B$, $Al_2Cu$-θ) in an LPBFed 2099 alloy, subjected to both in situ treatment, obtained by pre-heating the building platform at 220 °C, 320 °C and 520 °C, and post-building heat treatment (annealing at 80 °c, 450 °C and 520 °C). In situ treatment was found able to induce precipitation of both $T_1$ and $T_B$, the latter inducing negligible hardening. Noticeable precipitate-free zones (PFZ) were found along grain boundaries and were attributed to the local formation of Cu-rich phases as a consequence of local segregation of Cu. Post-building heat treatments appeared to induce relative hardening thanks to a fine precipitation of $T_1$ phase, but could not match the results of the 520 °C in situ treatment. In [237] a 2195 alloy displayed a non-uniform elemental distribution in the as-built state and was subjected to a T6 treatment (solution treatment at 520 °C for 1 h, ageing at 170 °C for 6 h). After solution treatment and ageing, a uniform distribution of alloying elements was achieved, grain growth was avoided and δ' ($Al_3Li$) and $T_1$ precipitates were formed. Such precipitation allowed a considerable improvement in tensile properties in T6 samples, at the expense of reduced ductility, as shown in Fig. 23.

### 5.2. Al-Zn-Mg alloys

The LPBF of Al-Zn-Mg alloys, which often comprise Cu, has been actively trialled to match the high mechanical performance, usually displayed by the corresponding wrought 7xxx series alloys. Most of the available works have challenged the LPBF production of the famous ENAW 7075 alloy and its thermal treatment [70,241–244]; moreover, other alloys, including a 7068 derivative [230] and a generic Al-Zn-Mg-Cu alloy with high Zn content [245] have been studied. It should be noted that most of these alloys are not processed without any modifications, but rather enriched in Si (directly or through blending with Al-Si alloy powders) or in both Si and $TiB_2$ inoculants [246], to improve their processability. Therefore, strengthening phases and precipitation sequences may be slightly different in the LPBFed alloys with respect to the original ones. Table 4 collects the mechanical properties of some of the considered alloys. It may be immediately appreciated that the data reported in Table 4 refer to modified alloys only, since the unmodified alloys do not show sufficient integrity to allow tensile tests to be performed.

Montero Sistiaga et al. [70] observed the progressive overlapping of η and β precipitation sequences when increasing the Si content in the original 7075 alloy. T5 treatment (150 °C for 6 h) was confirmed to yield better results than the T6 treatment (solution treatment at 470 °C for 2 h, ageing at 150 °C for 6 h) because it avoided the spheroidization of the fine Si network. However, the authors wondered if this temperature was sufficient for obtaining stress release, and claimed that further optimisation of heat treatments was necessary. The mechanical resistance of the wrought alloy could not be reached because, among other causes, selective evaporation of Zn and Mg during processing resulted in precipitation potential. As shown in Fig. 24, similar results, that is better performance of T5 over T6 treatment and interaction between Si morphology modification and η precipitation, were reported in [230] for a Si-modified 7068 alloy. Aversa et al. [242] obtained Al-5,3Si-2Zn-0,8Cu-1,6Mg (wt.%) alloy by blending AlSi10Mg and 7075 powders. Assuming that the aluminium matrix was sufficiently supersaturated, the authors explored T5 treatments at different

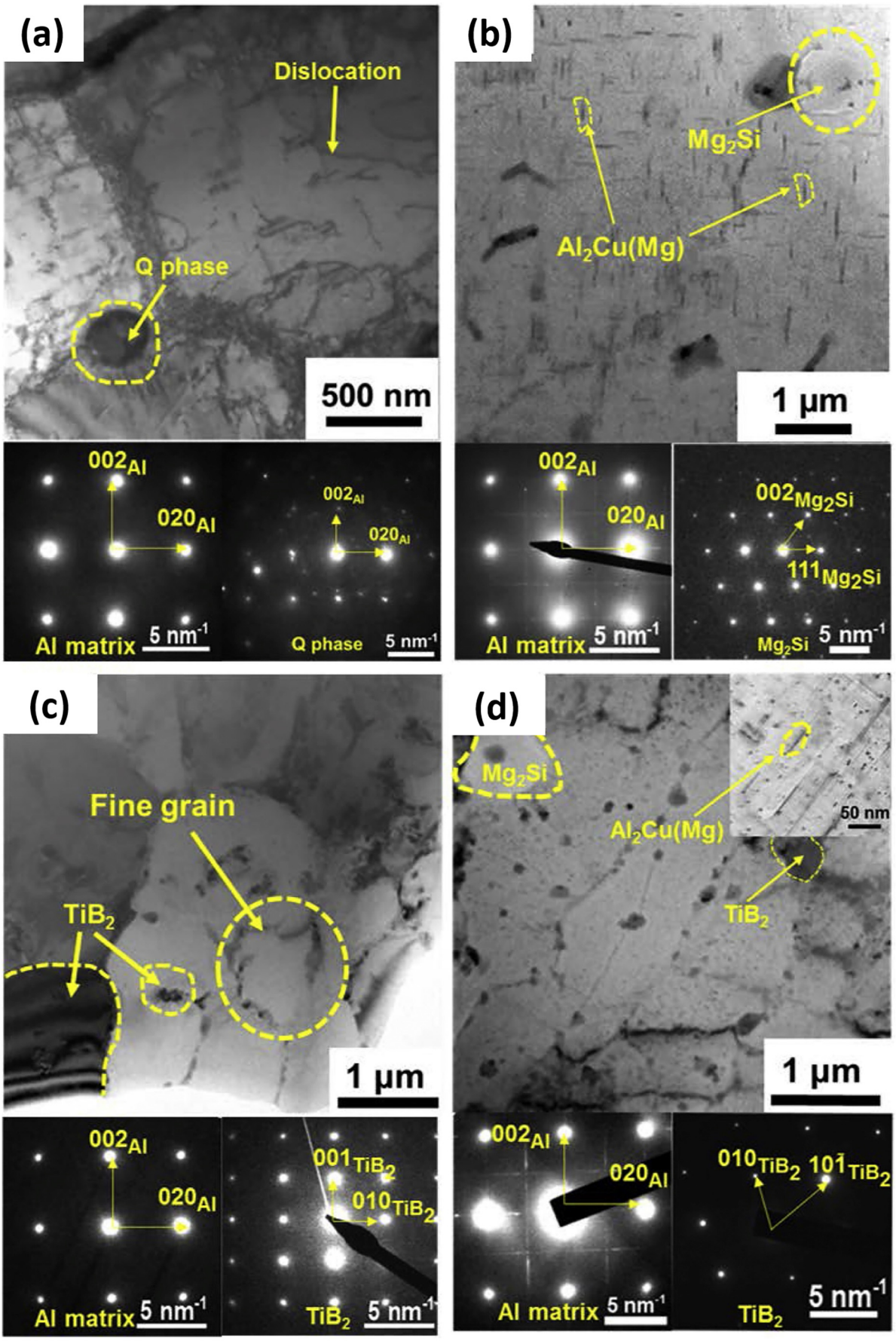
(a)
Dislocation
Q phase
500 nm
002Al
020Al
Al matrix
5 nm-1
002Al
020Al
Q phase
5 nm-1
(b)
Mg2Si
Al2Cu(Mg)
1 μm
002Al
020Al
Al matrix
5 nm-1
002Mg2Si
111Mg2Si
Mg2Si
5 nm-1
(c)
Fine grain
TiB2
1 μm
002Al
020Al
Al matrix
5 nm-1
001TiB2
010TiB2
TiB2
5 nm-1
(d)
Mg2Si
Al2Cu(Mg)
50 nm
TiB2
1 μm
002Al
020Al
Al matrix
5 nm-1
010TiB2
101TiB2
TiB2
5 nm-1

temperatures, obtaining a 11 % increase in yield strength after ageing at 160 °C for 6 h. In [241,231] the authors obtained somewhat surprising results exploring the heat treatment of a lean LPBFed 7075 alloy. Although a remarkable 87 % hardness increase was obtained through a double ageing treatment (solution treatment at 470 °C for 1 h, ageing at 110 °C for 5 h, and at 150 °C for 14 h), the authors attributed this result to the precipitation of S and θ phases, claiming that no η precipitate could be found due to Zn evaporation during processing. However, the reported TEM images show very coarse $Al_2Cu$ and $Al_2CuMg$ particles, whose presence may be ascribed to eutectic solidification rather than to precipitation. In [245] the T6 treatment was found to be more effective in the LPBFed than in the cast alloy owing to the precipitation of a finer η' dispersion.

In summary, solubilisation and ageing treatment appears to be more effective than direct ageing for lean 7xxx alloys and, in this context, it produces finely dispersed precipitates and attractive mechanical properties. This may be due to the necessity of dissolving the eutectic $MgZn_2$ formed upon solidification to obtain an adequate reservoir of solute atoms, which later allows the controlled precipitation of η'. In contrast, direct ageing is preferable if Si has been added for processability improvement. Thus, the concurrent benefits of allowing η precipitation and keeping the original fine Si morphology intact may be exploited.

### 5.3. Al-Mg-Sc-(Zr) alloys

In recent years, the ever-lasting quest for higher mechanical properties has driven considerable research efforts towards the development of aluminium alloys, specifically designed for LPBF synthesis. Such alloys were meant to overcome the strength limitations imposed by Al-Si alloys and the processing problems posed by conventional high-resistance alloys, such as the previously mentioned Al-Cu and Al-Zn-Mg alloys. In particular, great attention has been paid to the study of Sc- and Zr-containing alloys, often derived from the 5xxx series Al-Mg alloys [248], which has also led to the definition of the renown Scalmalloy®. The effect of thermal treatments on the tensile properties of some of the studied alloys is shown in Table 5.

Ageing treatments have been successfully researched to improve the mechanical resistance of as-built alloys. Early works showed that a 72 HV hardness increase was possible through direct ageing [11,12] owing to the formation of further $Al_3Sc$ precipitates, in addition to the ones formed during the process itself [253]. A solution treatment step prior to ageing was not deemed necessary because the high cooling rate allowed the formation of a considerably supersaturated solid solution. An image of $Al_3Sc$ precipitates in both as-built and heat-treated samples is shown in Fig. 25. It may be appreciated that in both cases the FCC Al matrix and the $L1_2$ precipitates are coherent and that the heat treatment induced the formation of a greater amount of particles [254]. The numerosity and dimensions of such precipitates were studied in detail in [255], showing that after ageing at 325 °C, the density of $Al_3Sc_xZr_{(1-x)}$ increased by a factor of 3 – 10, whereas their size distribution remained approximately unchanged. A detailed kinetic analysis performed by Jia et al. [256], revealing that a 63 KJ/mol activation energy characterized the precipitation of $Al_3Sc$ precipitates, this value being largely smaller than the one typical of conventionally produced alloys. This was interpreted as being due to the presence of numerous dislocations, quenched-in vacancies and fine grain size in the as-built microstructure. The formation of precipitates belonging to different sequences, such as the $Mg_2Si$ or $Al_6Mn$ ones, are possible depending on the starting alloy composition [257].

Numerous studies have explored different ageing temperatures and durations in order to optimise the treatment procedure. It is generally recognised that optimal ageing, resulting in fine coherent precipitates, occurs at 325 – 350 °C for 4 – 5 h [250–252], similar to what happens for conventionally produced Al-Sc alloys [258,259]. At higher temperatures (> 370 °C), precipitates rapidly lose coherency, whereas at low temperatures, excessively long holding times are required. It is worth noting that typical ageing temperatures lie in the range usually exploited for stress relieving of other LPBFed aluminium alloys, thus presenting the advantage of allowing a contemporary strengthening and stress – relieving of the alloy [249,260]. Moreover, it shall be underlined that no grain growth has been reported at such temperatures owing to the pinning effect of $Al_3Sc$ primary particles [261]. Best et al. [262] studied the influence of heat treatment on hardness and homogeneity at a microscopic level. They demonstrated that precipitation hardening is more effective in coarse grain areas and can improve the already good isotropy along different directions. As far as the modification of mechanical properties is concerned, by observing Fig. 26, it may be appreciated that direct ageing effectively improves strength: whereas the as-built alloy displays a 362 MPa yield strength, a yield strength of 520 MPa is obtained after ageing at 350 °C for 2 h. Higher temperatures, or longer times, induce a decrease of strength and a steep deterioration of ductility because of the coarsening and loss of coherency of precipitates [251]. Conversely, ductility reaches a maximum (still lower than the one displayed by as-built parts) after ageing at 324 °C and then starts decreasing again.

It was reported in [263] that the advantages of ageing should be carefully considered during high temperature employment of LPBFed Al-Mg-Zr alloys. In fact, coarsening of precipitates decorating grain boundaries was shown to depress high temperature strength and short-term creep resistance with respect to the as-built condition; on the contrary differences in precipitate size were smoothed during prolonged exposure to high temperatures and therefore a nearly identical long-term creep behaviour was observed.

An undesired side effect of heat treatments lies in the reduction of corrosion resistance: as reported in [264] ageing at 325 °C for 4 h caused a decrease in pitting resistance and an increase in intergranular corrosion because of the formation of precipitates. Such numerous precipitates were shown to induce local galvanic couples, therefore locally destabilizing the protective oxide scale [265]. As a result, intergranular corrosion takes place in a more severe way in heat treated samples [264]: it is also likely that this feature may further increase the anisotropic nature of corrosion resistance in LPBFed Al-Mg-Sc alloys. In fact the different grain boundary concentration on xy and xz surfaces causes a marked difference in corrosion resistance between the two kind of surfaces, and further precipitation along grain boundaries is likely to widen this difference [266]. Finally, it is worth briefly discussing a rather odd work by Ma et al. regarding the effect of cold rolling on an LPBFed Al-Mg-Sc-Zr alloy [267]. As far as heat treatments are concerned, it appears that smaller precipitates were formed in the deformed alloy during ageing at 300 °C.

### 5.4. Other alloys

The present section aims at collecting and reviewing research results that deal with aluminium alloys that do not fall within the previously discussed families.

A peculiar study on the LPBF of commercial-purity aluminium was conducted by Kimura and Nakamoto [268]: annealing was conducted for 10 min in the 350 – 550 °C range, with subsequent furnace cooling.

**Fig. 22.** [100]Al TEM images and SAED patterns of the unreinforced Al-Cu-Mg-Si alloy and the $TiB_2$/Al-Cu-Mg-Si composite: as-built Al-Cu-Mg-Si alloy (a); T6-treated Al-Cu-Mg-Si alloy T6 and corresponding SAED patterns of the Al matrix and theMg2Si phase (b); as-built $TiB_2$/Al-Cu-Mg-Si composite and corresponding SAED pattern of the Al matrix and the TiB2 phase (c); T6-treated $TiB_2$/Al-Cu-Mg-Si composite and corresponding SAED patterns of the Al matrix and the TiB2 phase (d) (inset: $Al_2Cu$(Mg) phase at high magnification). Reproduced from [229].

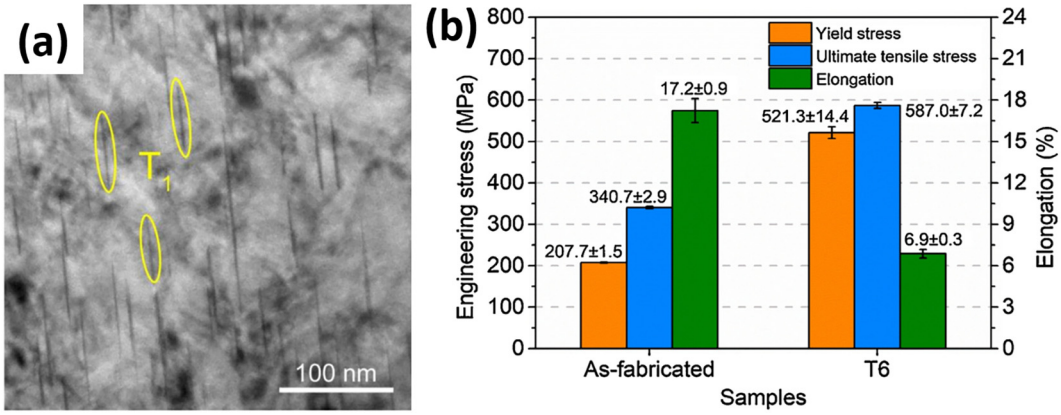


**Fig. 23.** TEM micrographs of T1 precipitates in a T6-treated LPBFed 2195 alloy (a); mechanical properties of the alloy in as-built and T6 conditions. Reproduced from [237].

**Table 4**
Mechanical properties at ambient temperature, evaluated through tensile tests, of LPBFed Al-Zn-Mg alloys in as-built and heat treated conditions

| Alloy | Reference | Thermal treatment | Sy (MPa) | UTS (MPa) | Ef (%) |
|---|---|---|---|---|---|
| AlSi10Mg-modified 7075 | [242] | As-built | 315 | 387 | 2,7 |
| | | 160 °C – 6 h | 350 | 415 | 2,3 |
| Si, $TiB_2$-modified 7075 | [246] | As-built | c.a 350 | 450 | c.a 2,7 |
| | | 490 °C – 1 h 120 °C – 18 h | c.a 460 | 556 | 4,5 |
| Zr-modified 7075 | [247] | 480 °C – 2 h, 120 °C – 18 h | 349 | 400 | 4,6 |
| Si-modified 7068 | [230] | As-built | 313 | 386 | 2,2 |
| | | 165 °C – 4 h | 370 | 432 | 1,4 |

**Table 5**
Mechanical properties at ambient temperature, evaluated through tensile tests, of LPBFed Al-Mg-Sc-(Zr) alloys in as-built and heat treated conditions

| Alloy | Reference | Thermal treatment | Sy (MPa) | UTS (MPa) | Ef (%) |
|---|---|---|---|---|---|
| Al-4,5Mn-1,3Mg-0,8Sc-0,7Zr | [249] | As-built | 431 | - | 21,5 |
| | | 300 °C – 5 h | 571 | - | 18,1 |
| Scalmalloy® | [250] | As-built | 287 | 427 | c.a 15 |
| | | 325 °C – 4 h | 450 | 515 | - |
| Al-4,0Mg-0,7Sc-0,4Zr-0,5Mn | [251] | As-built | 336 | 362 | 11,2 |
| | | 325 °C – 4 h | 504 | 511 | 7,3 |
| Al–4,5Mg–0,32Sc–0,66Zr | [252] | As-built | 291 | 368 | 25 |
| | | 360 °C – 6 h | 438 | 480 | 10 |
| Zr-modified 5083 | [248] | As-built | 212 | 317 | 22,3 |
| | | 400 °C – 2 h | 319 | 392 | 14,1 |

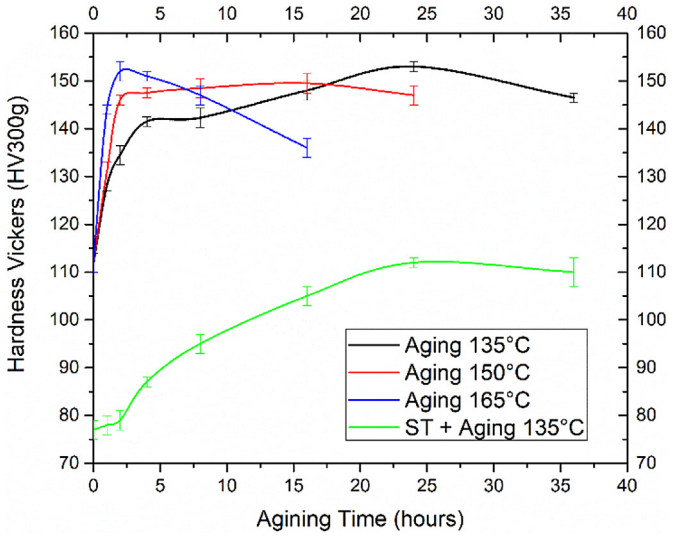


**Fig. 24.** Evolution of hardness of a LPBFed Si-modified 7068 alloy upon direct ageing at various temperatures and after solution treatment. The low hardness obtained by T6 treatment stems from the modification of the as-built Si structure taking place during solution treatment. Reproduced from [230].

They found that thermal conductivity progressively increased with an increase in the treatment temperature, reaching values higher than those displayed by the corresponding wrought alloy, while at the same time mechanical properties were only relatively degraded. This was attributed to increasing recrystallisation and grain growth, driven by residual stresses accumulated during solidification. Another alloy, which was developed for thermal conductivity purposes, is the Al-2,5Fe studied in [269]: the as-built alloy displayed a cellular structure with metastable $Al_6Fe$ secondary phases, which upon annealing at 300 °C were relatively unchanged, whereas they transformed into plate-like $Al_{13}Fe_4$ at 500 °C. Thermal conductivity and mechanical resistance were found to share a trade-off in different annealing conditions and the treatment at 300 °C was chosen as the best compromise, since it did not compromise strength while it largely improved conductivity.

Another group of investigated alloys is the so-called heat-resistant alloys, which usually contain elements such as Fe, to obtain stable intermetallic phases. In [270], Al-20Si-5Fe-3Cu-1Mg was annealed at 200 °C, 300 °C, and 400 °C, however, these treatments were not able to homogenise the highly non-uniform microstructure of the as-built condition. Moreover, they induced coarsening of the eutectic Si, precipitation of the β-$Al_5FeSi$, and reduced the solubility of Si. Consequently, although the paper did not discuss it, it is likely that the mechanical properties were lowered. In [271] an Al–Fe–V–Si alloy was studied: heat treatments at temperatures equal to or higher than 400 °C induced the precipitation of $Al_{12}(Fe,V)_3Si$ dispersoids, as revealed by calorimetry. These particles were found to be stable during successive holding at 425 °C, coarsened at 475 and 525 °C, whereas they decomposed into $Al_{13}(Fe,Si)_4$ and $Al_8Fe_2Si$ equilibrium phases at 600 °C, resulting in a steep reduction in hardness. Manca et al. [272] produced an Al-Si-Ni-Fe-(Cu) alloy, whose as-built microstructure was characterised by the presence of Si, $Al_5Fe(Ni,Cu)$, and $Al_3(Ni,Cu)$ phases. The T6 treatment did not modify the $Al_5Fe(Ni,Cu)$ and $Al_3(Ni,Cu)$ phases but caused a coarsening of Si particles, decreased solid-solution strengthening, and released residual stresses, thus markedly degrading the initial mechanical resistance (as-built: 186 HV; solution treated: 149 HV; aged: 124 HV). A novel heat-resistant Al-Ca-Ni-Mn alloy was produced by LPBF in

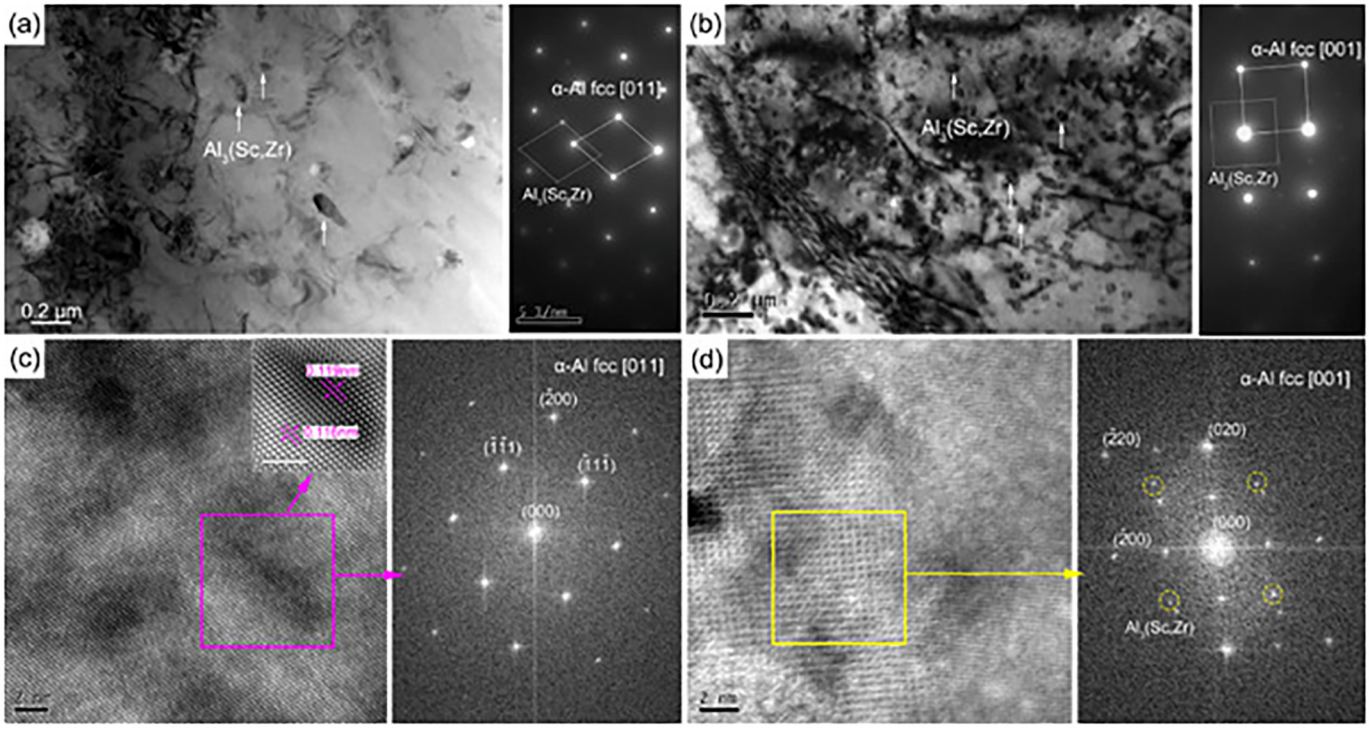


**Fig. 25.** TEM micrographs and SAED pattern (a, b); HRTEM image of α-Al and $Al_3(Sc,Zr)$ (c, d) in as-built (a,c) and aged (b,d) conditions. The evolution of the number of $Al_3Sc$ precipitates upon ageing and the coherency between the matrix and the $L1_2$ precipitates can be appreciated. Reproduced from [254].

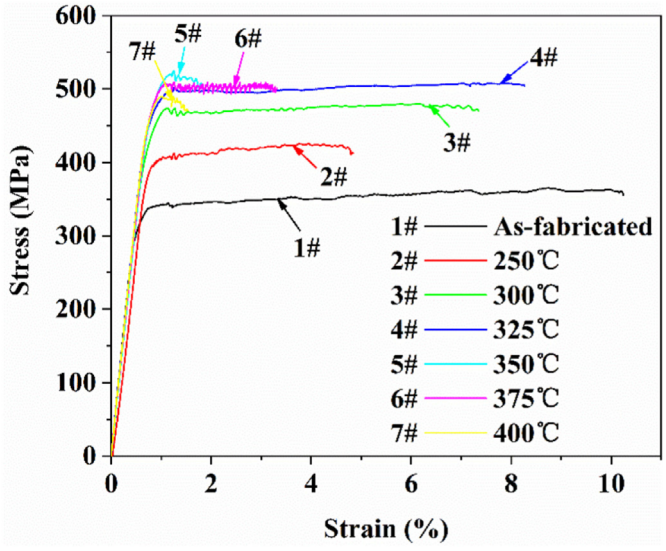


**Fig. 26.** tensile stress-strain curves of an LPBFed Al-4.0Mg-0.7Sc-0.4Zr-0.5Mn alloy directly aged at various temperatures for 2 h. Reproduced from [251].

[273]: the as-built microstructure displayed a fine cellular structure, whose border are likely composed of Ca- and Ni-rich intermetallic compounds; upon annealing at 400 °C such structure underwent breaking and spheroidisation, similarly to what happens in LPBFed Al-Si alloys. As a consequence, hardness reduction took place from 201 HV (as-built) to 161 HV (400 °C for 3 h). Although the number of studies in this field is still limited, LPBFed heat-resistant aluminium alloys definitively need heat treatments before employment in order to stabilise their microstructure, which would otherwise evolve in an uncontrolled way during service. The exact type of treatment will strongly depend on the alloy composition, but it may be reasonably inferred from the known literature that the stable temperature-resistant intermetallic phases will be limitedly affected by annealing, whereas the strengthening contributions of solid solution supersaturation and nanoscale precipitates present in the as-built condition will necessarily be degraded. Therefore, dedicated thermal treatments will need to find a balance between the lowering of strength and stability upon exposure to exercise temperatures.

## 6. Future perspectives of heat treatment of LPBFed aluminium alloys

As may be immediately appreciated through the analysis of the available literature, most of research efforts have been up to now directed to study and optimize the heat treatment of LPBFed Al-Si alloys, whereas a considerably smaller number of works has dealt with other alloying systems. As a consequence, it is logical to indicate that large room for improvement exists in the field of the various Al-Cu, Al-Mg-Sc-Zr and Al-Mg-Zn alloys, not including other less common formulations (heat resistant alloys, Li-based ones etcetera). In this respect, a large share of work can be expected to stem from the fact that the compositions of these alloys are frequently modified to improve their processability: each alloy may therefore present a peculiar as-built microstructure, whose response to thermal treatment has to be considered individually. Moreover, a real leap forward in the design of new LPBF-specific alloys could come if the necessity and consequences of the heat treatment were to be considered from the beginning of the alloy design process, which is currently mainly based on processability issues.

So far, the study of the effects of various heat treatments on LPBFed aluminium alloys has been mainly focused on the evolution of microstructural aspects and static mechanical behaviour. However, in the view of large scale fielding of additive manufactured aluminium components, other kinds of properties need to be properly investigated and used to further optimize thermal treatments. In particular, further developments are expected in the fields of mechanical behaviour under cyclic loading conditions (both fatigue

life and damping ability) and functional performances in selected applications (corrosion and wear resistance, thermal and electrical conductivity).

More generally, thermal treatment procedures will have to move further away from the ones typically applied to conventionally produced materials and towards ever more alloy- and application-specific treatments, formulated on the basis of the metallurgical understanding of the as-built conditions.

## 7. Summary and conclusions

Due to the ever-growing interest for the AM of metallic alloys, the present paper aims to collect and review the large share of research work, which has been devoted over the past years to the study and optimise the heat treatments for LPBFed aluminium alloys. Particularly, it should be noted that a rather profound knowledge of the metallurgy of the various alloys in the as-built state is now available and, as a consequence, the optimisation of dedicated thermal treatments is currently entering a state of maturity. Since most of the available works focus on the widespread Al–Si alloys, the efforts devoted to such family of alloys are likely to decrease in the near future, whereas promising developments can be expected for alloys based on different systems, which show an inherent good response to heat treatments.

Some concluding remarks are as follows:

- The peculiar solidification conditions induced by the LPBF process significantly affect the metallurgy of the produced alloy, and as thus, it is necessary to redefine suitable heat treatments. These treatments need to take into account the out-of-equilibrium condition of as-built parts to exploit their full potential. For example, solution treatments may be avoided owing to the supersaturation induced by rapid cooling. In contrast, precipitation kinetics appear to be only slightly affected by the LPBF process. This indicates that the ageing durations are likely to be similar to those commonly employed for conventionally produced alloys. A correct balance among strength, ductility, residual stresses, and possibly functional properties should be determined regularly based on the required in-service behaviour.
- The metallurgy of Al-Si alloys produced by LPBF is dominated by the presence of a fine cellular eutectic network, which also strongly influences the mechanical behaviour. Therefore, treatments may be roughly divided between the ones able to break such a network (solution treatment and ageing plus high-temperature annealing treatments) and the ones that keep it intact (direct ageing and low-temperature annealing). Solution treatment and ageing (T6) completely revolutionise the microstructure, leading to a fine Si dispersion that grants good ductility and strength (always lower than in the as-built condition). Direct ageing treatments have smaller effect on the hardness and are not able to release residual stresses. Annealing at intermediate temperatures can be fine-tuned to remove residual stresses, choose the desired level of strength, and eventually increase ductility. These treatments are particularly recommended if fatigue resistance is required.
- Al-Cu, Al-Zn-Mg, and Al-Mg-Sc alloys offer the greatest hardening potential when subjected to ageing treatments. Direct ageing generally leads to better results with respect to solution treatment followed by ageing, since rapid solidification grants a sufficient supersaturation of alloying elements in the Al matrix for successive precipitation. This condition does not hold if Si is added to the alloys' formulation to improve the processability. In such case the considerations drawn for Al-Si alloys are likely to prevail.
- The heat treatment of LPBFed heat-resistant aluminium alloys is definitely necessary to stabilise the microstructure prior to their employment. In addition, a large number of research advancements are still present in this field.

## Declaration of Competing Interest

The authors declare that they have no known competing financial interests or personal relationships that could have appeared to influence the work reported in this paper.

## Acknowledgements

The authors would like to acknowledge Accordo Quadro CNR - Regione Lombardia n. 3866 FHfFC for financial support. Special thanks also to Edoardo Fella, Simone Galli, Martina Verri and Giulio Gerosa for their contribution to this research topic during their thesis works.

## References

[1] A. Paolini, S. Kollmannsberger, E. Rank, Additive manufacturing in construction: A review on processes, applications, and digital planning methods, Addit. Manuf. 30 (2019) 100894, https://doi.org/10.1016/j.addma.2019.100894.
[2] A. Aversa, G. Marchese, A. Saboori, E. Bassini, D. Manfredi, S. Biamino, D. Ugues, P. Fino, M. Lombardi, New aluminum alloys specifically designed for laser powder bed fusion: a review, Materials (Basel) 12 (2019) https://doi.org/10.3390/ma12071007.
[3] M.K. Thompson, G. Moroni, T. Vaneker, G. Fadel, R.I. Campbell, I. Gibson, A. Bernard, J. Schulz, P. Graf, B. Ahuja, F. Martina, Design for additive manufacturing: trends, opportunities, considerations , and constraints, CIRP Ann. - Manuf. Technol. 65 (2016) 737–760, https://doi.org/10.1016/j.cirp.2016.05.004.
[4] A. Gisario, M. Kazarian, F. Martina, M. Mehrpouya, Metal additive manufacturing in the commercial aviation industry: a review, J. Manuf. Syst. 53 (2019) 124–149, https://doi.org/10.1016/j.jmsy.2019.08.005.
[5] P. Bajaj, A. Hariharan, A. Kini, P. Kürnsteiner, D. Raabe, E.A. Jägle, Steels in additive manufacturing: a review of their microstructure and properties, Mater. Sci. Eng. A 772 (2020) https://doi.org/10.1016/j.msea.2019.138633.
[6] L.C. Zhang, H. Attar, Selective laser melting of titanium alloys and titanium matrix composites for biomedical applications: a review, Adv. Eng. Mater. 18 (2016) 463–475, https://doi.org/10.1002/adem.201500419.
[7] C.Y. Yap, H.K. Tan, Z. Du, C.K. Chua, Z. Dong, Selective laser melting of nickel powder, Rapid Prototyp. J. 23 (2017) 750–757, https://doi.org/10.1108/RPJ-01-2016-0006.
[8] K. Bartkowiak, S. Ullrich, T. Frick, M. Schmidt, New developments of laser processing aluminium alloys via additive manufacturing technique, Phys. Procedia 12 (2011) 393–401, https://doi.org/10.1016/j.phpro.2011.03.050.
[9] J.P. Oliveira, T.G. Santos, R.M. Miranda, Revisiting fundamental welding concepts to improve additive manufacturing: from theory to practice, Prog. Mater. Sci. 107 (2020) 100590, https://doi.org/10.1016/j.pmatsci.2019.100590.
[10] P. Mercelis, J. Kruth, Residual stresses in selective laser sintering and selective laser melting, Rapid Prototyp. J. 5 (2006) 254–265, https://doi.org/10.1108/13552540610707013.
[11] K. Schmidtke, F. Palm, A. Hawkins, C. Emmelmann, Process and mechanical properties : applicability of a scandium modified Al-alloy for laser additive manufacturing, Phys. Procedia 12 (2011) 369–374, https://doi.org/10.1016/j.phpro.2011.03.047.
[12] F. Palm, K. Schmidtke, Exceptional grain refinement in directly built up Sc-modified AlMg-alloys is promising a quantum leap in ultimate light weight design, Trends Weld. Res. 2012 Proc. 9th Int. Conf 2013, pp. 108–116.
[13] E.O. Olakanmi, R.F. Cochrane, K.W. Dalgarno, A review on selective laser sintering / melting ( SLS / SLM ) of aluminium alloy powders : processing, microstructure , and properties, J. Prog. Mater. Sci. 74 (2015) 401–477, https://doi.org/10.1016/j.pmatsci.2015.03.002.
[14] J. Zhang, B. Song, Q. Wei, D. Bourell, Y. Shi, A review of selective laser melting of aluminum alloys: processing, microstructure, property and developing trends, J. Mater. Sci. Technol. 35 (2019) 270–284, https://doi.org/10.1016/j.jmst.2018.09.004.
[15] B.A.I. Mertens, J. Delahaye, J. Lecomte-beckers, Fusion-based additive manufacturing for processing aluminum alloys : state-of-the-art and challenges, 2017 1–13, https://doi.org/10.1002/adem.201700003.
[16] N.T. Aboulkhair, N.M. Everitt, I. Maskery, I. Ashcroft, C. Tuck, Selective laser melting of aluminium alloys, MRS Bull. 42 (2017) 311–319.
[17] T.B. Sercombe, X. Li, Selective laser melting of aluminium metal matrix composites: review, Mater. Technol. 31 (2016) 77–85, https://doi.org/10.1179/1753555715Y.0000000078.
[18] D. Manfredi, F. Calignano, M. Krishnan, R. Canali, E.P. Ambrosio, S. Biamino, D. Ugues, M. Pavese, P. Fino, Additive manufacturing of Al Alloys and aluminium matrix composites (AMCs), 2014 3–34.

[19] F. Trevisan, F. Calignano, M. Lorusso, J. Pakkanen, A. Aversa, E.P. Ambrosio, M. Lombardi, P. Fino, D. Manfredi, On the selective laser melting (SLM) of the AlSi10Mg alloy: Process, microstructure, and mechanical properties, Materials (Basel) 10 (2017) https://doi.org/10.3390/ma10010076.

[20] N.T. Aboulkhair, M. Simonelli, L. Parry, I. Ashcroft, C. Tuck, R. Hague, 3D printing of aluminium alloys: additive manufacturing of aluminium alloys using selective laser melting, Prog. Mater. Sci. 106 (2019) 100578, https://doi.org/10.1016/j.pmatsci.2019.100578.

[21] I.M. Kusoglu, B. Gökce, S. Barcikowski, Research trends in laser powder bed fusion of Al alloys within the last decade, Addit. Manuf. 36 (2020) 101489, https://doi.org/10.1016/j.addma.2020.101489.

[22] Z. Wang, R. Ummethala, N. Singh, S. Tang, C. Suryanarayana, J. Eckert, K.G. Prashanth, Selective laser melting of aluminum and its alloys, Materials (Basel). 13 (2020) 1–67, https://doi.org/10.3390/ma13204564.

[23] P. Wang, J. Eckert, K. Gokuldoss Prashanth, M. Wei Wu, I. Kaban, L. Xia Xi, S. Scudino, A review of particulate-reinforced aluminum matrix composites fabricated by selective laser melting, 2020 https://doi.org/10.1016/S1003-6326(20)65357-2.

[24] E. Sert, A. Öchsner, L. Hitzler, E. Werner, M. Merkel, Additive manufacturing: A review of the influence of building orientation and post heat treatment on the mechanical properties of aluminium alloys, Adv. Struct. Mater. 100 (2019) 349–366, https://doi.org/10.1007/978-3-030-30355-6_14.

[25] P. Ponnusamy, R.A.R. Rashid, S.H. Masood, D. Ruan, S. Palanisamy, Mechanical properties of slm-printed aluminium alloys: a review, Materials (Basel). 13 (2020) 1–51, https://doi.org/10.3390/ma13194301.

[26] H. Chen, C. Zhang, D. Jia, D. Wellmann, W. Liu, Corrosion behaviors of selective laser melted aluminum alloys: a review, Metals (Basel) 10 (2020) https://doi.org/10.3390/met10010102.

[27] Ó. Teixeira, F.J.G. Silva, L.P. Ferreira, E. Atzeni, A review of heat treatments on improving the quality and residual stresses of the Ti–6Al–4V parts produced by additive manufacturing, Metals (Basel) 10 (2020) https://doi.org/10.3390/met10081006.

[28] I.J. Polmear, Light Alloys: Metallurgy of the Light Metals, John Wiley & Sons Australia 1995.

[29] R.E. Smallman, J.W. Bishop, Modern Physical Metallurgy and Materials Engineering, Elsevier, 1999.

[30] F. Campbell, Elements of Metallurgy and Engineering Alloys, ASM International 2008.

[31] E. Ozawa, H. Kimura, Excess vacancies and the nucleation of precipitates in aluminum-silicon alloys, Acta Metall. 18 (1970) 995–1004.

[32] V. Fallah, A. Korinek, N. Ofori-Opoku, B. Raeisinia, M. Gallerneault, N. Provatas, S. Esmaeili, Atomic-scale pathway of early-stage precipitation in Al-Mg-Si alloys, Acta Mater. 82 (2015) 457–467, https://doi.org/10.1016/j.actamat.2014.09.004.

[33] L. Pedersen, L. Arnberg, The effect of solution heat treatment and quenching rates on mechanical properties and microstructures in AlSiMg foundry alloys, Metall. Mater. Trans. A. 32A (2001) 525, https://doi.org/10.1007/s11661-001-0069-y.

[34] I. Dutta, S.M. Allen, A calorimetric study of precipitation in aluminum alloy 6061, J. Mater. Sci. Lett. 10 (1991) 323–326, https://doi.org/10.1007/BF00719697.

[35] M.J. Starink, A.M. Zahra, Precipitation in a high silicon Al-Si alloy studied by isothermal calorimetry, Mater. Sci. Eng. A 241 (1998) 277–280, https://doi.org/10.1016/s0921-5093(97)00460-7.

[36] F. Lasagni, A. Falahati, H. Mohammadian-Semnani, H.P. Degischer, Precipitation of Si revealed by dilatometry in Al-Si-Cu/Mg alloys, Kov. Mater. 46 (2008) 1–6.

[37] P.J. Uggowitzer, E. Ogris, A. Wahlen, H. L, On the silicon spheroidization in Al – Si alloys, J. Light. Met. 2 (2003) 263–269, https://doi.org/10.1016/S1471-5317(03)00010-5.

[38] S.K. Pabi, On the dissolution kinetics of silicon in an aluminium-rich matrix, Mater. Sci. Eng. 43 (1980) 151–158.

[39] S.P. Ringer, T. Sakurai, I.J. Polmear, Origins of hardening in aged Al-Cu-Mg-(Ag) alloys, Acta Mater. 45 (1997) 3731–3744, https://doi.org/10.1016/S1359-6454(97)00039-6.

[40] S.C. Wang, M.J. Starink, Precipitates and intermetallic phases in precipitation hardening Al – Cu – Mg –( Li ) based alloys, Int. Mater. Rev. 50 (2013) 193–215, https://doi.org/10.1179/174328005X14357.

[41] Z. Gao, X. Zhang, M. Chen, Investigation on θ′ precipitate thickening in 2519A-T87 aluminum alloy plate impacted, J. Alloys Compd. 476 (2009) L1–L3, https://doi.org/10.1016/j.jallcom.2008.08.055.

[42] H. Liu, B. Bellón, J. LLorca, Multiscale modelling of the morphology and spatial distribution of θ′ precipitates in Al-Cu alloys, Acta Mater. 132 (2017) 611–626, https://doi.org/10.1016/j.actamat.2017.04.042.

[43] S.C. Wang, M.J. Starink, Two types of S phase precipitates in Al – Cu – Mg alloys, Acta Mater. 55 (2007) 933–941, https://doi.org/10.1016/j.actamat.2006.09.015.

[44] E.M. Elgallad, Z. Zhang, X.G. Chen, Effect of quenching rate on precipitation kinetics in AA2219 DC cast alloy, Phys. B Condens. Matter 514 (2017) 70–77, https://doi.org/10.1016/j.physb.2017.03.039.

[45] E.A. Starke, T.H. Sanders, I.G. Palmer, New approaches to alloy development in the Al-Li system, J. Meteorol. 33 (1981) 24–33, https://doi.org/10.1007/BF03339468.

[46] L.K. Berg, G. Waterloo, D. Schryvers, L.R. Wallenberg, GP-zones in Al–Zn–Mg alloys and their role in artificial ageing, Acta Mater. 49 (2001) 3443–3451.

[47] H. Löffler, I. Kovács, J. Lendvai, Decomposition processes in Al-Zn-Mg alloys, J. Mater. Sci. 18 (1983) 2215–2240, https://doi.org/10.1007/BF00541825.

[48] J. Gubicza, I. Schiller, N.Q. Chinh, J. Illy, Z. Horita, T.G. Langdon, The effect of severe plastic deformation on precipitation in supersaturated Al-Zn-Mg alloys, Mater. Sci. Eng. A 460–461 (2007) 77–85, https://doi.org/10.1016/j.msea.2007.01.001.

[49] P. Xu, F. Jiang, Z. Tang, N. Yan, J. Jiang, X. Xu, Y. Peng, Coarsening of Al3Sc precipitates in Al-Mg-Sc alloys, J. Alloys Compd. 781 (2019) 209–215, https://doi.org/10.1016/j.jallcom.2018.12.133.

[50] E.A. Marquis, D.N. Seidman, Nanoscale structural evolution of Al3Sc precipitates in Al(Sc) alloys, Acta Mater. 49 (2001) 1909–1919.

[51] J. Taendl, A. Orthacker, H. Amenitsch, G. Kothleitner, C. Poletti, Influence of the degree of scandium supersaturation on the precipitation kinetics of rapidly solidified Al-Mg-Sc-Zr alloys, Acta Mater. 117 (2016) 43–50, https://doi.org/10.1016/j.actamat.2016.07.001.

[52] K.B. Hyde, A.F. Norman, P.B. Prangnell, The effect of cooling rate on the morphology of primary Al3Sc intermetallic particles in Al-Sc alloys, Acta Mater. 49 (2001) 1327–1337.

[53] A.B. Spierings, K. Dawson, T. Heeling, P.J. Uggowitzer, R. Schäublin, F. Palm, K. Wegener, Microstructural features of Sc- and Zr-modified Al-Mg alloys processed by selective laser melting, Mater. Des. 115 (2017) 52–63, https://doi.org/10.1016/j.matdes.2016.11.040.

[54] H. Zhang, D. Gu, J. Yang, D. Dai, T. Zhao, C. Hong, A. Gasser, R. Poprawe, Selective laser melting of rare earth element Sc modified aluminum alloy: thermodynamics of precipitation behavior and its influence on mechanical properties, Addit. Manuf. 23 (2018) 1–12, https://doi.org/10.1016/j.addma.2018.07.002.

[55] S. Lee, A. Utsunomiya, H. Akamatsu, K. Neishi, M. Furukawa, Influence of scandium and zirconium on grain stability and superplastic ductilities in ultrafine-grained Al–Mg alloys, Acta Mater. 50 (2002) 553–564.

[56] A. Tolley, V. Radmilovic, U. Dahmen, Segregation in Al3(Sc,Zr) precipitates in Al–Sc–Zr alloys, Scr. Mater. 52 (2005) 621–625, https://doi.org/10.1016/j.scriptamat.2004.11.021.

[57] A. Tridello, J. Fiocchi, C.A. Biffi, G. Chiandussi, M. Rossetto, A. Tuissi, D.S. Paolino, Effect of microstructure, residual stresses and building orientation on the fatigue response up to 109 cycles of an SLM AlSi10Mg alloy, Int. J. Fatigue 137 (2020) 105659, https://doi.org/10.1016/j.ijfatigue.2020.105659.

[58] Y.J. Liu, Z. Liu, Y. Jiang, G.W. Wang, Y. Yang, L.C. Zhang, Gradient in microstructure and mechanical property of selective laser melted AlSi10Mg, J. Alloys Compd. 735 (2018) 1414–1421, https://doi.org/10.1016/j.jallcom.2017.11.020.

[59] Z.H. Xiong, S.L. Liu, S.F. Li, Y. Shi, Y.F. Yang, R.D.K. Misra, Role of melt pool boundary condition in determining the mechanical properties of selective laser melting AlSi10Mg alloy, Mater. Sci. Eng. A 740–741 (2019) 148–156, https://doi.org/10.1016/j.msea.2018.10.083.

[60] Q. Tan, Y. Yin, Z. Fan, J. Zhang, Y. Liu, M.-X. Zhang, Uncovering the roles of LaB6-nanoparticle inoculant in the AlSi10Mg alloy fabricated via selective laser melting, Mater. Sci. Eng. A 800 (2021) https://doi.org/10.1016/j.msea.2020.140365.

[61] P. Mair, L. Kaserer, J. Braun, N. Weinberger, I. Letofsky-Papst, G. Leichtfried, Microstructure and mechanical properties of a TiB2-modified Al–Cu alloy processed by laser powder-bed fusion, Mater. Sci. Eng. A 799 (2021) https://doi.org/10.1016/j.msea.2020.140209.

[62] L. Thijs, K. Kempen, J. Kruth, J. Van Humbeeck, Fine-structured aluminium products with controllable texture by selective laser melting of pre-alloyed AlSi10Mg powder, Acta Mater. 61 (2013) 1809–1819, https://doi.org/10.1016/j.actamat.2012.11.052.

[63] T. DebRoy, H.L. Wei, J.S. Zuback, T. Mukherjee, J.W. Elmer, J.O. Milewski, A.M. Beese, A. Wilson-Heid, A. De, W. Zhang, Additive manufacturing of metallic components – Process, structure and properties, Prog. Mater. Sci. 92 (2018) 112–224, https://doi.org/10.1016/j.pmatsci.2017.10.001.

[64] X. Zhang, C.J. Yocom, B. Mao, Y. Liao, Microstructure evolution during selective laser melting of metallic materials: a review, J. Laser Appl. 31 (2019), 031201, https://doi.org/10.2351/1.5085206.

[65] T. Mukherjee, H.L. Wei, A. De, T. DebRoy, Heat and fluid flow in additive manufacturing – Part II: Powder bed fusion of stainless steel, and titanium, nickel and aluminum base alloys, Comput. Mater. Sci. 150 (2018) 369–380, https://doi.org/10.1016/j.commatsci.2018.04.027.

[66] J.P. Oliveira, A.D. LaLonde, J. Ma, Processing parameters in laser powder bed fusion metal additive manufacturing, Mater. Des. 193 (2020) 1–12, https://doi.org/10.1016/j.matdes.2020.108762.

[67] S. Liu, H. Zhu, G. Peng, J. Yin, X. Zeng, Microstructure prediction of selective laser melting AlSi10Mg using finite element analysis, Mater. Des. 142 (2018) 319–328, https://doi.org/10.1016/j.matdes.2018.01.022.

[68] K.V. Yang, Y. Shi, F. Palm, X. Wu, P. Rometsch, Columnar to equiaxed transition in Al-Mg(-Sc)-Zr alloys produced by selective laser melting, Scr. Mater. 145 (2018) 113–117, https://doi.org/10.1016/j.scriptamat.2017.10.021.

[69] R. Casati, J.N. Lemke, A.Z. Alarcon, M. Vedani, Aging behavior of high-strength Al alloy 2618 produced by selective laser melting, Metall. Mater. Trans. A Phys. Metall. Mater. Sci (2016) https://doi.org/10.1007/s11661-016-3883-y.

[70] M.L. Montero, R. Mertens, B. Vrancken, X. Wang, B. Van Hooreweder, J. Kruth, J. Van Humbeeck, Changing the alloy composition of Al7075 for better processability by selective laser melting, J. Mater. Process. Technol. 238 (2016) 437–445, https://doi.org/10.1016/j.jmatprotec.2016.08.003.

[71] D.R. Manca, A.Y. Churyumov, A.V. Pozdniakov, A.S. Prosviryakov, D.K. Ryabov, A.Y. Krokhin, V.A. Korolev, D.K. Daubarayte, Microstructure and properties of novel heat resistant Al–Ce–Cu alloy for additive manufacturing, Met. Mater. Int. 25 (2019) 633–640, https://doi.org/10.1007/s12540-018-00211-0.

[72] P. Wang, C. Gammer, F. Brenne, K.G. Prashanth, R.G. Mendes, M.H. Rümmeli, T. Gemming, J. Eckert, S. Scudino, Microstructure and mechanical properties of a heat-treatable Al-3.5Cu-1.5Mg-1Si alloy produced by selective laser melting, Mater. Sci. Eng. A 711 (2018) 562–570, https://doi.org/10.1016/j.msea.2017.11.063.

[73] Q. Liu, H. Wu, M.J. Paul, P. He, Z. Peng, B. Gludovatz, J.J. Kruzic, C.H. Wang, X. Li, Machine-learning assisted laser powder bed fusion process optimization for

AlSi10Mg: new microstructure description indices and fracture mechanisms, Acta Mater. 201 (2020) 316–328, https://doi.org/10.1016/j.actamat.2020.10.010.
[74] N.V. Dynin, V.V. Antipov, D.V. Khasikov, I. Benarieb, A.V. Zavodov, A.G. Evgenov, Structure and mechanical properties of an advanced aluminium alloy AlSi10MgCu (Ce,Zr) produced by selective laser melting, Mater. Lett. 284 (2021) 128898, https://doi.org/10.1016/j.matlet.2020.128898.
[75] T. Maeshima, K. Oh-ishi, Solute clustering and supersaturated solid solution of AlSi10Mg alloy fabricated by selective laser melting, Heliyon. 5 (2019), e01186, https://doi.org/10.1016/j.heliyon.2019.e01186.
[76] N. Takata, M. Liu, H. Kodaira, A. Suzuki, M. Kobashi, Anomalous strengthening by supersaturated solid solutions of selectively laser melted Al–Si-based alloys, Addit. Manuf. 33 (2020) 101152, https://doi.org/10.1016/j.addma.2020.101152.
[77] J. Fiocchi, A. Tuissi, P. Bassani, C.A. Biffi, Low temperature annealing dedicated to AlSi10Mg selective laser melting products, J. Alloys Compd. 695 (2017) 3402–3409, https://doi.org/10.1016/j.jallcom.2016.12.019.
[78] S. Marola, D. Manfredi, G. Fiore, M.G. Poletti, M. Lombardi, P. Fino, L. Battezzati, A comparison of selective laser melting with bulk rapid solidification of AlSi10Mg alloy, J. Alloys Compd. 742 (2018) 271–279, https://doi.org/10.1016/j.jallcom.2018.01.309.
[79] J.H. Rao, Y. Zhang, K. Zhang, X. Wu, A. Huang, Selective laser melted Al-7Si-0.6Mg alloy with in-situ precipitation via platform heating for residual strain removal, Mater. Des. 182 (2019) 108005, https://doi.org/10.1016/j.matdes.2019.108005.
[80] C. Li, Z.Y. Liu, X.Y. Fang, Y.B. Guo, Residual stress in metal additive manufacturing, Procedia CIRP. 71 (2018) 348–353, https://doi.org/10.1016/j.procir.2018.05.039.
[81] A. Salmi, E. Atzeni, History of residual stresses during the production phases of AlSi10Mg parts processed by powder bed additive manufacturing technology, Virtual Phys. Prototyp. 12 (2017) 153–160, https://doi.org/10.1080/17452759.2017.1310439.
[82] J. Suryawanshi, K.G. Prashanth, S. Scudino, J. Eckert, O. Prakash, U. Ramamurty, Simultaneous enhancements of strength and toughness in an Al-12Si alloy synthesized using selective laser melting, Acta Mater. 115 (2016) 285–294, https://doi.org/10.1016/j.actamat.2016.06.009.
[83] S. Fu, D. Yi, H. Liu, Y. Jiang, B. Wang, Z. Hu, Effects of external stress aging on morphology and precipitation behavior of θ'' phase in Al — Cu alloy, Trans. Nonferrous Metals Soc. China 24 (2014) 2282–2288, https://doi.org/10.1016/S1003-6326(14)63345-8.
[84] J. Fiocchi, C.A. Biffi, A. Tuissi, Selective laser melting of high-strength primary AlSi9Cu3 alloy: Processability, microstructure, and mechanical properties, Mater. Des. 191 (2020) https://doi.org/10.1016/j.matdes.2020.108581.
[85] U. Tradowsky, J. White, R.M. Ward, N. Read, W. Reimers, M.M. Attallah, Selective laser melting of AlSi10Mg: Influence of post-processing on the microstructural and tensile properties development, Mater. Des. 105 (2016) 212–222, https://doi.org/10.1016/j.matdes.2016.05.066.
[86] F. Bosio, H. Shen, Y. Liu, M. Lombardi, P. Rometsch, X. Wu, Y. Zhu, A. Huang, Production strategy for manufacturing large-scale AlSi10Mg components by laser powder bed fusion, J. Mater. (2021) https://doi.org/10.1007/s11837-020-04523-8.
[87] R. Casati, M.H. Nasab, M. Coduri, V. Tirelli, M. Vedani, Effects of platform preheating and thermal-treatment strategies on properties of alsi10mg alloy processed by selective laser melting, Metals (Basel) 8 (2018) 954, https://doi.org/10.3390/met8110954.
[88] Y. Li, D. Gu, Parametric analysis of thermal behavior during selective laser melting additive manufacturing of aluminum alloy powder, Mater. Des. 63 (2014) 856–867, https://doi.org/10.1016/j.matdes.2014.07.006.
[89] A. Hadadzadeh, B.S. Amirkhiz, M. Mohammadi, Contribution of Mg2Si precipitates to the strength of direct metal laser sintered AlSi10Mg, Mater. Sci. Eng. A 739 (2019) 295–300, https://doi.org/10.1016/j.msea.2018.10.055.
[90] A. Hadadzadeh, B.S. Amirkhiz, J. Li, A. Odeshi, M. Mohammadi, Deformation mechanism during dynamic loading of an additively manufactured AlSi10Mg_200C, Mater. Sci. Eng. A 722 (2018) 263–268, https://doi.org/10.1016/j.msea.2018.03.014.
[91] A. Hadadzadeh, B.S. Amirkhiz, A. Odeshi, M. Mohammadi, Dynamic loading of direct metal laser sintered AlSi10Mg alloy: strengthening behavior in different building directions, Mater. Des. 159 (2018) 201–211, https://doi.org/10.1016/j.matdes.2018.08.045.
[92] A.B. Spierings, K. Dawson, P.J. Uggowitzer, K. Wegener, Influence of SLM scan-speed on microstructure, precipitation of Al3Sc particles and mechanical properties in Sc- and Zr-modified Al-Mg alloys, Mater. Des. 140 (2018) 134–143, https://doi.org/10.1016/j.matdes.2017.11.053.
[93] I. Raffeis, F. Adjei-Kyeremeh, U. Vroomen, S. Richter, A. Bührig-Polaczek, Characterising the microstructure of an additively built Al-Cu-Li alloy, Materials (Basel). 13 (2020) 1–18, https://doi.org/10.3390/ma13225188.
[94] J.H. Rao, Y. Zhang, K. Zhang, A. Huang, C.H.J. Davies, X. Wu, Multiple precipitation pathways in an Al-7Si-0.6Mg alloy fabricated by selective laser melting, Scr. Mater. 160 (2019) 66–69, https://doi.org/10.1016/j.scriptamat.2018.09.045.
[95] J. Wu, X.Q. Wang, W. Wang, M.M. Attallah, M.H. Loretto, Microstructure and strength of selectively laser melted AlSi10Mg, Acta Mater. 117 (2016) 311–320, https://doi.org/10.1016/j.actamat.2016.07.012.
[96] M. Hillert, M. Schwind, M. Selleby, Trapping of vacancies by rapid solidification, Acta Mater. 50 (2002) 3285–3293, https://doi.org/10.1016/s1359-6454(02)00150-7.
[97] M. van Rooyen, E.J. Mittemeijer, Precipitation of silicon in aluminum-silicon: A calorimetric analysis of liquid-quenched and solid-quenched alloys, Metall. Trans. A. 20 (1989) 1207–1214, https://doi.org/10.1007/BF02647402.
[98] V.C. Pierre, B. Anthony, T. Lore, V.H. Brecht, V. Kim, Heat treatment optimization via thermo-physical characterization of AlSi7Mg and AlSi10Mg manufactured by laser powder bed fusion (LPBF), Euro PM 2018 Congr. Exhib, 2018.
[99] L. Girelli, M. Tocci, M. Gel, A. Pola, Study of heat treatment parameters for additively manufactured AlSi10Mg in comparison with corresponding cast alloy, Mater. Sci. Eng. A 739 (2019) 317–328, https://doi.org/10.1016/j.msea.2018.10.026.
[100] J. Fiocchi, C.A. Biffi, C. Colombo, L.M. Vergani, A. Tuissi, Ad hoc heat treatments for selective laser melted Alsi10mg alloy aimed at stress-relieving and enhancing mechanical performances, J. Mater. (2020) https://doi.org/10.1007/s11837-019-03973-z.
[101] M. Rafieazad, M. Mohammadi, A.M. Nasiri, On microstructure and early stage corrosion performance of heat treated direct metal laser sintered AlSi10Mg, Addit. Manuf. 28 (2019) 107–119, https://doi.org/10.1016/j.addma.2019.04.023.
[102] E. Padovano, C. Badini, A. Pantarelli, F. Gili, F.D. Aiuto, A comparative study of the effects of thermal treatments on AlSi10Mg produced by laser powder bed fusion, J. Alloys Compd. 154822 (2020) https://doi.org/10.1016/j.jallcom.2020.154822.
[103] R. Casati, M. Vedani, Aging response of an A357 Al alloy processed by selective laser melting, Adv. Eng. Mater. (2018) https://doi.org/10.1002/adem.201800406.
[104] L.C. Doan, Y. Ohmori, K. Nakai, Precipitation and dissolution reactions in 6061 aluminum alloy, Mater. Trans. JIM 41 (2000) 300–305.
[105] S. Ichiro Fujikawa, K. Ichi Hirano, Y. Fukushima, Diffusion of silicon in aluminum, Metall. Trans. A. 9 (1978) 1811–1815, https://doi.org/10.1007/BF02663412.
[106] A. Paccagnella, G. Ottaviani, P. Fabbri, G. Ferla, G. Queirolo, Silicon diffusion in aluminium, Thin Solid Films 128 (1985) 217–223.
[107] P. Yang, L.A. Deibler, D.R. Bradley, D.K. Stefan, J.D. Carroll, Microstructure evolution and thermal properties of an additively manufactured, solution treatable AlSi10Mg part, J. Mater. Res. (2018) https://doi.org/10.1557/jmr.2018.405.
[108] M. Pellizzari, M. Malfatti, C. Lora, F. Deirmina, Properties of Laser Metal Fused AlSi10Mg Alloy Processed Using Different Heat Treatments, BHM Berg- Und Hüttenmännische Monatshefte, 2020 https://doi.org/10.1007/s00501-020-00956-5.
[109] Y.D. Jia, P. Ma, K.G. Prashanth, G. Wang, J. Yi, S. Scudino, F.Y. Cao, J.F. Sun, J. Eckert, Microstructure and thermal expansion behavior of Al-50Si synthesized by selective laser melting, J. Alloys Compd. 699 (2017) 548–553, https://doi.org/10.1016/j.jallcom.2016.12.429.
[110] C.A. Biffi, J. Fiocchi, A. Tuissi, Selective laser melting of AlSi10 Mg: influence of process parameters on Mg2Si precipitation and Si spheroidization, J. Alloys Compd. 755 (2018) 100–107, https://doi.org/10.1016/j.jallcom.2018.04.298.
[111] C.A. Biffi, J. Fiocchi, P. Bassani, A. Tuissi, Continuous wave vs pulsed wave laser emission in selective laser melting of AlSi10Mg parts with industrial optimized process parameters : Microstructure and mechanical behaviour, Addit. Manuf. 24 (2018) 639–646, https://doi.org/10.1016/j.addma.2018.10.021.
[112] F. Alghamdi, X. Song, A. Hadadzadeh, B. Shalchi-amirkhiz, M. Mohammadi, M. Haghshenas, Post heat treatment of additive manufactured AlSi10Mg : On silicon morphology, texture and small-scale properties, Mater. Sci. Eng. A 783 (2020) https://doi.org/10.1016/j.msea.2020.139296.
[113] L. Girelli, M. Tocci, L. Montesano, M. Gelfi, A. Pola, Optimization of heat treatment parameters for additive manufacturing and gravity casting AlSi10Mg alloy, IOP Conf. Ser. Mater. Sci. Eng 264 (2017) https://doi.org/10.1088/1757-899X/264/1/012016.
[114] M. Tocci, A. Pola, M. Gelfi, G. Marina, L.A. Vecchia, Effect of a new high-pressure heat treatment on additively manufactured AlSi10Mg alloy, Metall. Mater. Trans. A. (2020) https://doi.org/10.1007/s11661-020-05905-y.
[115] N.T. Aboulkhair, C. Tuck, I.A.N. Ashcroft, I.A.N. Maskery, N.M. Everitt, On the precipitation hardening of selective laser melted AlSi10Mg, Metall. Mater. Trans. A. 46 (2015) 3337–3341, https://doi.org/10.1007/s11661-015-2980-7.
[116] L. Hitzler, S. Hafenstein, E. Sert, Heat treatments and critical quenching rates in additively manufactured Al– Si–Mg Alloys, Materials (Basel) 13 (2020) https://doi.org/10.3390/ma13030720.
[117] A. Mertens, O. Dedry, D. Reuter, O. Rigo, J. Lecomte-Beckers, Thermal treatments of AlSi10Mg processed by laser beam melting, Proc. 26th Int. Solid Free. Fabr. Symp. 1 (2015) 1007–1016, https://doi.org/10.1017/CBO9781107415324.004.
[118] G. Sha, H. Mo, W.E. Stumpf, J.H. Xia, G. Govender, S.P. Ringer, Solute nanostructures and their strengthening effects in Al – 7Si – 0 . 6Mg alloy F357, Acta Mater. 60 (2012) 692–701, https://doi.org/10.1016/j.actamat.2011.10.029.
[119] R.X. Li, R.D. Li, Y.H. Zhao, L.Z. He, C.X. Li, H.R. Guan, Z.Q. Hu, Age-hardening behavior of cast Al – Si base alloy, Mater. Lett. 58 (2004) 2096–2101, https://doi.org/10.1016/j.matlet.2003.12.027.
[120] T. Kimura, T. Nakamoto, Microstructures and mechanical properties of A356 (AlSi7Mg0.3) aluminum alloy fabricated by selective laser melting, Mater. Des. 89 (2016) 1294–1301, https://doi.org/10.1016/j.matdes.2015.10.065.
[121] R. Casati, M.H. Nasab, V. Tirelli, M. Vedani, Effect of different heat treatment routes on microstructure and mechanical properties of AlSi7Mg, AlSi10Mg and Al-Mg-Zr-Sc alloys produced by selective laser melting, Euro PM 2018 Congr. Exhib 2020.
[122] W. Li, S. Li, J. Liu, A. Zhang, Y. Zhou, Q. Wei, C. Yan, Y. Shi, Effect of heat treatment on AlSi10Mg alloy fabricated by selective laser melting: microstructure evolution, mechanical properties and fracture mechanism, Mater. Sci. Eng. A 663 (2016) 116–125, https://doi.org/10.1016/j.msea.2016.03.088.
[123] L.F. Wang, J. Sun, X.L. Yu, Y. Shi, X.G. Zhu, L.Y. Cheng, H.H. Liang, B. Yan, L.J. Guo, Enhancement in mechanical properties of selectively laser-melted AlSi10Mg aluminum alloys by T6-like heat treatment, Mater. Sci. Eng. A 734 (2018) 299–310, https://doi.org/10.1016/j.msea.2018.07.103.
[124] F. Alghamdi, M. Haghshenas, Microstructural and small-scale characterization of additive manufactured AlSi10Mg alloy, SN Appl. Sci 1 (2019) https://doi.org/10.1007/s42452-019-0270-5.
[125] J. Sun, L. Qiu, F. Wang, Y. Yang, L. Guo, A new modification effect of eutectic Si in selective laser melted AlSi10Mg, Mater. Sci. Technol. 35 (2019) 709–715, https://doi.org/10.1080/02670836.2019.1589740.

[126] X.P. Li, X.J. Wang, M. Saunders, A. Suvorova, L.C. Zhang, Y.J. Liu, M.H. Fang, Z.H. Huang, T.B. Sercombe, A selective laser melting and solution heat treatment refined Al – 12Si alloy with a controllable ultrafine eutectic microstructure and 25 % tensile ductility, Acta Mater. 95 (2015) 74–82, https://doi.org/10.1016/j.actamat.2015.05.017.
[127] C. Silbernagel, I. Ashcroft, P. Dickens, M. Galea, Electrical resistivity of additively manufactured AlSi10Mg for use in electric motors, Addit. Manuf. 21 (2018) 395–403, https://doi.org/10.1016/j.addma.2018.03.027.
[128] L. Zhou, A. Mehta, E. Schulz, B. McWilliams, K. Cho, Y. Sohn, Microstructure, precipitates and hardness of selectively laser melted AlSi10Mg alloy before and after heat treatment, Mater. Charact. 143 (2018) 5–17, https://doi.org/10.1016/j.matchar.2018.04.022.
[129] K.V. Yang, P. Rometsch, C.H.J. Davies, A. Huang, X. Wu, Effect of heat treatment on the microstructure and anisotropy in mechanical properties of A357 alloy produced by selective laser melting, Mater. Des. 154 (2018) 275–290, https://doi.org/10.1016/j.matdes.2018.05.026.
[130] A.H. Maamoun, M. Elbestawi, G.K. Dosbaeva, S.C. Veldhuis, Thermal post-processing of AlSi10Mg parts produced by Selective Laser Melting using recycled powder, Addit. Manuf. 21 (2018) 234–247, https://doi.org/10.1016/j.addma.2018.03.014.
[131] L. Zhuo, Z. Wang, H. Zhang, E. Yin, Y. Wang, T. Xu, C. Li, Effect of post-process heat treatment on microstructure and properties of selective laser melted AlSi10Mg alloy, Mater. Lett. 234 (2019) 196–200, https://doi.org/10.1016/j.matlet.2018.09.109.
[132] Q. Han, Y. Jiao, Effect of heat treatment and laser surface remelting on AlSi10Mg alloy fabricated by selective laser melting, Int. J. Adv. Manuf. Technol. 102 (2019) 3315–3324, https://doi.org/10.1007/s00170-018-03272-y.
[133] R. Subbiah, J. Bensingh, A. Kader, S. Nayak, Influence of printing parameters on structures, mechanical properties and surface characterization of aluminium alloy manufactured using selective laser melting, Int. J. Adv. Manuf. Technol. (2020) 5137–5147, https://doi.org/10.1007/s00170-020-04929-3.
[134] C. Gao, Z. Liu, Z. Xiao, W. Zhang, K. Wong, A.H. Akbarzadeh, Effect of heat treatment on SLM-fabricated TiN/AlSi10Mg composites: microstructural evolution and mechanical properties, J. Alloys Compd. 853 (2021) 156722, https://doi.org/10.1016/j.jallcom.2020.156722.
[135] B. Vrancken, K. Kempen, L. Thijs, J.-P. Kruth, J. Van Humbeeck, Adapted heat treatment of selective laser melted materials, Euro PM 2014 Congr. Exhib. Proc, 2014.
[136] X. Yu, L. Wang, T6 heat-treated AlSi10Mg alloys additive-manufactured by selective laser melting, Procedia Manuf. 15 (2018) 1701–1707, https://doi.org/10.1016/j.promfg.2018.07.265.
[137] K. Zyguła, B. Nosek, H. Pasiowiec, N. Szysiak, Mechanical properties and microstructure of AlSi10Mg alloy obtained by casting and SLM technique, 104 (2018) 462–472.
[138] B. Chen, S.K. Moon, X. Yao, G. Bi, J. Shen, J. Umeda, K. Kondoh, Strength and strain hardening of a selective laser melted AlSi10Mg alloy, Scr. Mater. 141 (2017) 45–49, https://doi.org/10.1016/j.scriptamat.2017.07.025.
[139] L. Hitzler, C. Janousch, J. Schanz, M. Merkel, B. Heine, F. Mack, W. Hall, A. Öchsner, Direction and location dependency of selective laser melted AlSi10Mg specimens, J. Mater. Process. Technol. 243 (2017) 48–61, https://doi.org/10.1016/j.jmatprotec.2016.11.029.
[140] S. Heilgeist, B. Heine, M. Merkel, L. Hitzler, Z. Javanbakht, A. Öchsner, The influence of post-heat treatments on the tensile strength and surface hardness of selectively laser-melted AlSi10Mg, Mater. Werkst. 50 (2019) 546–552, https://doi.org/10.1002/mawe.201800236.
[141] L. Hitzler, A. Charles, A. Öchsner, The influence of post-heat-treatments on the tensile strength and surface hardness of selective laser melted AlSi10Mg, Defect Diffus. Forum. 370 (2017) 171–176, https://doi.org/10.4028/www.scientific.net/DDF.370.171.
[142] N.T. Aboulkhair, I. Maskery, C. Tuck, I. Ashcroft, N.M. Everitt, The microstructure and mechanical properties of selectively laser melted AlSi10Mg: The effect of a conventional T6-like heat treatment, Mater. Sci. Eng. A 667 (2016) 139–146, https://doi.org/10.1016/j.msea.2016.04.092.
[143] K. Kitazono, R. Tada, Y. Sugiyama, T. Miura, Impact energy absorbing system for space lander using hemispherical open-cell porous aluminum, Mater. Sci. Forum 933 (2018) 337–341, https://doi.org/10.4028/www.scientific.net/MSF.933.337.
[144] Y. Sugiyama, T. Miura, K. Kitazono, Effects of heat treatment on compressive behavior of porous aluminum manufactured by SLM, Mater. Sci. Forum 933 (2018) 142–147 MSF. 10.4028/www.scientific.net/MSF.933.142.
[145] P. Delroisse, P.J. Jacques, E. Maire, O. Rigo, A. Simar, Effect of strut orientation on the microstructure heterogeneities in AlSi10Mg lattices processed by selective laser melting, Scr. Mater. 141 (2017) 32–35, https://doi.org/10.1016/j.scriptamat.2017.07.020.
[146] A. Mauduit, S. Pillot, F. Frascati, Application study of AlSi10Mg alloy by selective laser melting: physical and mechanical properties, microstructure, heat treatments and manufacturing of aluminium metallic matrix composite (MMC), Metall. Res. Technol. 112 (2015) https://doi.org/10.1051/metal/2015039.
[147] I. Maskery, N.T. Aboulkhair, M.R. Corfield, C. Tuck, A.T. Clare, R.K. Leach, R.D. Wildman, I.A. Ashcroft, R.J.M. Hague, Quantification and characterisation of porosity in selectively laser melted Al-Si10-Mg using X-ray computed tomography, Mater. Charact. 111 (2016) 193–204, https://doi.org/10.1016/j.matchar.2015.12.001.
[148] W.H. Kan, Y. Nadot, M. Foley, L. Ridosz, G. Proust, J.M. Cairney, Factors that affect the properties of additively-manufactured AlSi10Mg: Porosity versus microstructure, Addit. Manuf. 29 (2019) 100805, https://doi.org/10.1016/j.addma.2019.100805.
[149] N.O. Larrosa, W. Wang, N. Read, M.H. Loretto, C. Evans, J. Carr, U. Tradowsky, M.M. Attallah, P.J. Withers, Linking microstructure and processing defects to mechanical properties of selectively laser melted AlSi10Mg alloy, Theor. Appl. Fract. Mech. 98 (2018) 123–133, https://doi.org/10.1016/j.tafmec.2018.09.011.
[150] K.V. Yang, P. Rometsch, T. Jarvis, J. Rao, S. Cao, C. Davies, X. Wu, Porosity formation mechanisms and fatigue response in Al-Si-Mg alloys made by selective laser melting, Mater. Sci. Eng. A 712 (2018) 166–174, https://doi.org/10.1016/j.msea.2017.11.078.
[151] A. Majeed, Y.F. Zhang, J.X. Lv, T. Peng, S. Waqar, Z. Atta, Study the effect of heat treatment on the relative density of SLM built parts of alsi10mg alloy, Proc. Int. Conf. Comput. Ind. Eng. CIE 2018 (2018) Decem.
[152] A. Majeed, M. Muzamil, J. Lv, B. Liu, F. Ahmad, Heat treatment influences densification and porosity of AlSi10Mg alloy thin-walled parts manufactured by selective laser melting technique, J. Braz. Soc. Mech. Sci. Eng. 41 (2019) 1–13, https://doi.org/10.1007/s40430-019-1769-9.
[153] J.N. Domfang Ngnekou, Y. Nadot, G. Henaff, J. Nicolai, L. Ridosz, Influence of defect size on the fatigue resistance of AlSi10Mg alloy elaborated by selective laser melting (SLM), Procedia Struct. Integr. 7 (2017) 75–83, https://doi.org/10.1016/j.prostr.2017.11.063.
[154] I. Maskery, N.T. Aboulkhair, C. Tuck, R.D. Wildman, I.A. Ashcroft, N.M. Everitt, R.J.M. Hague, Fatigue performance enhancement of selectively laser melted aluminium alloy by heat treatment, Solid Free. Fabr. Symp. (2015) 1017–1025.
[155] N.T. Aboulkhair, I. Maskery, C. Tuck, I. Ashcroft, N.M. Everitt, Improving the fatigue behaviour of a selectively laser melted aluminium alloy: Influence of heat treatment and surface quality, Mater. Des. 104 (2016) 174–182, https://doi.org/10.1016/j.matdes.2016.05.041.
[156] E. Brandl, U. Heckenberger, V. Holzinger, D. Buchbinder, Additive manufactured AlSi10Mg samples using selective laser melting (SLM): microstructure, high cycle fatigue, and fracture behavior, J. Mater. 34 (2012) 159–169, https://doi.org/10.1016/j.matdes.2011.07.067.
[157] J.H. Rao, Y. Zhang, A. Huang, X. Wu, K. Zhang, Improving fatigue performances of selective laser melted Al-7Si-0 . 6Mg alloy via defects control, Int. J. Fatigue 129 (2019) 105215, https://doi.org/10.1016/j.ijfatigue.2019.105215.
[158] I. Serrano-munoz, J. Buffiere, C. Verdu, Y. Gaillard, P. Mu, Y. Nadot, Influence of surface and internal casting defects on the fatigue behaviour of A357-T6 cast aluminium alloy, Int. J. Fatigue 82 (2016) 361–370, https://doi.org/10.1016/j.ijfatigue.2015.07.032.
[159] S. Bagherifard, N. Beretta, S. Monti, M. Riccio, M. Bandini, M. Guagliano, On the fatigue strength enhancement of additive manufactured AlSi10Mg parts by mechanical and thermal post-processing, Mater. Des. 145 (2018) 28–41, https://doi.org/10.1016/j.matdes.2018.02.055.
[160] X. Lesperance, P. Ilie, A. Ince, Very high cycle fatigue characterization of additively manufactured AlSi10Mg and AlSi7Mg aluminium alloys based on ultrasonic fatigue testing, Fatigue Fract. Eng. Mater. Struct. (2020) 1–9, https://doi.org/10.1111/ffe.13406.
[161] M.T. Di Giovanni, J.T.O. de Menezes, G. Bolelli, E. Cerri, E.M. Castrodeza, Fatigue crack growth behavior of a selective laser melted AlSi10Mg, Eng. Fract. Mech. 217 (2019) 106564, https://doi.org/10.1016/j.engfracmech.2019.106564.
[162] C. Zhang, H. Zhu, H. Liao, Y. Cheng, Z. Hu, X. Zeng, Effect of heat treatments on fatigue property of selective laser melting AlSi10Mg, Int. J. Fatigue 116 (2018) 513–522, https://doi.org/10.1016/j.ijfatigue.2018.07.016.
[163] R.I. Revilla, D. Verkens, G. Couturiaux, L. Malet, L. Thijs, S. Godet, I. De Graeve, galvanostatic anodizing of additive manufactured Al-Si10-Mg alloy, J. Electrochem. Soc. 164 (2017) C1027.
[164] X.H. Gu, J.X. Zhang, X.L. Fan, L.C. Zhang, Corrosion behavior of selective laser melted AlSi10Mg alloy in NaCl solution and its dependence on heat treatment, Acta Metall. Sin. English Lett 33 (2020) 327–337, https://doi.org/10.1007/s40195-019-00903-5.
[165] M. Cabrini, F. Calignano, P. Fino, S. Lorenzi, M. Lorusso, D. Manfredi, C. Testa, T. Pastore, Corrosion behavior of heat-treated AlSi10Mg manufactured by laser powder bed fusion, Materials (Basel) 11 (2018) https://doi.org/10.3390/ma11071051.
[166] P. Wei, Z. Chen, S. Zhang, X. Fang, B. Lu, L. Zhang, Z. Wei, Effect of T6 heat treatment on the surface tribological and corrosion properties of AlSi10Mg samples produced by selective laser melting, Mater. Charact. 110769 (2020) https://doi.org/10.1016/j.matchar.2020.110769.
[167] X. Gu, J. Zhang, X. Fan, L. Zhang, Corrosion behavior of selective laser melted AlSi10Mg alloy in NaCl solution and its dependence on heat treatment, Acta Metall. Sin. English Lett (2019) https://doi.org/10.1007/s40195-019-00903-5.
[168] M. Fousová, D. Dvorský, A. Michalcová, D. Vojtěch, Changes in the microstructure and mechanical properties of additively manufactured AlSi10Mg alloy after exposure to elevated temperatures, Mater. Charact. 137 (2018) 119–126, https://doi.org/10.1016/j.matchar.2018.01.028.
[169] A. Aversa, M. Lorusso, F. Trevisan, E. Ambrosio, F. Calignano, D. Manfredi, S. Biamino, P. Fino, M. Lombardi, M. Pavese, Effect of process and post-process conditions on the mechanical properties of an A357 alloy produced via laser powder bed fusion, Metals (Basel) 7 (2017) 68, https://doi.org/10.3390/met7020068.
[170] J. Fite, S.E. Prameela, J. Slotwinski, T. Weihs, Evolution of the microstructure and mechanical properties of additively manufactured AlSi10Mg during room temperature holds and low temperature aging, Addit. Manuf (2020) https://doi.org/10.1016/j.addma.2020.101429.
[171] T. Rubben, R.I. Revilla, I. De Graeve, Influence of heat treatments on the corrosion mechanism of additive manufactured AlSi10Mg, Corros. Sci. 147 (2019) 406–415, https://doi.org/10.1016/j.corsci.2018.11.038.
[172] M. Albu, R. Krisper, J. Lammer, G. Kothleitner, J. Fiocchi, P. Bassani, Microstructure evolution during in-situ heating of AlSi10Mg alloy powders and additive

manufactured parts, Addit. Manuf. 36 (2020) 101605, https://doi.org/10.1016/j.addma.2020.101605.
[173] C. Colombo, C.A. Biffi, J. Fiocchi, D. Scaccabarozzi, B. Saggin, A. Tuissi, L.M. Vergani, Modulating the damping capacity of SLMed AlSi10Mg trough stress-relieving thermal treatments, Theor. Appl. Fract. Mech. 107 (2020) 1–6, https://doi.org/10.1016/j.tafmec.2020.102537.
[174] J.T. Oliveira de Menezes, E.M. Castrodeza, R. Casati, Effect of build orientation on fracture and tensile behavior of A357 Al alloy processed by Selective Laser Melting, Mater. Sci. Eng. A 766 (2019) 138392, https://doi.org/10.1016/j.msea.2019.138392.
[175] I. Rosenthal, R. Shneck, A. Stern, Heat treatment effect on the mechanical properties and fracture mechanism in AlSi10Mg fabricated by additive manufacturing selective laser melting process, Mater. Sci. Eng. A 729 (2018) 310–322, https://doi.org/10.1016/j.msea.2018.05.074.
[176] C. Colombo, C.A. Biffi, J. Fiocchi, A. Tuissi, L.M. Vergani, Effect of optimized heat treatments on the tensile behavior and residual stresses of selective laser melted AlSi10Mg samples, Key Eng. Mater. 813 (2019) 364–369 KEM. 10.4028/www.scientific.net/KEM.813.364.
[177] Renishaw plc, Laser meting: aluminum AlSi10Mg_25μm_AM250-400W parameter validation, 2014.
[178] SLM Solutions, EN AC-AlSi10Mg Material Data Sheet, Lubeck 2020.
[179] EOS GmbH, Aluminium AlSi10Mg Material data sheet, Munchen 2014.
[180] K.G. Prashanth, S. Scudino, H.J. Klauss, K.B. Surreddi, L. Löber, Z. Wang, A.K. Chaubey, U. Kühn, J. Eckert, L. Löber, Z. Wang, A.K. Chaubey, U. Kühn, J. Eckert, Microstructure and mechanical properties of Al-12Si produced by selective laser melting: Effect of heat treatment, Mater. Sci. Eng. A 590 (2014) 153–160, https://doi.org/10.1016/j.msea.2013.10.023.
[181] C. Zhang, H. Zhu, Y. Qi, X. Zeng, The effect of annealing on microstructure and mechanical properties of selective laser melting AlSi10Mg, IOP Conf. Ser. Mater. Sci. Eng 538 (2019) https://doi.org/10.1088/1757-899X/538/1/012023.
[182] P. Yang, M.A. Rodriguez, L.A. Deibler, B.H. Jared, J. Griego, A. Kilgo, A. Allen, D.K. Stefan, Effect of thermal annealing on microstructure evolution and mechanical behavior of an additive manufactured AlSi10Mg part, J. Mater. Res. (2018) https://doi.org/10.1557/jmr.2018.82.
[183] J. Fiocchi, C.A. Biffi, P. Bassani, A. Tuissi, Tailored thermal treatment for SLM built aluminum alloy product, Proc. Eur., Milan, 2017.
[184] D. Martinez-Maradiaga, O. Mishin, K. Engelbrecht, Thermal properties of selectively laser melted AlSi10Mg products with different densities, J. Alloys Compd. (2019) 1–8.
[185] N. Takata, H. Kodaira, K. Sekizawa, A. Suzuki, M. Kobashi, Change in microstructure of selectively laser melted AlSi10Mg alloy with heat treatments, Mater. Sci. Eng. A 704 (2017) 218–228, https://doi.org/10.1016/j.msea.2017.08.029.
[186] M. Liu, T. Wada, A. Suzuki, N. Takata, M. Kobashi, M. Kato, Effect of annealing on anisotropic tensile properties of al–12%si alloy fabricated by laser powder bed fusion, Crystals. 10 (2020) 1–14, https://doi.org/10.3390/cryst10111007.
[187] M. Wang, B. Song, Q. Wei, Y. Zhang, Y. Shi, Effects of annealing on the microstructure and mechanical properties of selective laser melted AlSi7Mg alloy, Mater. Sci. Eng. A 739 (2019) 463–472, https://doi.org/10.1016/j.msea.2018.10.047.
[188] T. Chen, L. Wang, S. Tan, Effects of vacuum annealing treatment on microstructures and residual stress of AlSi10Mg parts produced by selective laser melting process, Mod. Phys. Lett. B. 30 (2016) 1650255, https://doi.org/10.1142/S0217984916502559.
[189] S. Siddique, M. Imran, E. Wycisk, C. Emmelmann, F. Walther, Influence of process-induced microstructure and imperfections on mechanical properties of AlSi12 processed by selective laser melting, J. Mater. Process. Technol. 221 (2015) 205–213, https://doi.org/10.1016/j.jmatprotec.2015.02.023.
[190] X. Jiang, W. Xiong, L. Wang, M. Guo, Z. Ding, Heat treatment effects on microstructure-residual stress for selective laser melting AlSi10Mg, Mater. Sci. Technol. 36 (2020) 168–180, https://doi.org/10.1080/02670836.2019.1685770.
[191] A. Salmi, E. Atzeni, L. Iuliano, M. Galati, Experimental analysis of residual stresses on AlSi10Mg parts produced by means of selective laser melting ( SLM ), Procedia CIRP. 62 (2017) 458–463, https://doi.org/10.1016/j.procir.2016.06.030.
[192] N. Kang, P. Coddet, M.R. Ammar, H. Liao, C. Coddet, Characterization of the microstructure of a selective laser melting processed Al-50Si alloy: Effect of heat treatments, Mater. Charact. 130 (2017) 243–249, https://doi.org/10.1016/j.matchar.2017.06.026.
[193] S. Zhang, P. Ma, Y. Jia, Z. Yu, R. Sokkalingam, X. Shi, P. Ji, J. Eckert, K.G. Prashanth, Microstructure and mechanical properties of Al-(12-20)Si Bi-material fabricated by selective laser melting, Materials (Basel) 12 (2019) https://doi.org/10.3390/ma12132126.
[194] C.A. Biffi, J. Fiocchi, A. Tuissi, Laser weldability of AlSi 10 Mg alloy produced by selective laser melting: microstructure and mechanical behavior, J. Mater. Eng. Perform. (2019) 0–5, https://doi.org/10.1007/s11665-019-04402-7.
[195] P.J. Noell, J.M. Rodelas, Z.N. Ghanbari, C.M. Laursen, Microstructural modification of additively manufactured metals by electropulsing, Addit. Manuf 33 (2020) https://doi.org/10.1016/j.addma.2020.101128.
[196] Z. Li, Z. Li, Z. Tan, D. Xiong, Q. Guo, Stress relaxation and the cellular structure-dependence of plastic deformation in additively manufactured AlSi10Mg alloys, Int. J. Plast. 127 (2020) https://doi.org/10.1016/j.ijplas.2019.12.003.
[197] Y. Cao, X. Lin, Q.Z. Wang, S.Q. Shi, N. Kang, W.D. Huang, Microstructure evolution and mechanical properties at high temperature of selective laser melted AlSi10Mg, Mater. Sci. Technol. (2020) https://doi.org/10.1016/j.jmst.2020.04.066.
[198] R.S. Fachyrtdinov, P.E. Kuznetsova, I.D. Savichev, Structure, properties and heat treatment of aluminum alloy BAC1 synthesized by 3D printing, IOP Conf. Ser. Mater. Sci. Eng 934 (2020) https://doi.org/10.1088/1757-899X/934/1/012043.
[199] S. Kleiner, J. Zürcher, O. Bauer, P. Margraf, Heat treatment response of selectively laser melted AlSi10Mg, HTM - J. Heat Treat. Mater. 75 (2020) 327–341, https://doi.org/10.3139/105.110418.
[200] P. Ma, K.G. Prashanth, S. Scudino, Y. Jia, H. Wang, C. Zou, Z. Wei, Influence of annealing on mechanical properties of Al-20Si processed by selective laser melting, Metals (Basel). 4 (2014) 28–36, https://doi.org/10.3390/met4010028.
[201] V.J. Matjeke, C. Moopanar, A.S. Bolokang, J.W. van der Merwe, Effect of heat treatment time on the microstructure and mechanical deformation behavior of additive-manufactured AlSi10Mg components, Prog. Addit. Manuf. 5 (2020) 379–385, https://doi.org/10.1007/s40964-020-00139-1.
[202] D. Dai, D. Gu, H. Zhang, J. Zhang, Y. Du, T. Zhao, C. Hong, A. Gasser, R. Poprawe, Heat-induced molten pool boundary softening behavior and its effect on tensile properties of laser additive manufactured aluminum alloy, Vacuum. 154 (2018) 341–350, https://doi.org/10.1016/j.vacuum.2018.05.030.
[203] Y. Bai, Y. Yang, Z. Xiao, M. Zhang, D. Wang, Process optimization and mechanical property evolution of AlSiMg0.75 by selective laser melting, Mater. Des. 140 (2018) 257–266, https://doi.org/10.1016/j.matdes.2017.11.045.
[204] A. Iturrioz, E. Gil, M.M. Petite, F. Garciandia, A.M. Mancisidor, M. San Sebastian, Selective laser melting of AlSi10Mg alloy: influence of heat treatment condition on mechanical properties and microstructure, Weld. World. 65 (2018) 417–424, https://doi.org/10.1007/s40194-018-0592-8.
[205] P. Rodriguez, S. Venkadesan, Serrated plastic flow, Solid State Phenom. 42–43 (1995) 257–266, https://doi.org/10.4028/www.scientific.net/SSP.42-43.257.
[206] J.M. Robinson, Serrated flow in aluminium base alloys, Int. Mater. Rev. 39 (1994) 217–227, https://doi.org/10.1179/095066094790151017.
[207] Z. Hua Li, Y. Fei Nie, B. Liu, Z. Zhou Kuai, M. Zhao, F. Liu, Mechanical properties of AlSi10Mg lattice structures fabricated by selective laser melting, Mater. Des. 192 (2020) 108709, https://doi.org/10.1016/j.matdes.2020.108709.
[208] A. Suzuki, K. Sekizawa, M. Liu, N. Takata, M. Kobashi, Effects of heat treatments on compressive deformation behaviors of lattice-structured AlSi10Mg alloy fabricated by selective laser melting, Adv. Eng. Mater. 21 (2019) 1–9, https://doi.org/10.1002/adem.201900571.
[209] M. Liu, N. Takata, A. Suzuki, M. Kobashi, Effect of heat treatment on gradient microstructure of AlSi10Mg lattice structure manufactured by laser powder bed fusion, Materials (Basel) 13 (2020) https://doi.org/10.3390/ma13112487.
[210] P. Ponnusamy, S.H. Masood, D. Ruan, S. Palanisamy, R.A.R. Rashid, R. Mukhlis, N.J. Edwards, Dynamic compressive behaviour of selective laser melted AlSi12 alloy: effect of elevated temperature and heat treatment, Addit. Manuf. 36 (2020) 101614, https://doi.org/10.1016/j.addma.2020.101614.
[211] M. Giovagnoli, M. Tocci, A. Fortini, M. Merlin, M. Ferroni, A. Migliori, A. Pola, Effect of different heat-treatment routes on the impact properties of an additively manufactured AlSi10Mg alloy, Mater. Sci. Eng. A 802 (2021) 140671, https://doi.org/10.1016/j.msea.2020.140671.
[212] H.J. Rathod, T. Nagaraju, K.G. Prashanth, U. Ramamurty, Tribological properties of selective laser melted Al–12Si alloy, Tribol. Int. 137 (2019) 94–101, https://doi.org/10.1016/j.triboint.2019.04.038.
[213] Y. Zhou, L. Duan, S. Wen, Q. Wei, Y. Shi, Enhanced micro-hardness and wear resistance of Al-15Si/TiC fabricated by selective laser melting, Compos. Commun. 10 (2018) 64–67, https://doi.org/10.1016/j.coco.2018.06.009.
[214] A. Tridello, D.S. Paolino, VHCF response of AM materials: a literature review, Mater. Des. Process Commun. 2 (2020) 10–16, https://doi.org/10.1002/mdp2.121.
[215] A.M. Grande, S. Cacace, A.G. Demir, G. Sala, Fracture and fatigue behaviour of AlSi7Mg0. 6 produced by Selective Laser Melting: effects of thermal-treatments, 25th Conf. Ital. Assoc. Aeronaut. Astronaut. (AIDAA 2019) 2019, pp. 1138–1144.
[216] S. Siddique, M. Awd, J. Tenkamp, F. Walther, High and very high cycle fatigue failure mechanisms in selective laser melted aluminum alloys, J. Mater. Res. 32 (2017) 4296–4304, https://doi.org/10.1557/jmr.2017.314.
[217] L. Wang, J. Sun, X. Zhu, L. Cheng, Y. Shi, L. Guo, B. Yan, Effects of T2 heat treatment on microstructure and properties of the selective laser melted aluminum alloy samples, Materials (Basel) 11 (2018) https://doi.org/10.3390/ma11010066.
[218] E. Strumza, O. Yeheskel, S. Hayun, The effect of texture on the anisotropy of thermophysical properties of additively manufactured AlSi10Mg, Addit. Manuf. 29 (2019) 100762, https://doi.org/10.1016/j.addma.2019.06.013.
[219] B.J. Mfusi, N.R. Mathe, L.C. Tshabalala, P.A.I. Popoola, The effect of stress relief on the mechanical and fatigue properties of additively manufactured AlSi10Mg parts, Metals (Basel). 9 (2019) 1–15, https://doi.org/10.3390/met9111216.
[220] A. Tridello, J. Fiocchi, C.A. Biffi, G. Chiandussi, M. Rossetto, A. Tuissi, D.S. Paolino, VHCF response of Gaussian SLM AlSi10Mg specimens: effect of a stress relief heat treatment, Int. J. Fatigue 124 (2019) 435–443, https://doi.org/10.1016/j.ijfatigue.2019.02.020.
[221] A. Tridello, J. Fiocchi, C.A. Biffi, G. Chiandussi, M. Rossetto, A. Tuissi, D.S. Paolino, Influence of the annealing and defects on the VHCF behavior of an SLM AlSi10Mg alloy, Fatigue Fract. Eng. Mater. Struct. 42 (2019) 2794–2807, https://doi.org/10.1111/ffe.13123.
[222] M. Cabrini, S. Lorenzi, C. Testa, T. Pastore, D. Manfredi, M. Lorusso, Statistical approach for electrochemical evaluation of the effect of heat treatments on the corrosion resistance of AlSi10Mg alloy by laser powder bed fusion, Electrochim. Acta 305 (2019) 459–466, https://doi.org/10.1016/j.electacta.2019.03.103.
[223] M. Cabrini, S. Lorenzi, T. Pastore, S. Pellegrini, E.P. Ambrosio, F. Calignano, D. Manfredi, M. Pavese, P. Fino, Effect of heat treatment on corrosion resistance of

DMLS AlSi10Mg alloy, Electrochim. Acta 206 (2016) 346–355, https://doi.org/10.1016/j.electacta.2016.04.157.
[224] X. Gu, J. Zhang, X. Fan, N. Dai, Y. Xiao, L.C. Zhang, Abnormal corrosion behavior of selective laser melted AlSi10Mg alloy induced by heat treatment at 300 °C, J. Alloys Compd. 803 (2019) 314–324, https://doi.org/10.1016/j.jallcom.2019.06.274.
[225] M. Rafieazad, P. Fathi, M. Mohammadi, A.M. Nasiri, Low temperature heat-treatment cycle on AlSi10Mg_200C alloy fabricated by direct laser metal sintering: microstructural evolution and corrosion resistivity, Proc. 16th Int. Alum. Alloy. Conf., 2018.
[226] H. Zhang, H. Zhu, T. Qi, Z. Hu, X. Zeng, Selective laser melting of high strength Al – Cu – Mg alloys : processing , microstructure and mechanical properties, Mater. Sci. Eng. A 656 (2016) 47–54, https://doi.org/10.1016/j.msea.2015.12.101.
[227] X. Nie, H. Zhang, H. Zhu, Z. Hu, L. Ke, X. Zeng, Analysis of processing parameters and characteristics of selective laser melted high strength Al-Cu-Mg alloys: from single tracks to cubic samples, J. Mater. Process. Technol. 256 (2018) 69–77, https://doi.org/10.1016/j.jmatprotec.2018.01.030.
[228] F. Belelli, R. Casati, M. Riccio, A. Rizzi, M.Y. Kayacan, M. Vedani, Development of a novel high-temperature Al alloy for laser powder bed fusion, Metals (Basel). 11 (2021) 125–170. doi:10.3390/ met11010035.
[229] P. Wang, C. Gammer, F. Brenne, T. Niendorf, J. Eckert, S. Scudino, A heat treatable TiB2/Al-3.5Cu-1.5Mg-1Si composite fabricated by selective laser melting: Microstructure, heat treatment and mechanical properties, Compos. Part B Eng 147 (2018) 162–168, https://doi.org/10.1016/j.compositesb.2018.04.026.
[230] R. Casati, M. Coduri, M. Riccio, A. Rizzi, M. Vedani, Development of a high strength Al–Zn–Si–Mg–Cu alloy for selective laser melting, J. Alloys Compd. 801 (2019) 243–253, https://doi.org/10.1016/j.jallcom.2019.06.123.
[231] P. Liu, J. Ying Hu, H. Xue Li, S. Yu Sun, Y. Bin Zhang, Effect of heat treatment on microstructure, hardness and corrosion resistance of 7075 Al alloys fabricated by SLM, J. Manuf. Process. 60 (2020) 578–585, https://doi.org/10.1016/j.jmapro.2020.10.071.
[232] M.C.H. Karg, B. Ahuja, S. Wiesenmayer, S.V. Kuryntsev, M. Schmidt, Effects of process conditions on the mechanical behavior of aluminium wrought alloy EN AW-2219 (AlCu6Mn) additively manufactured by laser beam melting in powder bed, Micromachines. 8 (2017) 1–11, https://doi.org/10.3390/mi8010023.
[233] Q. Tan, J. Zhang, Q. Sun, Z. Fan, G. Li, Y. Yin, Y. Liu, M.X. Zhang, Inoculation treatment of an additively manufactured 2024 aluminium alloy with titanium nanoparticles, Acta Mater. 196 (2020) 1–16, https://doi.org/10.1016/j.actamat.2020.06.026.
[234] A.V. Pozdniakov, A.Y. Churyumov, I.S. Loginova, D.K. Daubarayte, D.K. Ryabov, V.A. Korolev, Microstructure and properties of novel AlSi11CuMn alloy manufactured by selective laser melting, Mater. Lett. 225 (2018) 33–36, https://doi.org/10.1016/j.matlet.2018.04.077.
[235] Y. Qi, H. Zhang, J. Zhu, X. Nie, Z. Hu, H. Zhu, X. Zeng, Mechanical behavior and microstructure evolution of Al-Cu-Mg alloy produced by laser powder bed fusion: effect of heat treatment, Mater. Charact. 165 (2020) 110364, https://doi.org/10.1016/j.matchar.2020.110364.
[236] P. Wang, A. Gebert, L. Yan, H. Li, C. Lao, Z. Chen, K. Kosiba, U. Kühn, S. Scudino, Corrosion of Al-3.5Cu-1.5 Mg–1Si alloy prepared by selective laser melting and heat treatment, Intermetallics 124 (2020) 106871, https://doi.org/10.1016/j.intermet.2020.106871.
[237] Y. Qi, H. Zhang, X. Nie, Z. Hu, H. Zhu, X. Zeng, A high strength Al–Li alloy produced by laser powder bed fusion: densification, microstructure, and mechanical properties, Addit. Manuf. 101346 (2020) https://doi.org/10.1016/j.addma.2020.101346.
[238] Z. Hu, Y. Qi, S. Gao, X. Nie, H. Zhang, H. Zhu, X. Zeng, Aging responses of an Al-Cu alloy fabricated by selective laser melting, Addit. Manuf. 101635 (2020) https://doi.org/10.1016/j.addma.2020.101635.
[239] M. Roudnická, O. Molnárová, D. Dvorský, L. Křivský, D. Vojtěch, Specific response of additively manufactured AlSi9Cu3Fe alloy to precipitation strengthening, Met. Mater. Int. (2019) https://doi.org/10.1007/s12540-019-00504-y.
[240] I. Raffeis, F. Adjei-Kyeremeh, U. Vroomen, P. Suwanpinij, S. Ewald, A. Bührig-Polazcek, Investigation of the lithium-containing aluminum copper alloy (AA2099) for the laser powder bed fusion process [L-PBF]: effects of process parameters on cracks, porosity, and microhardness, J. Mater. 71 (2019) 1543–1553, https://doi.org/10.1007/s11837-019-03367-1.
[241] S. Sun, P. Liu, J. Hu, C. Hong, X. Qiao, S. Liu, R. Zhang, C. Wu, Effect of solid solution plus double aging on microstructural characterization of 7075 Al alloys fabricated by selective laser melting (SLM), Opt. Laser Technol. 114 (2019) 158–163, https://doi.org/10.1016/j.optlastec.2019.02.006.
[242] A. Aversa, G. Marchese, D. Manfredi, M. Lorusso, F. Calignano, S. Biamino, M. Lombardi, P. Fino, M. Pavese, Laser Powder Bed Fusion of a High Strength Al-Si-Zn-Mg-Cu Alloy, Metals (Basel). (2018) 1–12. doi:https://doi.org/10.3390/met8050300.
[243] W. Reschetnik, J.P. Brüggemann, M.E. Aydinöz, O. Grydin, K.P. Hoyer, G. Kullmer, H.A. Richard, Fatigue crack growth behavior and mechanical properties of additively processed en AW-7075 aluminium alloy, Procedia Struct. Integr. 2 (2016) 3040–3048, https://doi.org/10.1016/j.prostr.2016.06.380.
[244] J. Ying Hu, P. Liu, S. Yu Sun, Y. Hua Zhao, Y. Bin Zhang, Y. Shuang Huo, Relation between heat treatment processes and microstructural characteristics of 7075 Al alloy fabricated by SLM, Vacuum 177 (2020) 109404, https://doi.org/10.1016/j.vacuum.2020.109404.
[245] P. Wang, H.C. Li, K.G. Prashanth, J. Eckert, S. Scudino, Selective laser melting of Al-Zn-Mg-Cu: heat treatment, microstructure and mechanical properties, J. Alloys Compd. 707 (2017) 287–290, https://doi.org/10.1016/j.jallcom.2016.11.210.
[246] S.Y. Zhou, Y. Su, H. Wang, J. Enz, T. Ebel, M. Yan, Selective laser melting additive manufacturing of 7xxx series Al-Zn-Mg-Cu alloy: cracking elimination by co-incorporation of Si and TiB2, Addit. Manuf 36 (2020) https://doi.org/10.1016/j.addma.2020.101458.
[247] J.H. Martin, B.D. Yahata, J.M. Hundley, J.A. Mayer, T.A. Schaedler, T.M. Pollock, 3D printing of high-strength aluminium alloys, Nat. Publ. Gr. (2017) https://doi.org/10.1038/nature23894.
[248] L. Zhou, H. Hyer, S. Park, H. Pan, Y. Bai, K.P. Rice, Y. Sohn, Microstructure and mechanical properties of Zr-modified aluminum alloy 5083 manufactured by laser powder bed fusion, Addit. Manuf. 28 (2019) 485–496, https://doi.org/10.1016/j.addma.2019.05.027.
[249] Q. Jia, P. Rometsch, S. Cao, K. Zhang, X. Wu, Towards a high strength aluminium alloy development methodology for selective laser melting, Mater. Des. 174 (2019) 107775, https://doi.org/10.1016/j.matdes.2019.107775.
[250] A.B. Spierings, K. Dawson, K. Kern, F. Palm, K. Wegener, SLM-processed Sc- and Zr-modi fi ed Al-Mg alloy: mechanical properties and microstructural e ff ects of heat treatment, Mater. Sci. Eng. A 701 (2017) 264–273, https://doi.org/10.1016/j.msea.2017.06.089.
[251] R. Ma, C. Peng, Z. Cai, R. Wang, Z. Zhou, X. Li, X. Cao, Manipulating the microstructure and tensile properties of selective laser melted Al e Mg-Sc-Zr alloy through heat treatment, J. Alloys Compd. 831 (2020) 154773, https://doi.org/10.1016/j.jallcom.2020.154773.
[252] A.Y. Churyumov, A.V. Pozdniakov, A.S. Prosviryakov, I.S. Loginova, D.K. Daubarayte, D.K. Ryabov, V.A. Korolev, A.N. Solonin, M.D. Pavlov, S.V. Valchuk, Microstructure and mechanical properties of a novel selective laser melted Al – Mg alloy with low Sc content, Mater. Res. Express 6 (2019) https://doi.org/10.1088/2053-1591/ab5bea.
[253] Z. Sheng, L. Wu, L. Lu, E.A. Ja, J. Risse, A. Weisheit, D. Raabe, Precipitation reactions in age-hardenable alloys during laser additive manufacturing, J. Mater. 68 (2016) 943–949, https://doi.org/10.1007/s11837-015-1764-2.
[254] R. Li, H. Chen, C. Chen, H. Zhu, M. Wang, T. Yuan, B. Song, Selective laser melting of gas atomized Al–3.02Mg–0.2Sc–0.1Zr alloy powder: microstructureand mechanical properties, Adv. Eng. Mater. 1800650 (2019) 1–15, https://doi.org/10.1002/adem.201800650.
[255] A.B. Spierings, K. Dawson, P. Dumitraschkewitz, S. Pogatscher, K. Wegener, Microstructure characterization of SLM-processed Al-Mg-Sc-Zr alloy in the heat treated and HIPed condition, Addit. Manuf. 20 (2018) 173–181, https://doi.org/10.1016/j.addma.2017.12.011.
[256] Q. Jia, F. Zhang, P. Rometsch, J. Li, J. Mata, M. Weyland, L. Bourgeois, M. Sui, X. Wu, Precipitation kinetics, microstructure evolution and mechanical behavior of a developed Al–Mn–Sc alloy fabricated by selective laser melting, Acta Mater. 193 (2020) 239–251, https://doi.org/10.1016/j.actamat.2020.04.015.
[257] J. Bi, Z. Lei, Y. Chen, X. Chen, Z. Tian, X. Qin, J. Liang, X. Zhang, Effect of Al3(Sc, Zr) and Mg2Si precipitates on microstructure and tensile properties of selective laser melted Al-14.1Mg-0.47Si-0.31Sc-0.17Zr alloy, Intermetallics 123 (2020) 106822, https://doi.org/10.1016/j.intermet.2020.106822.
[258] J. Røyset, N. Ryum, Kinetics and mechanisms of precipitation in an Al–0.2 wt.% Sc alloy, Mater. Sci. Eng. A 396 (2005) 409–422, https://doi.org/10.1016/j.msea.2005.02.015.
[259] C.B. Fuller, D.N. Seidman, D.C. Dunand, Mechanical properties of Al(Sc, Zr) alloys at ambient and elevated temperatures, Acta Mater. 51 (2003) 4803–4814, https://doi.org/10.1016/S1359-6454(03)00320-3.
[260] Q. Jia, P. Rometsch, P. Kürnsteiner, Q. Chao, A. Huang, M. Weyland, L. Bourgeois, X. Wu, Selective laser melting of a high strength Al-Mn-Sc alloy: alloy design and strengthening mechanisms, Acta Mater. 171 (2019) 108–118, https://doi.org/10.1016/j.actamat.2019.04.014.
[261] J. Bi, Z. Lei, Y. Chen, X. Chen, Z. Tian, N. Lu, X. Qin, J. Liang, Microstructure, tensile properties and thermal stability of AlMgSiScZr alloy printed by laser powder bed fusion, J. Mater. Sci. Technol. 69 (2021) 200–211, https://doi.org/10.1016/j.jmst.2020.08.033.
[262] J.P. Best, X. Maeder, J. Michler, A.B. Spierings, Mechanical anisotropy investigated in the complex SLM-processed Sc- and Zr-Modified Al – Mg alloy microstructure, 1801113 (2019) 1–6, https://doi.org/10.1002/adem.201801113.
[263] S. Griffiths, J.R. Croteau, M.D. Rossell, R. Erni, A. De Luca, N.Q. Vo, D.C. Dunand, C. Leinenbach, Coarsening- and creep resistance of precipitation-strengthened Al–Mg–Zr alloys processed by selective laser melting, Acta Mater. 188 (2020) 192–202, https://doi.org/10.1016/j.actamat.2020.02.008.
[264] H. Zhang, D. Gu, D. Dai, C. Ma, Y. Li, M. Cao, Influence of heat treatment on corrosion behavior of rare earth element Sc modified Al-Mg alloy processed by selective laser melting, Appl. Surf. Sci. 509 (2020) 1–11, https://doi.org/10.1016/j.apsusc.2020.145330.
[265] J. Bi, Z. Lei, Y. Chen, X. Chen, N. Lu, Z. Tian, X. Qin, An additively manufactured Al-14.1Mg-0.47Si-0.31Sc-0.17Zr alloy with high specific strength, good thermal stability and excellent corrosion resistance, J. Mater. Sci. Technol. 67 (2021) 23–35, https://doi.org/10.1016/j.jmst.2020.06.036.
[266] D. Gu, H. Zhang, D. Dai, C. Ma, H. Zhang, Y. Li, S. Li, Anisotropic corrosion behavior of Sc and Zr modified Al-Mg alloy produced by selective laser melting, Corros. Sci. 170 (2020) 108657, https://doi.org/10.1016/j.corsci.2020.108657.
[267] R. Ma, C. Peng, Z. Cai, R. Wang, Z. Zhou, X. Li, Enhanced strength of the selective laser melted Al-Mg-Sc-Zr alloy by cold rolling, Mater. Sci. Eng. A 775 (2020) 1–9, https://doi.org/10.1016/j.msea.2020.138975.

[268] T. Kimura, T. Nakamoto, Thermal and mechanical properties of commercial-purity aluminum fabricated using selective laser melting * 1, Mater. Trans. 58 (2017) 167–173.

[269] X. Qi, N. Takata, A. Suzuki, M. Kobashi, M. Kato, Managing both high strength and thermal conductivity of a laser powder bed fused Al–2.5Fe binary alloy: effect of annealing on microstructure, Mater. Sci. Eng. A (2020) 140591, https://doi.org/10.1016/j.msea.2020.140591.

[270] P. Ma, Y. Jia, K.G. Prashanth, S. Scudino, Z. Yu, J. Eckert, Microstructure and phase formation in Al-20Si-5Fe-3Cu-1Mg synthesized by selective laser melting, J. Alloys Compd. 657 (2016) 430–435, https://doi.org/10.1016/j.jallcom.2015.10.119.

[271] S. Sun, L. Zheng, J. Liu, H. Zhang, Selective laser melting of an Al – Fe – V – Si alloy : microstructural evolution and thermal stability, J. Mater. Sci. Technol. 33 (2017) 389–396, https://doi.org/10.1016/j.jmst.2016.09.015.

[272] D.R. Manca, A.Y. Churyumov, A.V. Pozdniakov, D.K. Ryabov, V.A. Korolev, D.K. Daubarayte, Novel heat-resistant Al-Si-Ni-Fe alloy manufactured by selective laser melting, Mater. Lett. 236 (2019) 676–679, https://doi.org/10.1016/j.matlet.2018.11.033.

[273] P.K. Shurkin, N.V. Letyagin, A.I. Yakushkova, M.E. Samoshina, D.Y. Ozherelkov, T.K. Akopyan, Remarkable thermal stability of the Al-Ca-Ni-Mn alloy manufactured by laser-powder bed fusion, Mater. Lett. 129074 (2020)https://doi.org/10.1016/j.matlet.2020.129074.